Scuola Internazionale Superiore Studi Avanzati -S.I.S.S.A

International School for Advanced Studies -I.S.A.S

Trieste, Italy

Characterization of molecular mechanisms underlying VRAC activation

Thesis submitted for the degree of
''Doctor Philosophiae''

CANDIDATE:

Sara Bertelli

SUPERVISORS

Prof. Anna Menini
Dr. Michael Pusch

SISSA - Via Bonomea 265 - 34136 Trieste - Italy

Table of contents

ABSTRACT

Multicellular organisms evolved mechanisms to accurately regulate cellular volume to counteract swelling or shrinkage which can in turn affect cell integrity.

The Volume Regulated Anion Channel (VRAC) is ubiquitously found in all vertebrate cells and turned out to be a key player in the cell-intrinsic regulatory processes which tend to restore the original volume upon osmotic challenges. In combination with potassium export mechanisms, this is achieved by the swelling-induced increased VRAC activity allowing release of halide ions and organic osmolytes, that subsequently drive water efflux through the membrane, in the so-called regulatory volume decrease process.

Difficulties encountered in the molecular identification of the channel greatly undermined biophysical characterization of VRAC and the mechanism underlying channel activation is not resolved.

Several biochemical and mechanical events have been implicated in the capability of VRAC to respond to a hypotonic challenge. The most relevant among these include: a foreground role for reactive oxygen species (ROS) and channel oxidation; the involvement of phosphorylation with several kinases and signalling pathways leading to a differential modulation of the channel; and finally the sensing of low intracellular ionic strength.

Molecular identification of genes encoding VRAC and recently solved cryo-EM structures of LRRC8A homomers revealed that the channel is a hexamer formed by members of the leucine rich repeat containing protein 8 (LRRC8) family, with the obligatory LRRC8A subunit, essential for channel functioning, and at least one of the other closely related members, which in total comprise five paralogues (LRRC8A-E). Little is known about the relevant stoichiometry, even if the high variability of the expression patterns depending on the cell type suggests that subunit composition is modified to meet physiological demand.

In this project, I followed parallel strategies to obtain a deeper insight the relevant trigger events which underlie channel activation.

By means of site-directed mutagenesis and electrophysiological analysis I elucidated mechanism of oxidation dependent VRAC modulation with the goal to understand which structural motifs are involved. Using oocytes as a heterologous expression system, I confirmed that oxidation sensitivity is subunit specific, a finding that was previously supported by the work of (Gradogna et al, 2017): LRRC8A-LRRC8E (8A-8E) heteromers are activated by oxidation, whereas 8A-8C heteromers are inhibited.

A chimeric approach allowed to identify regions responsible of the divergent effect mediated by the application of oxidant component. Swapping the C-terminus leucine-rich repeat domains (LRRD) between 8E and 8C subunits resulted in a corresponding interchange of the respective oxidation sensitivity.

Further specific targeted site-directed mutagenesis led to the identification of cysteines C424 and C448 unique to the 8E subunit, as those responsible of the dramatic increase of the current upon oxidative stimulation, with both 8A/8E_{C424F} and 8A/8E_{C448S} heteromers losing their capability to activate upon oxidant application.

In a parallel set of experiments I investigated the role played by phosphorylation in swelling dependent VRAC activation. On this purpose I mutated several residues with a high prediction score to be target of kinases from the first intracellular loop (IL1) of LRRC8A. By means of a chimeric strategy I finally disclosed that mutating residue T169 to alanine (A) or serine (S), gave rise to channels that completely lost their ability to undergo activation upon hypotonic stimulation. Surprisingly, mutation T169S retained activation by low intracellular ionic strength.

Overall, the results obtained in this thesis provide strong evidence in support of a role of oxidation in the subunit dependent VRAC modulation. In parallel, the identification of T169 as a determinant residue for channel functioning lays the groundwork to further investigation to disclose whether its importance might rely on phosphorylation or other unknown mechanisms.

1. INTRODUCTION

1.1 Ion homeostasis and cell volume regulation

Metazoan cells are constantly challenged by a variety of stimuli. A key element that distinguishes plant, bacterial, and yeast cells from animal cells is that the latter lack a rigid cell wall, being surrounded only by a flexible plasma membrane permeable to water that can therefore follow its gradient.

During evolution, multicellular organisms acquired mechanisms to accurately maintain a constant cell volume to survive and enable normal cell function. Although complex systemic osmoregulation acts to maintain the composition of extracellular fluids tightly regulated, changes in extracellular osmolarity do, however, occur under physiological conditions. Nevertheless, cell volume challenges mostly originate from disturbances in intracellular osmolarity. Indeed, at the level of single cells, normal metabolic processes, e.g., epithelial transport, cell division, growth and migration, constantly perturb the intracellular osmotic equilibrium. Necessity of volume regulation stems from the evidence that even small changes may affect the concentrations of cellular constituents and thereby interfere with biochemical reactions, trafficking and signalling, compromising overall cellular function. Indeed, impairments of cell volume regulation are closely associated with several pathophysiological states such as diabetes mellitus, ischemia, hypoxia or intracellular acidosis due both to plasma osmolality changes and increase of cellular osmolytes. Similarly, even though less critical for cell survival, cell shrinkage can occur, as described below.

Mammalian cells can only sustain a limited expansion before rupturing, leaving restricted space to volume deviation. Increases of cell surface mainly rely on amounts of pre-existing membrane reserves in the form of invaginations (Groulx et al, 2006) or in case of extreme swelling by intracellular endomembrane insertion.

Given the overall limited capacity of cells to tolerate excessive increases in cell volume, which may impair cellular structural integrity, intrinsic regulatory mechanisms are activated to restore the original cell size.

This thesis is focused on a critical player of the volume regulation process: the volume regulated anion channel (VRAC). To understand the role of VRAC role in regulatory volume decrease (RVD), the basic principles of ion and volume homeostasis shall be introduced.

The net transport of small inorganic osmolytes into and out of the cell is determined by their electrochemical gradients and the presence and activity of passive and/or secondary active membrane transporters that catalyse their transport In addition, cells contain a large number of practically membrane-impermeable charged compounds that create an osmotic pressure across the cell membrane, resulting in a constant tendency to swell throughout life. This condition is well described by the Donnan effect that defines the steady-state equilibrium of diffusible and non-diffusible species. As the osmolyte content of cells is higher than that of the extracellular space, the resulting pressure is defined as the force needed to stop water from entering a compartment. Thus, constant cell volume is ultimately maintained by net

osmolyte efflux via ion pumps, (mainly the Na^+/K^+-ATPase, [NKA]) which works against diffusional leaks of Na^+ and K^+, and secondary active transporters that exploit the large Na^+ gradient.

Integrative models of physiology still provide a framework and play an enormously important role in codifying our understanding of physiology. The pump-leak mechanism (PLM) provides a mathematical framework of how the action of NKA stabilizes cell volume against osmotic forces that drive water in (Dusterwald et al, 2018). It generates a small electric current by extruding three Na^+ ions while taking in only two K^+ ions in each cycle. Besides diminishing the Na^+ concentration, intracellular levels of Cl^- are reduced as well compared to the extracellular space, which again creates “osmotic space” for the cellular organic osmolytes.

The osmolarity of the extracellular fluid is generally tightly regulated and varies only in a narrow window. Extracellular changes of osmolarity are, therefore, usually limited to cells of the intestine, kidney or blood which can be exposed to solutions with highly varying osmolarity. Particularly important is the role of impermeant molecules, mostly anions, but also uncharged organic osmolytes, such as taurine, myo-inositol and sorbitol that are trapped in the cytoplasm and exert both osmotic and electrical effects. These types of molecules within a cell are a sizeable fraction of the contributors to the osmolarity and essentially provide the need for stabilizing the cell against inundation by water.

The processes by which swollen or shrunken cells return to their normal size are called regulatory volume decrease (RVD) and regulatory volume increase (RVI), respectively. This is achieved by the activations of channels and transporters, depending on the cell type, that transport Na^+, K^+, Cl^- or organic osmolytes (Figure 1).

RVI is mostly driven by transporters like the ubiquitously expressed Na^+/H^+-exchanger NHE1 in conjunction with the Na^+/Cl^- cotransporter NKCC1 and $Cl^-/HCO3^-$-antiporters of the anion exchanger (AE) family. They mediate a net uptake of NaCl, which provides the osmotic driving force for water influx and thereby counteract the shrinkage of the cell (Hoffmann et al, 2009).

Regulatory volume decrease (RVD) mechanisms generally involve stimulation of K^+ and Cl^- channels, as well as K^+-Cl^- (KCC) and other electroneutral cotransporters, leading to a loss of KCl and other solutes thus to reduce cell swelling. Especially for K^+, several channels and transporters turned out be critical in volume regulation. Among them are the calcium activated K^+ channels containing the small, intermediate, and big conductance K^+ channels (SK, IK, and BK), the voltage-gated K^+ channels of the KCNK-family (KCNK2, KCNK5, KCNK4) and the KCNQ family (KCNQ1, KCNQ4 and KCNQ5) (Wehner, 2006).

The current underlying the increase in Cl^- efflux occurring during RVD is termed $I_{Cl,vol}$.

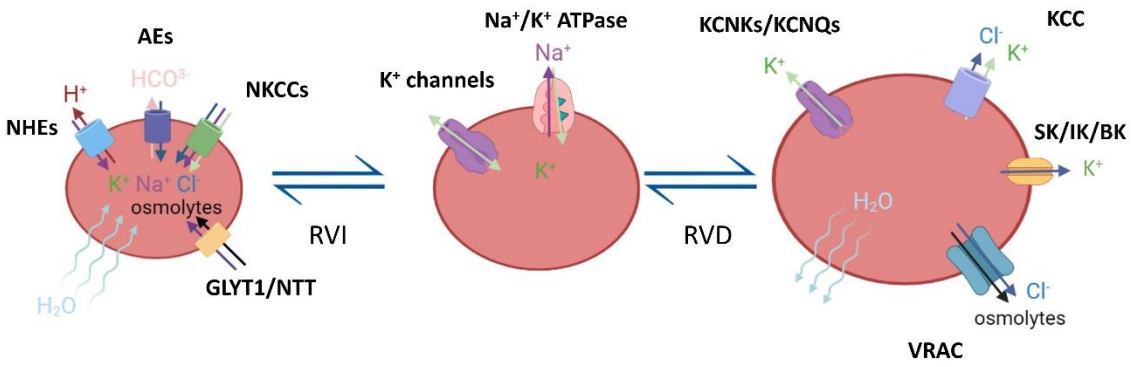

Figure 1. Schematic view of main channels and transporters involved in RVI and RVD mechanisms. See text for details.

Difficulties encountered in molecular identification of genes underlying $I_{Cl,vol}$, greatly impeded progress in the field for almost 30 years.

Many efforts have produced a number of molecular candidates, all of which turned out to be wrong. Among them the list of most prominent proteins included members of the CLC family of chloride channels and transporters, bestrophins, members of the TMEM16/anoctamin family, pICln and P-glycoprotein just to name a few (Jentsch, 2016).

Since then, the underlying channel has been referred to by different terms including volume-regulated anion channel (VRAC), volume-sensitive outwardly rectifying channel (VSOR) and volume-sensitive organic osmolyte and anion channel (VSOAC). Only the molecular identification could finally unveil that all the above descriptions were indeed referring to the same molecular entity (see dedicated paragraph 1.2.2).

Since VRAC is the major topic of this work, its biophysical properties, regulatory mechanisms and physiological relevance will be all discussed in detail in the following sections.

1.2 The volume-regulated anion channel VRAC

Chloride is the most abundant and predominant anion in the human body, constituting approximately 70% of total anionic species. Therefore, membrane channels for anionic electrolytes mostly mediate chloride current, even if their usually low selectivity allows passage of other anions. Nevertheless, they are referred to as chloride channels.

Mammalian anion channels are ordinarily classified into six major groups according to their regulatory mechanisms. 1) Ligand-gated anion channels, including GABA (y-aminobutyric acid) and glycine activated channels; 2) Voltage-gated anion channels, formed by several types of CLC family members; 3) Ca^{2+}-activated Cl^- channels (CaCCs); 4) acid-sensitive outwardly rectifying anion channel (ASOR), which is

activated by extracellular acidification; 5) PKA-activated epithelial CFTR; and finally, 6) volume-regulated anion channels that are slowly activated by cell swelling (VRAC) (Okada et al, 2019).

Regarding the class of volume regulated anion channels, a further clarification is necessary. Several channels have been described to be sensitive to changes in cell volume. For example, bestrophins and some members of the TMEM16 family have been reported to be dually regulated by $[Ca^{2+}]_i$ and cell swelling (Hoffmann et al, 2015; Pedersen et al, 1998). This has created certain confusion in the past years when referring to the group they belong to, frequently leading to misclassification. Yet, in the absence of an increase in intracellular Ca^{2+} these channels fail to activate upon hypotonic swelling. In a similar way, ClC-2 channels have been shown to be swelling-activated but convincing evidence for a determinant role in volume regulation is lacking (Gründer et al, 1992).

Thus, all these channels must be distinguished from canonical volume-regulated anion channels (VRAC), which display a distinct, well-studied biophysical fingerprint, and for which swelling is the primary mechanism of activation.

1.2.1 Biophysical properties of $I_{Cl,vol}$ /VRAC

The VRAC current (known as $I_{Cl,vol}$) was first described in human lymphocytes and epithelial cells in 1988 (Cahalan & Lewis, 1988; Hazama & Okada, 1988). $I_{Cl,vol}$ has then been observed in almost every vertebrate cell type investigated (Jentsch, 2016).

$I_{Cl,vol}$ are slowly activated upon hypotonic challenges (Figure 2A) and decrease by raising the osmolarity of the extracellular environment. There is evidence that the channel can be activated also under isovolumic conditions, for example by pro-apoptotic stimuli, intracellular application of GTPγS, or by decreasing intracellular ionic strength, which will be all discussed in depth in the next section.

A distinctive feature that characterizes VRAC current is its mild outward rectification, with larger current observed at positive membrane potentials and (variable) inactivation occurring at large positive membrane voltages (Figure 2B-C).

These characteristics are in strong contrast to other anion channels like ClC-2, that shows an inwardly rectifying current and different anion selectivity (Gründer et al, 1992; Thiemann et al, 1992), bestrophins with a linear I-V-relationship (Hartzell et al, 2009) or anoctamins with a steep outward rectification at low $[Ca^{2+}]_i$ and linearity at high $[Ca^{2+}]_i$ (Grubb et al, 2013; Juul et al, 2014; Pifferi et al, 2009; Schroeder et al, 2008).

Additionally, none of the above channels inactivate at positive potentials. The specific fingerprint of VRAC currents allows to clearly distinguish them among other Cl^- conductances mediated by different anion channels.

VRAC show a higher permeability to larger halide anions than Cl^- and displays a selectivity sequence which corresponds to the Eisenmann type I sequence $I^- > Br^- > Cl^-$ as determined from shifts in the reversal

potential of $I_{Cl,vol}$ upon anion substitution. This feature is typical for channels with low affinity binding sites and has been used to calculate the pore diameter of VRAC that was estimated around 1.1 nm (Nilius et al, 1999). A further characteristic is its virtual exclusion of cations (Akita & Okada, 2014; Nilius & Droogmans, 2003; Nilius et al, 1997; Okada, 1997). VRAC can conduct small organic osmolytes due to its weak discrimination among halides, but also uncharged compounds, like taurine, which play a critical role in volume regulatory processes (Figure 2D). These substrates include some excitatory amino acids and their derivatives, for which significant current have been recorded (e.g. glycine, gluconate, aspartate, glutamate), and ATP. Their permeation through VRAC channels has been proposed to be important for signalling and toxicity in glia and other cell types (Gaitán-Peñas et al, 2016; Lutter et al, 2017; Nilius et al, 1997; Pedersen et al, 2016; Strange et al, 2019).

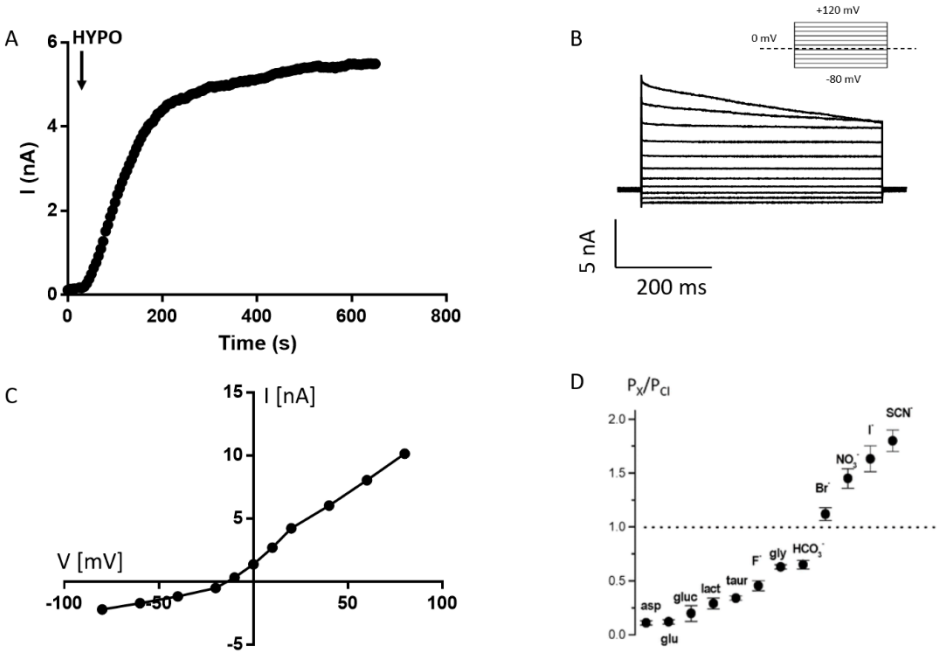

Figure 2. (A) Representative time course of activation of $I_{Cl,vol}$ in HEK-5X-KO cells transiently transfected with 8A/8E heteromers and patched in the whole cell configuration upon hypotonic perfusion. (B) Currents from the same cell elicited by the voltage protocol shown above. (C) Current–voltage (I–V) curves obtained at steady-state. Note the mild outward rectification of $I_{Cl,vol.}$ (D) Permeation properties of $I_{Cl,vol}$: permeability ratios calculated from the shifts in Erev by substitution of Cl^-. Note the permeation of large anion such as taurine, aspartate, and glutamate. Panel D is modified from (Pedersen et al, 2016).

1.2.2 Molecular identification of genes underlying VRAC current

Difficulties encountered in the molecular identification of genes underlying VRAC greatly thwarted progress in the field for almost 26 years. Many efforts have produced several molecular candidates, all of which turned out to be wrong. Among the main factors that hindered conventional approaches used to identify the channel mediating $I_{Cl,vol}$ was the fact that VRAC is ubiquitously expressed in all vertebrate cells, including Xenopus oocytes, a tool often used in the past to clone and characterize ion channels. Thus, no

heterologous system devoid of a significant $I_{Cl,vol}$ background was available. Moreover, no blockers with a high enough specificity and affinity for VRAC are known and this contributed to the difficulties experienced in the attempt to biochemically purify related protein(s).

One of the more specific blockers of VRAC is the ethacrynic-acid derivative DCPIB (4-(2butyl-6,7-dichlor-2-cyclopentyl-indan-1-on-5-yl) oxybutyric acid), which potently inhibits $I_{Cl,vol}$ in several cell lines and tissues in the micromolar range (Decher et al, 2001; Liu et al, 2009). However this compound has also been reported to target connexin hemichannels, the glutamate transporter GLT-1 (Bowens et al, 2013)(Bowens et al., 2013), the gastric H^+,K^+-ATPase (Fujii et al, 2015) and K2P channels (Minieri et al, 2013).

Another issue was the heterogeneity of some properties of VRAC currents, like e.g. inactivation and permeation fingerprint, which slightly varied according to the cell type investigated, suggesting the involvement of more than one protein or even a heteromeric channel with functionally redundant subunits according to tissue specific expression pattern.

Unfortunately, none of these candidates withstood the test of experimental verification by other laboratories (Strange et al, 2019).

A major breakthrough came in 2014 when two groups independently identified the genes encoding VRAC using genome-wide RNA silencing methods and high-throughput fluorescence assays of channel activity (Syeda et al, 2016; Voss et al, 2014). In principle the assay consisted in the siRNA knockdown of all putative candidates and the screening criteria were defined by the maximal slope of fluorescence quenching upon hypotonic stimulation.

These milestone works demonstrated that VRAC is a heteromeric channel encoded by members of the Leucine Rich Repeat Containing 8 (LRRC8) gene family, which comprises the five members *LRRC8A–E*. Using CRISPR/Cas9 technology the group of Jentsch established cell lines in which all 5 genes had been knocked out (KO^{8A-8E}), allowing to study and characterize the channel in a background devoid of endogenous VRAC (Voss et al, 2014). This paved the way for the discovery that the channel is a multimer formed by the essential, but not sufficient LRRC8A subunit that needs to be co-expressed with at least one more additional subunit among LRRC8B, LRRC8C, LRRC8D and LRRC8E (Voss et al, 2014). The LRRC8B subunit is the least understood one because co-transfection of LRRC8A with LRRC8B in KO^{8A-8E} cells did not produce $I_{Cl,vol}$ currents, while cells in which the three genes LRRC8C-E were knocked out, i.e. with intact LRRC8A and LRRC8B genes, retained $I_{Cl,vol}$ (Voss et al, 2014).

Expression of LRRC8A alone only elicits negligible currents upon hypotonic stimulation, while co-expression of LRRC8A with LRRC8C, D or E subunits results in a large VRAC current response, with characteristic kinetics of inactivation that depend on the subunit composition. The details will be discussed in the next paragraph.

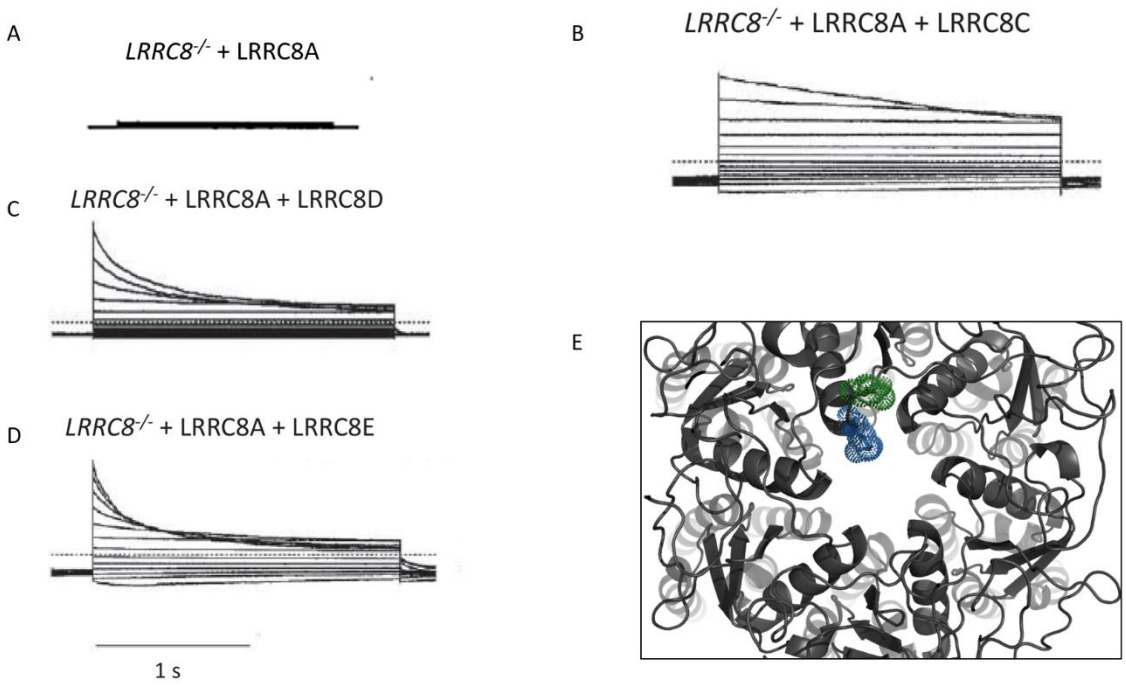

Figure 3. Subunit composition determines channel inactivation kinetics.
Panels A-D illustrate different kinetics of inactivation of currents measured in LRRC8 knockout cells transfected with the indicated subunits; applied voltages range from -120 to 120 mV. In (A) cells transfected with 8A alone do not elicit any current (modified from (Voss et al, 2014)). In (E) are highlighted with dots residues D100 and R103, which define respectively the narrowest part of the pore (R103), and properties of inactivation kinetics (D100).

1.2.3 Voltage dependence

A distinctive feature that characterizes $I_{Cl,vol}$ is its time-dependent inactivation at depolarizing voltage steps. The voltage sensitivity of the inactivation process was shown to differ drastically among different cell lines and native tissues (Nilius et al, 1997). At inside-positive potentials above a certain threshold, VRAC currents decrease slowly, and further depolarizing voltage steps accelerate the current decay, which saturates on a timescale of tens of milliseconds at sufficiently strong depolarizations. Inactivation is not complete with around 10–20% of the initial peak current which persists. However the remaining current might partially differ from $I_{Cl,vol}$ since swollen cells also variably activate leak currents that are particularly prominent at highly depolarized voltages where inactivation is most pronounced.

Negative potentials facilitate recovery from inactivation which occurs more rapidly at more hyperpolarized potentials (Nilius et al, 1997; Okada, 1997). Both inactivation and recovery are well described by double exponential functions in some (Jackson & Strange, 1995; Voets et al, 1997a), but not all cell types (Voets et al, 1997a), suggesting a more complex kinetic process.

The molecular identification of LRRC8 genes underlying VRAC shed light on the variability observed in different cell types. In this respect a pivotal role was played by the work of Jentsch and collaborators, who

generated LRRC8$^{-/-}$ quintuple knockout, as well as single, double, and triple knockout of various cell line, including HEK293, HCT116 and HS60.

Besides demonstrating that LRRC8A is essential for $I_{Cl,vol}$ and fundamental for correct trafficking of the channel to the plasma membrane, they found that the pattern of differential voltage-dependent inactivation was strictly dependent on subunit composition. LRRC8A/LRRC8E complexes exhibit profound and rapid kinetic of inactivation at positive voltages, similarly to LRRC8A/LRRC8D channels, even if in this case current decay is slightly slower and less pronounced (Gaitán-Peñas et al, 2016; Voss et al, 2014). Conversely LRRC8A/LRRC8C complexes yield currents with much larger time constants of inactivation.

While generally the time constant of inactivation (τ) of LRRC8A/E reaches steady state at voltages more positive than ~80 mV, LRRC8A/C currents do not reach similar inactivation time constants even at 120 mV (Ullrich et al, 2016). However, it is also conceivable that smaller differences could partially originate from variation in cellular environment such as membrane components or composition of extracellular and intracellular solutions (Ullrich, 2016).

The composition of the extracellular medium can significantly affect the voltage-dependent properties of $I_{Cl,vol}$. Various reports showed that an acidic extracellular pH accelerates the inactivation of the channel and shifts the inactivation curve to less positive voltages (Hernandez-Carballo et al, 2010; Nilius et al, 1997; Voets et al, 1997a).

Divalent cations in the extracellular bath solution were found to facilitate inactivation with their efficacy decreasing in the order $Mg^{2+} > Ca^{2+} > Sr^{2+} > Ba^{2+}$ (Anderson et al, 1995; Braun & Schulman, 1996; Voets et al, 1997a). It was proposed that divalent cations may bind to extracellular sites of the channel thus altering its gating properties (Nilius et al, 1997). Similarly, low pH may act by protonation of extracellular site(s) on VRAC.

Overall, voltage-dependent inactivation is unlikely to be of physiological relevance since the membrane potential in most cells is usually much more negative than the voltage required for inactivation. However, the understanding of this phenomenon is important to elucidate the general gating mechanisms of VRAC. Exploiting the kinetic differences between LRRC8A/8E and LRRC8A/8C heteromers and a chimeric approach, Ullrich et al. identified the C-terminal half of the first extracellular loop (EL1) as a major determinant of VRAC inactivation (Ullrich et al, 2016). Their functional results together with the recently available structural information suggest that inactivation involves a conformational change of the external pore constriction, hinting that inactivation may reflect a closure of the outer pore entrance (see dedicated section 1.4). It still remains to be determined whether positive voltages lead directly to inactivation, by acting on charged VRAC protein segments, or indirectly, e.g. by interaction of permeating substrates with the protein, and if the inactivation process is mechanistically coupled to the general mechanism of VRAC activation by hypotonicity. Only the comprehension of the basic activation mechanism could help in addressing this unsolved point (Bertelli et al, 2021).

1.3 Putative mechanisms of VRAC modulation

The mechanisms by which VRAC channels can sense cell volume changes leading to their activation are not fully resolved. From its first discovery, several stimuli have been associated with VRAC modulation. These included pro-apoptotic compounds, second messengers, signalling pathways and other molecules that showed at least a permissive effect. However, only few of them could be replicated and gave evidence to be effectively required for $I_{Cl,vol}$. (Akita & Okada, 2014; Pedersen et al, 2015).

One of the crucial questions is if VRAC itself is able to sense volume changes or if it relies on an extrinsic sensor which could be coupled to the channel either directly or via a signal transduction cascade (Ullrich, 2016).

A leading hypothesis to explain how the channel detects cell volume changes that immediately follow the hypotonic stimulus is the sensing of a low intracellular ionic strength. Nilius and collegues in 1998 provided a first insight of this concluding that a decrease in ionic strength can activate $I_{Cl,vol}$ even in the absence of cell swelling, under isotonic conditions (Nilius et al, 1998).

After molecular identification, the group of Patapoutian succeeded in purifying and reconstituting LRRC8A homomeric and heteromeric complexes into lipid bilayers at the interface between two droplets, to form VRAC channels. With a minimalistic approach they managed to study VRAC activation in the absence of cellular components that have were thought to be involved in this process, such as cytoskeleton, caveoli, enzymes and second messenger systems. Under these conditions they found that mechanically-induced stresses on the membrane were not sufficient to induce channel activation, but when bilayers were injected with a lower ionic strength in the cytoplasmic side droplet, VRAC current could be directly gated (Syeda et al, 2016).

Several works of the latest 90's indicated that $I_{Cl,vol}$ amplitudes and the time course of activation correlated better with ionic strength than with cell volume, and swelling induced by a hypertonic intracellular solution of high ionic strength even inhibited VRAC (Voets et al, 1999). However, as reviewed in detail by Strange et al. (Strange et al, 2019), several pieces of evidence argue strongly against the idea that low ionic strength is the physiologically relevant stimulus. Notably, the reduction of ionic strength necessary to elicit VRAC current in patch-clamp recordings is much larger than what would be expected from physiological activation by hypotonicity. Moreover, during patch clamp recordings in the whole cell configuration under normal ionic strength, the intracellular ion concentrations upon application of a hypotonic extracellular solution is practically "clamped" through the patch pipette even close to the membrane (Bertelli et al, 2021). Thus, in these conditions, activation of VRAC occurs without reduction of intracellular ionic strength.

As final consideration, VRAC can be activated in a variety of conditions that are not coupled to alteration of ionic strength or extracellular osmolarity. For example application of GTPγS through the patch pipette

activates VRAC in chromaffin cells (Doroshenko, 1991). The potential physiological role of intracellular ionic strength needs to be determined.

Mechanical activation of VRAC through membrane stretch has been matter of debate for many years (Nilius & Droogmans, 2001; Nilius et al, 1997; Okada, 1997). Notably, $I_{Cl,vol}$ could be induced by application of positive pressure (blowing into) through the patch pipette. Nonetheless, it has been argued that osmotic swelling might not actually induce membrane stretch, as cells have great amounts of membrane invaginations which may unfold during volume increase (Okada, 1997).

Another matter of debate is the dependency of VRAC on the intracellular concentration of ATP. It has been reported that swelling-induced activation of the channel requires a permissive concentration of ATP or nonhydrolyzable ATP analogues. This suggested that its hydrolysis is probably not necessary for channel gating, but ATP might presumably bind directly to VRAC channels. Yet, the relevant ATP binding site has not been identified so far, and it cannot be excluded that ATP is acting indirectly on other essential proteins. It was proposed that the ATP requirement might correlate with reduced cellular energy states to prevent the rundown of metabolically expensive organic osmolytes, thus providing a feedback to counteract the loss of carbon sources (Jackson et al, 1994).

In many cells, swelling and subsequent VRAC activation is often accompanied by a rise in intracellular calcium, $[Ca^{2+}]_i$. However, the role of $[Ca^{2+}]_i$ in the activation of VRAC remains enigmatic. The channel is generally recognized not to be Ca^{2+}-dependent in the classical sense (Kubo & Okada, 1992; Nilius et al, 1997; Nilius et al, 1994; Strange et al, 1996). Similarly to the ATP dependence, full activation of $I_{Cl,vol}$ requires permissive Ca^{2+} concentrations (≥50 nM free $[Ca^{2+}]_i$ in some, but not all cell types investigated, while higher concentrations do not influence the current density (Nilius et al, 1997; Szücs et al, 1996).

Moreover, at least in some systems, VRAC current could be elicited even under conditions of heavy buffering of $[Ca^{2+}]_i$ by the application of the specific chelator BAPTA (1,2-bis(o-aminophenoxy)ethane-N,N,N',N'-tetraacetic acid (Kubo & Okada, 1992). This characteristic firmly distinguishes VRAC channels from other Ca^{2+}-activated Cl^- channels like bestrophins and TMEM16 family members, which fail to activate in the absence of increases in $[Ca^{2+}]_i$, upon hypotonic swelling (Jentsch, 2016).

1.3.1 Reactive oxygen species (ROS) and role of oxidation

A biochemical event that has been linked to VRAC activation in several cellular systems is the increase in reactive oxygen species (ROS) level. Several works reported that the exogenous application of hydrogen peroxide (H_2O_2) could elicit a current with VRAC biophysical properties that could be thereafter inhibited by the application of antioxidant enzymes, e.g. catalase and/or the reducing agent dithiothreitol (DTT) (Crutzen et al, 2012; Jiao et al, 2006; Shimizu et al, 2004; Varela et al, 2007). A regulatory role was suggested for NADPH oxidase-generated ROS in apoptotic signalling with subsequent activation of VRAC leading to apoptotic volume decrease (AVD) (Jiao et al, 2006; Okada et al, 2006; Shimizu et al, 2004). In

support of this hypothesis, VRAC was shown to be activated under isovolumic conditions by several pro-apoptotic stimuli, including staurosporine (Coca-Prados et al, 1995; Okada et al, 2006; Shimizu et al, 2004), the death receptor ligand TNFα (Nietsch et al, 2000; Schumann et al, 1993)or doxorubicin (de Tassigny et al, 2004).

Even though oxidative compounds are generally known for their deleterious effects, it is now generally recognised that mild oxidative stress is a key element leading to cell adaptation and survival. Physiologically, ROS signalling plays a critical role in the immune system (Muralidharan & Mandrekar, 2013); for example neutrophils can eliminate pathogens by production of superoxide and other free oxygen radicals in phagosomes (DeCoursey, 2003).

Notably, T lymphocytes were among the first cells in which VRAC currents have been identified (Cahalan & Lewis, 1988; Gradogna et al, 2017; Lewis et al, 1993).

Oxidative stress can activate several signalling pathways within the cell, culminating in reactive oxygen species (ROS) production which can directly react with proteins on cysteine and methionine residues. In this regard, an important question is whether VRACs are directly or indirectly affected by oxidation.

In a previous work Gradogna et al. showed that Chloramine-T (Chl-T), an oxidant that reacts with cysteine and methionine residues, had a divergent effect when applied to oocytes expressing LRRC8A-E heteromers, where it resulted in a strong activation of the current, compared to the effect observed when applied in oocytes expressing LRRC8A-C heteromers, that conversely resulted in a inhibition of the constitutive current (Gradogna et al, 2017).

Exploiting cysteine modifying compounds (e.g. MTT, $MTSEST^+$, $MTSET^-$), that react with cysteines blocking their further oxidation, they concluded that the relevant residues undergoing oxidation in 8A/8E heteromers are intracellularly localized.

While it was shown that the target of Chl-T within the 8E subunit were cysteine residues, the application of MTSET on 8C and 8D subunits could not completely abolish the effect of the subsequent application of Chl-T, suggesting methionine residues as the putative target of oxidation, but leaving open the possibility of a combined effect of Cys and Met.

It has also to be highlighted that the application of another oxidant, tertbutyl hydroperoxide (TBHP), had slightly different effects compared to Chl-T. While 8A-8E heteromers were activated by TBHP as well, the compound had no effect at all on 8A-8C heteromers (Figure 4).

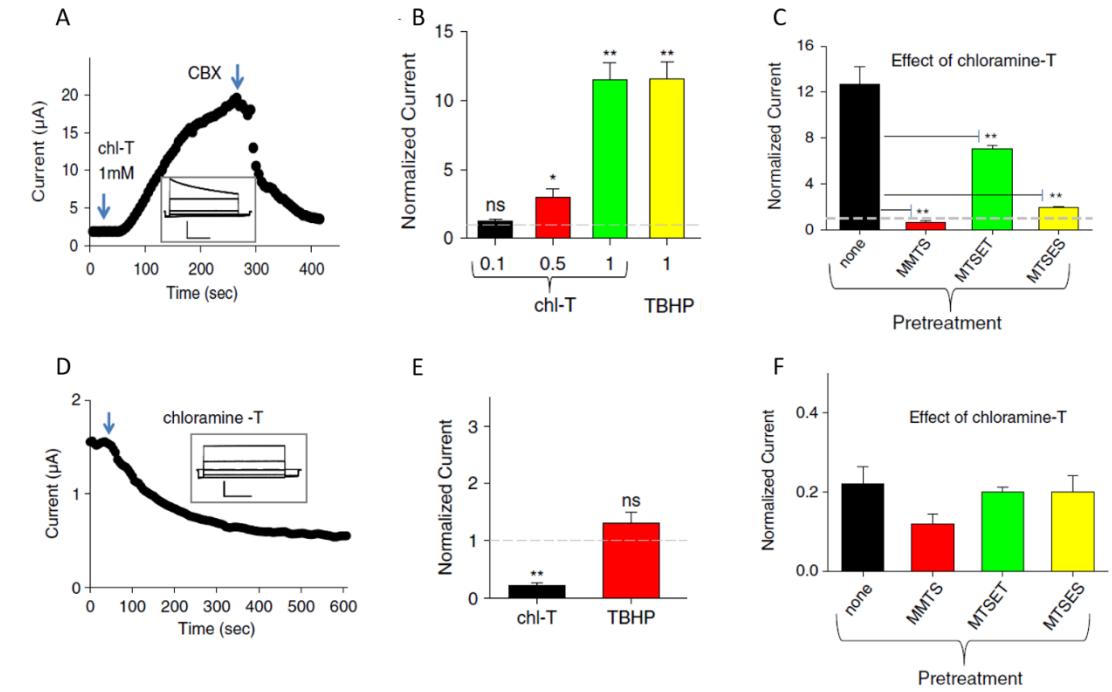

.

Figure 4. **Oxidation sensitivity is strictly subunit dependent.**
Figure modified from (Gradogna et al, 2017). Figure 4. A -D representative traces of the effect of application of chloramine-T to oocytes co-expressing 8A-VFP and 8E-mCh. The concentration is indicated in the figure. B-F average current response to the indicated stimuli, normalized to the initial current. Dashed lines indicate basal current level with respect to chloramine-T (chl-T). C-F average response to the application of 1 mM chloramine-T after pretreatment with cysteine-modifying reagents, normalized to the current before chloramine-T application.

1.3.2 Role of phosphorylation in swelling induced VRAC activation

During the first decade of investigation of VRAC, special attention has been devoted to the role of post-translational modification on channel modulation. In particular, many studies devoted their efforts to explore a possible role of phosphorylation as the trigger event upon hypotonic challenges.

It was shown that the direct application of specific inhibitors of protein tyrosine kinases (PTKs), like e.g. genistein, could prevent VRAC activation upon hypotonic perfusion (Bryan-Sisneros et al, 2000; Crepel et al, 1998; Sorota, 1995; Tilly et al, 1993; Voets et al, 1998). In line with this finding, the application of protein tyrosine phosphatase (PTP) inhibitors, like Na_3VO_4 and dephostatin could elicit VRAC currents even in isotonic conditions suggesting a fine-tuned mechanism of this kinase family in regulating VRAC state upon cells swelling (Bertelli et al, 2021). However, it needs to be highlighted that other works as well could not find a similar effect of tyrosine kinases, while in contradiction with the above observations, other studies reported an increase of VRAC upon the application of PTK inhibitors (Du et al, 2004; Ren & Baumgarten, 2005), and protein tyrosine phosphatase (PTP) inhibitors were shown to suppress VRAC, conversely suggesting an opposite mechanism where dephosphorylation is determinant in the activation of the

channel (Doroshenko, 1998; Thoroed et al, 1999). It was proposed that an interplay of PTKs and their corresponding signalling cascades differentially modulates the gating of the channel in different cell types. In any case, since no candidate proteins underlying VRAC current were known at that time, no evidence of a direct effect of phosphorylation on channel subunits could be investigated. Indeed, these results left unsolved the crucial question, whether the effect of tyrosine kinases on VRAC gating could be attributed to an upstream regulator or to the channel itself. Also, it remained unclear which tyrosine kinase family may be involved in this regulatory mechanism, even if indirect evidence pointed toward the Src family.

In parallel a large amount of literature suggested a primary role of protein kinase C (PKC) in VRAC activation. Many works showed that the use of PKC blockers was able to prevent channel activation upon swelling, which could be rescued by the PKC activator phorbol 12-myristate,13-acetate (PMA) (Chou et al, 1998; Gong et al, 2004; Hermoso et al, 2004; Meyer & Korbmacher, 1996). Notably, two independent studies provided a direct indication of a swelling-induced translocation of PKC-α in the cytoskeleton fraction that subsequently underwent phosphorylation in the cell membrane (Chou et al, 1998; Hermoso et al, 2004). Furthermore, other experiments conducted in a cell line stably expressing dominant negative PKC variants pointed out an essential role of PKCα isoforms in swelling-dependent VRAC activation (Hermoso et al, 2004). For an overview of the major contributions on PTKs and PKCs role in VRAC activation see (Bertelli et al, 2021).

In a recent publication, Stauber and collaborators developed a sensor to measure intra-complex Förster resonance energy transfer (FRET) to monitor VRAC activity in a spatio-temporally resolved manner. Performing simultaneously cFRET and whole-cell current measurements they found that protein kinase D (PKD) activity may be critically involved in hypotonicity-induced activation of VRAC (Figure 3) (König et al, 2019).

Given the ability of this kinase isoform to converts transient diacylglycerol (DAG) signals into physiological effects downstream of PKC, this suggested serine/threonine phosphorylation as the putative final event for VRAC regulation.

Overall, these data suggest that phosphorylation can play an important part in VRAC modulation, but leave as an open question whether it represents a critical step in swelling dependent VRAC activation.

Several hypotheses have been made to partially justify some controversial findings. First, the divergent effects observed on kinase activity can rely on tissue- or species-specific mechanisms, but also cell-type specific channel composition and stoichiometry. Moreover, broad-spectrum inhibitors, as the most commonly used genistein, can mask antagonistic effects of specific PTKs subfamilies.

Interestingly, few years before the molecular identity of VRAC was disclosed, Abascal & Zardoya correctly predicted LRRC8 proteins to form hexameric ion channels, and speculated around the importance of the intracellular loop connecting the TM pore to the LRR domain as a potential target of post-translational modification (Abascal & Zardoya, 2012). In particular, since the primary sequence of this region is

particularly rich of serine, threonine and tyrosine amino acids they performed proteomic data base analysis, leading to the proposal that part of these residues in the first intracellular loop undergo phosphorylation (Abascal & Zardoya, 2012).

Recently, the group of Strange analyzed several regions of the LRRC8 for their functional importance. Among these was the intracellular loop connecting TM2 and TM3, which will be called IL-loop throughout the thesis. Within the IL-loop, Yamada & Strange identified a short minimal stretch comprising amino acids 182 to 206 as particularly interesting (we will call this stretch YSS-stretch for simplicity). Introducing the YSS-stretch from 8A to replace the same region in the background of other isoforms, was sufficient to give rise to functional homomeric chimeric channels that are otherwise non-functional (Yamada & Strange, 2018). Performing a PONDR analysis (Predictor of Natural Disordered Regions), they found out that the IS-stretch, which is not resolved in any of the structures described so far, significantly diverges among LRRC8A, LRRC8C, LRRC8D, and LRRC8E proteins (Yamada & Strange, 2018). This finding brought them to conclude that such dips in the PONDR score of intrinsically disordered protein regions may predict the existence of molecular recognition elements or other features (Strange et al, 2019). All these parallel findings of a possible relevance of the intracellular loop, suggests that this region could be the target of post-translational modifications. Yet, it needs to be assessed whether the region plays a central role in channel gating (i.e. activation), or whether it is, more indirectly, required for folding, membrane targeting, protein-protein interaction or other physiological roles.

1.3.3 GTP-binding proteins

The role of GTPγS was deeply investigated. The intracellular application of the non-hydrolysable GTP analogue guanosine 5'-O-(3-thiotriphosphate) was shown to elicit VRAC current even under isotonic conditions (Doroshenko & Neher, 1992; Estevez et al, 2001; Voets et al, 1998). Conversely, application of GDPβS, a non-hydrolysable analogue of GDP that competes with GTP for binding to G proteins, caused a time-dependent inhibition of VRAC, which was more pronounced when the current was activated upon hypotonic conditions. Yet, GDPβS could not prevent activation of anion currents in all the cell types investigated (Botchkin & Matthews, 1993). Some studies also reported that treatment of cells with Clostridium Difficile, a toxin which causes glycosylation of GTP-binding proteins of the Rho/Ras family and thereby their inactivation, strongly reduced swelling induced VRAC current (Carton et al, 2002; Tilly et al, 1996).

Rho proteins are involved in the organization of the cytoskeleton, and other multiple Rho-dependent cellular processes. Tilly and co-workers (Tilly et al, 1996) found that the activation of the Ras-related GTPase p21rho was accompanied by a transient reorganization of the F-actin cytoskeleton. They proposed an involvement of the Rho pathway in the signalling cascade that leads to the rearrangement of the actin filaments finally resulting in VRAC activation.

Nevertheless, transfection of calf pulmonary artery endothelial cells with constitutively active isoforms of Gα (a Rho activating heterotrimeric G protein subunit), Rho, or Rho kinase alone failed to induce VRAC activation (Carton et al, 2002). Also, GTPγS alone has no effect when applied in Xenopus oocytes in isotonic conditions (Ackerman et al, 1994).

Overall, the actual knowledge concerning the role of GTPγS signalling in VRAC modulation are not comprehensive to conclude a crucial involvement in channel activation under hypo-osmotic conditions, but rather weighs in favour of a permissive or cell-subtype-specific effect.

Following studies provided insight that several G-protein-coupled receptors, like P2Y receptors leads to a limited isovolumic activation of VRAC in astrocytes (Akita et al, 2011; Darby et al, 2003; Fisher et al, 2008; Fisher et al, 2010; Franco et al, 2008; Mongin & Kimelberg, 2005; Takano et al, 2005).

1.4 LRRC8 paralogues and orthologues

LRRC8 is a protein family comprising five paralogues, each of them being about 800 amino acids long. The first half (~400 amino acids) is organized in four transmembrane domains, while the last ~400 amino acids, which constitute the C-terminus of the protein are characterized by 17 cytosolic leucine rich repeats (LRRs) (Abascal & Zardoya, 2012; Kubota et al, 2004; Smits & Kajava, 2004). Even before 2014, some pre-existing literature about these proteins was present, although limited, and their biology remained poorly understood. In their pioneering work, Abascal & Zardoya performed a bioinformatic study that evidenced a close evolutionary relationship of LRRC8 proteins and pannexins, a class of channels forming plasma membrane proteins structurally related to the gap junction forming connexins (Abascal & Zardoya, 2012).

The N-terminal transmembrane domain of these protein families shares well-conserved sequences and structural motifs, and possesses a very similar topology, which consists of four TM segments that are likely to associate into heteromeric channels (Abascal & Zardoya, 2012). Connexins, despite been related to pannexins and LRRC8 proteins, do not share significant sequence similarity. These proteins assemble into hexameric channel pores and dock with identical structures in an adjacent cell, giving rise to highly specialized structures called gap junctions. Similarly, non-chordates use the related innexin protein family to form octameric structures that assemble into hexadecameric intercellular channels that serve a similar purpose (Abascal & Zardoya, 2012).

In contrast, pannexins rather act as single membrane channels that connect the cytosol and the extracellular space. These proteins are thought to allow the direct passage of ions and small molecules and have been associated to paracrine signalling and ATP release under a variety of physiological and pathological conditions.

LRRC8s originated from the evolutionary combination of a pannexin and an LRR-containing protein and share a common ancestor at the origin of chordates (Abascal & Zardoya, 2012) (Figure 4).

LRRC8 and pannexin paralogues diverged under different evolutionary constraints and this explains the fact that sequence similarity between LRRC8 paralogues is higher than with pannexin. Moreover, two recent studies revealed that Pannexin1 assembles as a heptameric channel (Michalski et al, 2020; Ruan et al, 2020), an important difference with LRRC8s forming hexamers, whose detailed structure and assembly will be discussed in the next paragraph.

Leucine Rich Repeat motifs (LRRs) are present in a large number of proteins from viruses to eukaryotes (Enkhbayar et al, 2004) and cover a variety of functions including immune response, apoptosis, autophagy, nuclear mRNA transport and

neuronal development. The eponymous LRRs refer to motifs characterized by the presence of a consensus sequence LxxLxLxx(N/C)xL with x = any amino acid; and L = leucine, valine, isoleucine or phenylalanine (Kobe & Kajava, 2001) comprising 20 to 30 amino acids, that arrange in a peculiar horseshoe shape constituted by the alternation of parallel beta-sheet and alpha helices.

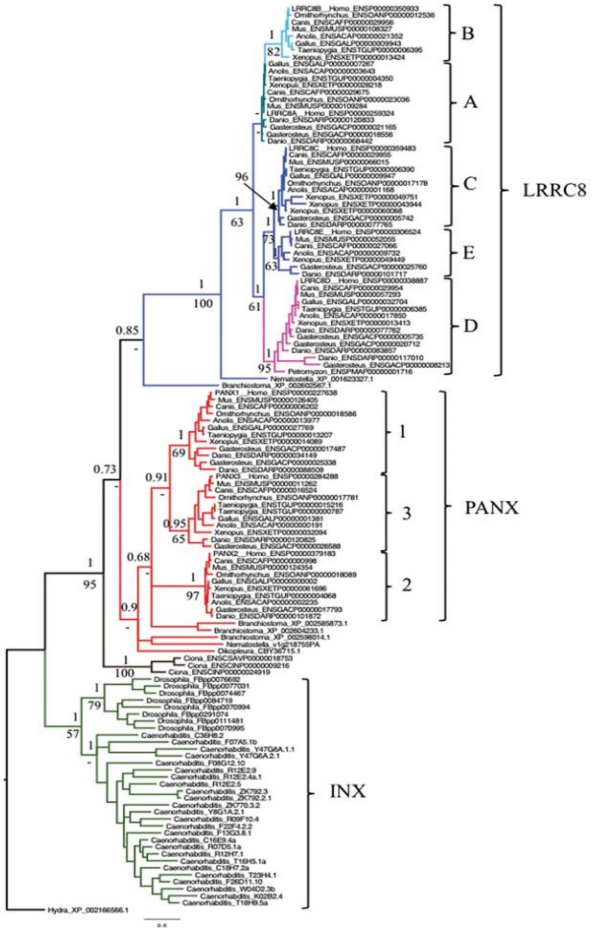

Figure 5. ML phylogeny of LRRC8 proteins, non-chordate (i.e. innexins) and chordate pannexins. A cnidarian (Hydra) innexin was used as the outgroup. Modified from (Abascal & Zardoya, 2012).

Most LRRD-containing receptors, including Toll-like receptors and several hormone receptors have extracellular LRRDs (Dolan et al, 2007; Gay et al, 2014), whose topology is usually supposed to mediate protein-protein recognition and binding (Kobe & Kajava, 2001).

In contrast to their previously proposed role as receptors, LRRC8 topology with the C-terminal LRRs oriented toward the cytosolic side, suggested a potential role of LRRC8s as membrane proteins involved in the organisation and regulation of intracellular signalling cascades and in direct or indirect cell-cell communication. Only the discovery that LRRC8 paralogues underlie VRAC currents finally revealed their role in cell volume regulation.

Given that the extended C-terminal cytosolic LRRD is a unique structural feature that distinguishes them from connexins and pannexins, and that channels formed by LRRC8 subunits are volume sensitive, while connexins and pannexins are not, it is likely that the LRRDs are involved in VRAC activation. Direct evidence that LRRD separation or reorientation accompanies channel activation was provided by FRET measurements. Moreover, the finding that attachment of fluorescent proteins to the C-terminus of LRRC8 subunits results in channels that display a constitutive activity in the absence of hypotonic stimulation (Gaitán-Peñas et al, 2016; Gaitán-Peñas et al, 2018) strongly corroborates this hypothesis.

1.5 Cryo-EM structure and topology of LRRC8A-hexamer

Recently, four studies revealed the general architecture of VRAC by determining the structure of homomeric mouse and human LRRC8A complexes (Deneka et al, 2018; Kasuya et al, 2018; Kefauver et al, 2018; Kern et al, 2019) (Figure 5).

Even if the physiological relevance of LRRC8A homomers is uncertain, the high sequence similarity among the different subunits suggests that the general architecture is well conserved, thus providing a powerful tool to derive structural functional insight(s). Moreover, the first published work of Deneka and colleagues additionally solved the structure of LRRC8A/C heteromers at 8 Å resolution (Deneka et al, 2018).

Four different high-resolution cryo-EM structures fully confirmed the predictions of Abascal & Zardoya (Abascal & Zardoya, 2012), and the experimental evidence of Voss et al (Voss et al, 2014) with LRRC8 proteins assembling into hexameric complexes and displaying a topology in which both N- and C-termini are localized in the cytosol.

The transmembrane domains of each subunit contribute to the formation of a relatively loosely packed, membrane imbedded, ion pore. Each subunit is composed of several distinct domains. The transmembrane domain (TMD) is formed by four helices (TM1-TM4) with TM1 and TM2 contributing to pore lining mostly characterized by hydrophobic residues. The maximum channel pore is formed by TMH1 and TMH2 in the lower part of the transmembrane region and reach approximately ∼35 Å. Two threonine residues, T44 and T48 line the pore.

The extracellular domain (ED) consists of several beta strands stabilized by intra-subunit disulphide bonds and is formed by a ring of arginines, R103, of the first extracellular loop (EL1H) which narrows the pore to a minimum diameter of ∼6–8 Å. Kern and co-workers solved the structure of LRRC8A together with the inhibitor DCPIB, finding that R103 is involved in the blockage mechanism (Kern et al, 2019).

The residue D100 is the most “extracellularly” exposed residue within the solved part of the homomeric LRRC8A structure and a major determinant of inactivation. Indeed, a point mutation of D100 in LRRC8A and equivalent residues in LRRC8C and -E were found to strongly alter the kinetics and voltage dependence of inactivation (Ullrich et al, 2016).

The N terminus is 23 amino acids long and appears to be largely unstructured (Deneka et al, 2018; Kasuya et al, 2018; Kefauver et al, 2018; Kern et al, 2019) except for a short N-terminal coil that possibly projects into the channel pore, as in connexins and innexins (Kefauver et al, 2018). It needs to be highlighted that mutations in the amino termini of contributing LRRC8A/C heteromers turned out to drastically affect channel function, including anion selectivity, rectification, and inactivation (Zhou et al, 2018).

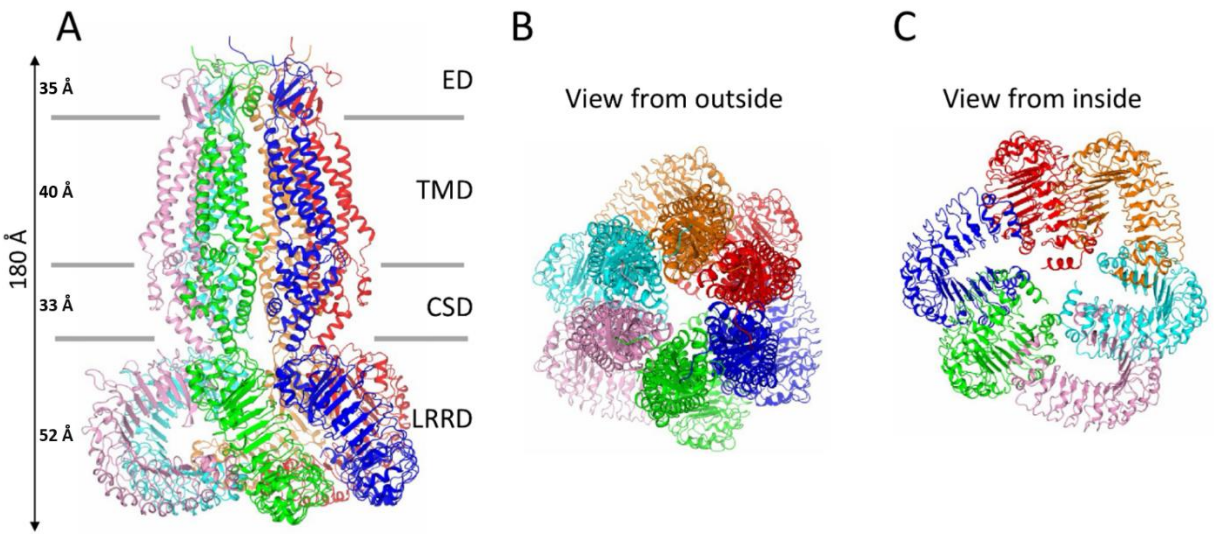

Figure 6. Structure of homomeric LRRC8A.
The different views were prepared with Pymol based on the mLRRC8A homomeric channel structure (pdb 6g9l) (Deneka et al, 2018). Each subunit is shown in a different color (ED, extracellular domain; TMD transmembrane domain; CSD, cytoplasmic subdomain; LRRD, leucine rich repeat domain).In A) the relative size of each domain is indicated.

Notably, the cytosolic side of the channel is not only formed by the leucine rich repeat domain (LRRD) as it was predicted, but by additional intracellular loops connecting TM2 and TM3 (IL1) and TM4 to the C-terminus (IL2) form a consistent part of the cytosolic subdomain (CSD) with a relatively long stretch that has not been resolved in the cryoEM structures. The downstream leucine rich repeats (LRR) domain comprises an N terminus (LRR NT) containing an α-helix and, as predicted from its sequence, consists of up to 17 structural repeats, each containing a β-strand followed by an α-helix and a C terminus (LRR CT) containing three α-helices. The parallel stacking in tandem LRRs leads to a solenoid structure divided in four parts that consist of a concave surface, ascending loops, a convex surface, and descending loops (Matsushima et al, 2019).

Overall, the structures described in the 4 studies are similar with only minor differences. A major feature that diverges among the four solved structures concerns the symmetry of the channel. In the works of Deneka et al., Kefauver et al. and Kasuya et al. (Deneka et al, 2018; Kasuya et al, 2018; Kefauver et al, 2018) the transmembrane structure together with the ED exhibits a six-fold symmetry while the CSD exhibits a complex structure with the six-fold symmetry that is broken at the level of the LRR domains and assemble as trimer of dimers giving rise to a C3 symmetry. In the more recent work of Kern et al. (Kern et al, 2019), the authors observed an overall C6 symmetry in the extracellular domain, TM, and intracellular loop regions and an asymmetric and heterogeneous arrangement of the LRR regions. Also, the TMD is more loosely packed, with several lipid molecules intercalating into the membrane pore wall.

Classification of the cryo-EM images of Kern et al. predicted two different structures, a "constricted" structure and a "relaxed" structure, in which the intracellular opening of the pore is dilated by ~4 Å. These two structural states may reflect channel gating conformations (Kern et al, 2019).

Notably, the structures described by Kern et al. (Kern et al, 2019) were obtained from LRRC8A reconstituted in lipid nanodiscs, which may more closely approximate the cell membrane in contrast to earlier studies where LRRC8As were reconstituted in detergent (Deneka et al, 2018; Kasuya et al, 2018; Kefauver et al, 2018).

Kern et al. (Kern et al, 2019) proposed that the arrangement of LRRC8A subunits is modified by the hydrophobic environment in which the protein is embedded. The trimer-of-dimer modelled from digitonin-solubilized VRACs would expand the possibilities for differential interaction within heteromers because the position of a subunit within the complex influences its biophysics.

Even among these structures, all of which were modelled from digitonin-solubilized VRACs, a subset of particles showed a heterogeneous arrangement of the LRRD. Together, this suggests high flexibility and various orientations of the LRRDs within a VRAC.

Which of the two classes of structures is more relevant to native heteromeric LRRC8 structures remains to be determined (Bertelli et al, 2021).

1.6 Emergent physiological and pathological roles of VRAC channels

A large body of literature indicates that in addition to its role in volume regulation VRAC is involved in several physiological and pathophysiological mechanisms. Since its first discoveries, VRAC was mentioned as an important determinant in all relevant mechanism used by cells for self-maintenance as e.g., proliferation, migration and differentiation.

Various works revealed that inhibition of VRAC by means of different blockers of $I_{Cl,vol}$ inhibited cell proliferation (Burg, 2002; Dubois & Rouzaire-Dubois, 2004; Lang et al, 2000; Rouzaire-Dubois et al, 2005) and affected angiogenesis in different model systems (Manolopoulos et al, 2000; Nilius & Droogmans, 2001; Ziegelhoeffer et al, 2003). Indeed, cell proliferation was found to be stimulated by swelling and

inhibited by shrinkage and progression through cell cycle phases correlated with concerted arrangements of cell volume changes in different cell types (Chen et al, 2007; Habela & Sontheimer, 2007; Klausen et al, 2007; Michea et al, 2000; Pappas & Ritchie, 1998; Pendergrass et al, 1991; Rouzaire-Dubois et al, 2000; Shen et al, 2000; Voets et al, 1995; Wondergem et al, 2001). Interestingly, switching from proliferation to differentiation led to downregulation of VRAC currents in myoblasts (Manolopoulos et al, 1997; Voets et al, 1997b), revealing a critical role of the channel in determining the progression through different stages of cell development.

Cell motility has been shown to at least partially rely on localized cell volume changes (Schwab et al, 2012). Since cell migration is important for tumor metastasis, specific interference with this process may be beneficial for the containment of malignant carcinoma.

VRAC like currents can be induced without cell swelling by the direct application of pro-apoptotic compounds (as discussed before). These currents probably play a major part in apoptotic volume decrease (AVD), which is a hallmark of programmed cell death and is thought to be one of the earliest triggers for the induction of the apoptotic cascade through yet undefined mechanisms. Planells-Cases et al. revisited the role of VRAC in drug resistance, apoptosis, and organic osmolyte transport and provided evidence that the channel conducts the anticancer drugs cisplatin as well as the cellular osmolyte taurine in a largely LRRC8D dependent manner (Planells-Cases et al, 2015). This finding, besides demonstrating that the RVD mechanism is not carried solely by the extrusion of KCl, but also of uncharged organic osmolytes, is of great relevance as it disclosed LRRC8D as an attainable marker to predict drug responsiveness of tumours and to improve chemotherapy success rates.

In the brain, VRAC is thought to be a major pathway for the release of excitatory amino acids, like e.g., aspartate and glutamate. This has an impact both on physiological brain function (such as astrocyte-neuron signalling) and neuropathology. Indeed, upon ischaemia, astrocytes and neurons swelling can undergo to an excess of glutamate release through VRAC and the consequent massive activation of glutamate receptors, thus resulting in an influx of Na^+ and Ca^{2+} that causes widespread excitotoxic neuronal death (Mongin, 2016).

After the molecular identification of the VRAC mediating genes, various conditional knockout mice have been developed. This allowed to obtain deeper insight into VRAC function in different tissues. In pancreatic beta cells, VRAC was shown to be involved in glucose sensing, where it mediates membrane depolarization and thereby increase in Ca^{2+} influx which finally leads to insulin secretion (Kang et al, 2018; Stuhlmann et al, 2018). The channel turned out to be of great relevance also in spermatogenesis, where the disruption of Lrrc8a in the germ-cell line led to abnormal sperm and male infertility in mice (Bao et al, 2018; Lück et al, 2018). An early study suggested a role of LRRC8C in adipocyte differentiation and the gene was thereafter named (initially) fad158 (for factor for adipocyte differentiation) (Tominaga et al, 2004).

More recently discovered roles include myogenesis (Chen et al, 2019; Kumar et al, 2020), reduction of intracellular chloride concentration (Chen et al, 2020), release and uptake of cyclic di-nucleotides, which are important in the STING defense pathway (Lahey et al, 2020; Zhou et al, 2020), and the permeability to glutathione proposed to modulate epithelial-to-mesenchymal transition (Friard et al, 2019).

Several functional roles of LRRC8 proteins appear to be related to the ability of VRAC to decrease cell volume by allowing chloride and osmolyte efflux. For example, in spermiogenesis, cells have to reduce their volume and LRRC8A defects lead to swollen plasma and deformations of late spermatids (Lück et al, 2018). In contrast, other functions appear to be unrelated to changes in cell volume but closely linked to the ability of VRACs to allow the permeation of specific large anionic molecules, like cyclic di-nucleotides [44, 45] or excitatory amino acids (Lahey et al, 2020; Zhou et al, 2020).

Certainly, to be able to comprehend VRAC relevance in all the above cited physiological and non-physiological mechanisms, thus, to exploit such knowledge as a powerful tool to modulate channel activity under specific conditions, we cannot prescind from elucidating the molecular basis underlying its activation mechanism.

2. AIMS

The specific aim of my project was to get deeper into the relevant mechanisms underlying VRAC activation. On this purpose I followed 2 parallel strategies:

I. Elucidation of mechanisms of oxidation dependent activation with the final goal to disclose structural motifs involved.

II. Investigation of the role of phosphorylation in VRAC gating upon cell swelling.

3. MATERIALS AND METHODS

3.1 Bacterial transformation and plasmid purification

Plasmids were transformed in chemically competent cells (DH5α, SDM) using a maximal amount of 100 ng. Bacteria aliquots were thawed on ice before usage for 20 minutes. After addition of plasmids, DNA-bacteria mixtures were incubated for 30 minutes on ice. Heat shock was performed by incubation of bacteria at 42 °C for 45 seconds, and a following incubation for two minutes on ice. Then 350 µl of pre-warmed SOC medium was added, and cells incubated for one hour at 37 °C before plating on either ampicillin or kanamycin containing LB-agar plates (o/n). Colonies were picked and incubated o/n in 50 ml LB medium before DNA purification (NucleoSpin Plasmid QuickPure, Macherey-Nagel). To check for the correct insert sequence, plasmids were Sanger-sequenced (Microsynth Seqlab GmbH).

For PCR mutagenesis, Phusion (Thermo Fisher Scientific- Massachusetts) or Q5 mutagenesis kit (New England Biolabs-Roboklon) DNA polymerase were used. Oligonucleotides were ordered from Eurofins genomics (Luxembourg) or TransGen Biotech (Beijing, China). Isolation of plasmid DNA from *E. coli* cultures or agarose gel fragments was performed using the Nucleo Spin® Plasmid QuickPure or the Nucleo Spin® Gel and PCR Clean-up kit (Macherey & Nagel), respectively. Agarose gels were prepared using UltraPure agarose (Invitrogen) in TAE buffer (40 mM Tris, 40 mM acetic acid, 1 mM EDTA, pH 8.0) and samples were mixed with 6x DNA loading buffer (60 mM Tris-HCl (pH 8.0), 60% glycerol, 60 mM EDTA, 0.4% Orange G) before submitting them to agarose gel electrophoresis.

3.2 Molecular cloning

For heterologous expression in Xenopus oocytes, we used the constructs in which the human LRRC8A–E cDNA, C-terminally fused with VFP for 8A and with mCherry for 8E and 8C cloned into the pCSDest vector (Gaitán-Peñas et al, 2016). For heterologous expression in HEK-5X-KO cells we used LRRC8A and LRRC8E cDNAs cloned in the background of pcDNA3.1 plasmids (Gaitán-Peñas et al, 2016) and/or PEGFP-N1-Cerulean/Venus plasmids (König et al, 2019). To generate chimeric constructs or insert modified sequences in the background of all the constructs used in this thesis (see Table 1) different approaches were adopted. The chimeras and sub-chimeras of LRRC8E/C-mCh were all generated by standard cloning strategies, consisting of 3 PCRs, where each region of interest was amplified using the respective template of LRRC8E/C mCh pCSDest constructs, by means of specifically designed primers.

Two flanking primers (F-ext and R-ext) are designed to mark the 5’ ends of both strands complementary to the target plasmids and to be external but in proximity (~50bp) to restriction enzymes sites, so that the final PCR product can be cloned into the desired expression vector. Two chimeric internal primers (F-chim and R-chim) are designed, all consisting of an 18-nucleotide annealing segment and a 15-nucleotide anchor

segment corresponding to the adjacent regions of the final template. The first step involves two independent PCRs to generate two PCR products, called PCR I and PCR II, respectively. The chimeric internal primers generate overlapping complementary 3' ends on the intermediate segments, PCRi and PCRii, and introduce sequences of the adjacent regions of the final desired template. PCRi and PCRii are used as template for a third recombinant PCR, where overlapping strands of PCRi and PCRii hybridize and are extended using the external primers to generate the full-length product (PCR III). Both the PCRiii product and the expression vector are then digested with the selected restriction enzymes to proceed with the cloning. Vector ligations were all performed using a T4 Ligase (Fermentas).

The 2A-peptides are short (~18-25 aa) peptides derived from viruses, used as linkers to co-express multiple ORFs under the control of a single promoter allowing to express multiple proteins from a single mRNA transcript (Tang et al, 2009). 2A-peptides function by inducing the ribosome to skip the synthesis of the glycine and proline peptide bond at the C-terminal end of the 2A element, causing separation between the end of the 2A sequence and the downstream peptide. As a result, the upstream protein will have a few extra 2A residues added to its C terminus while the downstream protein will have an extra proline added to its N terminus.

To investigate the role of oxidation in VRAC modulation we screened all cysteine and methionine residues in the background of 8E and 8C. To substitute the first methionine residue (M1) in the background of 8C we had to find a strategy to bypass the problem of protein synthesis initiation, given that the first methionine is mandatory for ribosome assembling and protein synthesis to start. We thus exploited the T2A linker technology to generate a bicistronic construct called LRRC8A-VFP-T2A-LRRC8C(M1L)-mCh where the sequence of 8C (where M1 was substituted by L) was inserted at the 5' of 8A ORF following the T2A linker (and 8A ORFs) thus to obtain two protein from a single mRNA transcript. To obtain LRRC8A-VFP-T2A-LRRC8C(M1L)-mCh bicistronic constructs we used three vectors as templates: 8A-VFP, 8C-mCh and a 8A-T2A-8E construct kindly provided by Héctor Gaitán-Peñas and Raùl Estévez (Barcelona). Exploiting a 4 PCR cloning strategy we succeeded in generating LRRC8A-VFP-T2A-LRRC8C(M1L)-mCh and LRRC8A-VFP-T2A-LRRC8C-mCh. The cloning strategy is described in detail in Figure 6. The construct has not been tested so far.

The $IL1_{\Delta p}$ sequences of the 8A(IL), and 8E(IL) were synthetized by the TWIST company and then cloned in the respective background of LRRC8A-pcDNA3.1 and LRRC8E-pcDNA3.1 (see Table 1) using a cloning strategy with AfeI, SexAI, and HindIII restriction enzymes.

LRRC8A-CFP pEGFP-N1 and LRRC8E-VFP pEGFP-N1 plasmids were kindly provided by Tobias Stauber (Berlin). All mutations mentioned in this thesis (both single point mutations and IL1-Δp inserts) were inserted into their background by cloning.

To avoid confusion, I summarize above all names of inserts, domains, or stretch of sequences corresponding to specific subdomains of LRRC8 subunits which are frequently recalled in the thesis, and are highlighted in Figure 7:

IL1: refers to the full length of the first intracellular loop between TM2 and TM3 highlighted in purple.

Yamada-Strange stretch (YSS): this is the stretch of 25 aminoacids of LRRC8A IL1 identified by Yamada and Strange (Yamada & Strange, 2018).

8A-IL1$_{\Delta p}$: refers to the stretch of aminoacids within positions (144-265) of the 8A IL1 where 16 threonine and serine residues with high score to undergo phosphorylation were mutated to alanine (see Table 2).

8E-IL1$_{\Delta p}$: refers to the stretch of aminoacids within position (137-256) of the 8E IL1 where the corresponding 9 threonine and serine residues of 8E were mutated to alanine (see Table 3).

For ease of viewing, Figure 7 shows only the 8A subunit, given the overall similarity of IL1 of 8A and 8E.

Table 1. In the table are listed all chimeric constructs designed and used in this thesis.

Construct name	**Plasmid**	**Heterlogous expression system**
8A-IL(Δp)	pcDNA3.1	HEK-5X-KO
8A-IL (Δp-wt)	pcDNA3.1	HEK-5X-KO
8A-IL (wt-Δp)	pcDNA3.1	HEK-5X-KO
8A-IL (4A)	pcDNA3.1	HEK-5X-KO
8A-IL (3E)	pcDNA3.1	HEK-5X-KO
8A- IL (Δp)-Cerulean	pEGFP-N1	HEK-5X-KO, HELA
8A-IL (Δp-wt)-Cerulean	pEGFP-N1	HEK-5X-KO, HELA
8A-IL (wt-Δp)-Cerulean	pEGFP-N1	HEK-5X-KO, HELA
8E-LRRD(8C)	pCSDEST	Oocytes
8C-LRRD(8E)	pCSDEST	Oocytes
8E- LRRD(CE)	pCSDEST	Oocytes
8E- LRRD(EC)	pCSDEST	Oocytes
8E-LRRD(ECEE)	pCSDEST	Oocytes
8E-LRRD(CEEE)	pCSDEST	Oocytes
8A-VFP-T2A-8C-mCh	pCSDEST	Oocytes
8A-VFP-T2A-8C-M1L-mCh	pCSDEST	Oocytes

Table 2. The table lists the residues within the LRRC8A IL1 mutated to alanine to generate 8A-IL1$_{(\Delta p)}$, 8A-IL1$_{(\Delta p/wt)}$ and 8A-IL1$_{(wt/\Delta p)}$ constructs.

8A Residue	IL1$_{(\Delta p)}$	IL1$_{(\Delta p/wt)}$	IL1$_{(wt/\Delta p)}$
S150	A	A	S
S151	A	A	S
S158	A	A	S
T169	A	A	T
S174	A	A	S
T176	A	A	T
S181	A	A	S
S188	A	A	S
S193	A	S	A
S198	A	S	A
S199	A	S	A
T200	A	T	A
S202	A	S	A
S217	A	S	A
T229	A	T	A
T252	A	T	A

Table 3. The table lists the residues within the LRRC8A IL1 mutated to alanine to generate 8E-IL1$_{(\Delta p)}$

8E Residue	IL1$_{(\Delta p)}$
T142	A
S153	A
S144	A
S159	A
T162	A
S167	A
S170	A
T180	A

3.3 Cell culture

The cell line HEK-5X-KO *lrrc8*-/- (for short: HEK-5X-KO) used for patch clamp recordings were knock-out for all five genes encoding lrrc8 subunits and were kindly provided by Thomas Jentsch (Berlin). HEK-5X-KO were cultured in Dulbecco's Modified Eagle Medium (DMEM, Pan Biotech) supplemented with 10% FBS, 1% penicillin/streptomycin and 1% glutamine and maintained at 37 °C in a 5% CO_2, 100% humidity atmosphere. Same conditions were adopted for Hela cells used for FRET experiments. Cells were grown on plastic tissue culture dishes and divided every 3–4 days.

Transfection was performed by means of the Effectene Kit from Qiagen according to manufacturer's protocol. The amount of cDNA used for transfection differed depending on the experiments and was always accompanied by co-transfection of a fixed amount of a vector expressing CD8 (50 ng) used as reporter (Jurman et al, 1994).

The ratio between the co-transfected of LRRC8 subunits ranged from 1:1 to 1:5 (8a:8e or 8c). One day after transfection, cells were plated at low density on plastic Petri dishes or onto glass coverslips (ø15 mm) coated with poly-L-lysine (for YFP assays or when LRRC8 isoforms C-terminally fused to CFP/YFP were used) and patch clamp recordings were performed in the following 24-48 hours.

3.4 Electrophysiology

$I_{Cl,vol}$ currents were recorded using the patch clamp technique in the whole-cell configuration using an Axopatch 200B amplifier and the GePulse acquisition program (http://users.ge.ibf.cnr.it/pusch/programs-mik.htm). Transfected cells were visualized by addition to the extracellular media of beads binding to cells expressing CD8 or by their fluorescence (in case of fluorescently C-terminal tagged LRRC8 subunits). Recordings were performed at room temperature (22–25 °C).

Patch pipettes were made of borosilicate glass and pulled with a List-Medical vertical puller. Series resistance, RS, was between 2 and 4 MOhm, and the cell capacitance was between 10 and 40 pF. Currents were sampled at 50 kHz and low-pass filtered at 10 kHz. The holding potential was −25 mV.

The standard current-voltage protocol (IV) for stimulation consisted of 500 ms-long voltage steps ranging from -80 to 120 mV in 20 mV increments.

The response of $I_{Cl,vol}$ to the various stimuli were monitored using the "time course protocol", which consisted of successive steps of 50 ms pulses to −75, −25, 0, 25 and 75 mV every 5 s. These steps allowed to verify the absence of a significant leak conductance because the expected reversal potential is −25 mV and VRAC currents are slightly outwardly rectifying under the ionic conditions used.

Data were analysed with the program Ana (available at http://users.ge.ibf.cnr.it/pusch/programs-mik.htm) and Sigma Plot Systat Software, Inc. (SPSS) 2107, San Jose, CA, USA.

Solutions with different ionic composition and osmolarity were used for experiments:

The standard extracellular isotonic solution contained in mM: 145 NaCl, 6 KCl, 1.5 $CaCl_2$, 1 $MgCl_2$, 10 HEPES, 10 glucose (pH 7.4, 310 mOsm). For activation of VRAC current by extracellular hypotonicity, cells were perfused with a solution containing in mM: 105 NaCl, 6 CsCl, 1.5 $CaCl_2$, 1 $MgCl_2$, 10 HEPES, 10 glucose (pH7.4, 230 mOsm). Experiments to monitor VRAC activation under oxidative conditions were performed by addition of fresh Chloramine-T (500 µM or 1 mM) to the respective extracellular solutions.

Intracellular solutions varied depending on experiments performed.

The standard pipette solution to monitor VRAC activation upon hypotonic perfusion contained (in mM) 100 K-Gluconate, 40 CsCl, 2 $MgCl_2$, 1.9 $CaCl_2$, 5 EGTA-NMDG,1 Na_2ATP, and 10 HEPES-NMDG, pH 7.3 with CsOH (290 mOsm). The free Ca^{2+} concentration in this solution was calculated to be approximately ~80 nM.

To test activation of the channel by low intracellular ionic strength the following solution was used (in mM): 75 NMDG-Cl, 150 Mannitol, 1 EGTA, 3 Na_2ATP, 10 Hepes-NMDG, pH 7.3 with NMDG-OH, 300 mOsm, while cells were kept in isotonic bath.

Zinc experiments were performed using a pipette solution containing: 100 K-Gluconate, 40 CsCl, 2 $MgCl_2$, 1.9 $CaCl_2$, 10 Citrate,1 Na_2ATP, 10 HEPES-NMDG,and 1 $ZnCl_2$, pH 7.3 with CsOH (290 mOsm). The program WinMAXC (C. Patton, Stanford University, Palo Alto, CA USA) was used to calculate free Zn^{2+} concentrations in buffered solutions.

3.4 Preparation of oocytes and voltage clamp experiments

Xenopus oocytes are commonly used for heterologous expression of membrane proteins involved in ion and solute transport (Stühmer, 1998). Oocytes were surgically extracted from Xenopus Laevis frogs under anaesthesia and the follicular layer was removed by 1 hour incubation under shaking with collagenase type I A (Sigma-Aldrich). For expression in Xenopus oocytes, the plasmids were linearized by NotI and then transcribed using the mMessage mMachine SP6 kit (Thermo Fischer, Waltham, USA) to obtain the cRNA of human LRRC8 proteins as described (Gaitán-Peñas et al, 2016). Depending on the aim of the experiments we used either untagged constructs as well as constructs in which Venus fluorescent protein (VFP) or mCherry (mCh) were fused to the C-terminus of LRRC8A/C/E (Gaitán-Peñas et al, 2016). Fifty nanolitres of solution containing different concentrations of cRNAs were injected, depending on the expression level required for the experiments. Oocytes were then incubated at 18°C in a solution containing (in mM): 90 NaCl, 2 KCl, 1 $MgCl_2$, 1 $CaCl_2$, 10 HEPES (pH 7.5).

Injection pipettes were pulled using a standard pipette puller. The tips of the pipettes were broken under a microscope until they had an opening diameter of about 20 µm, with a sharp protrusion.

All voltage clamp experiments were performed at room temperature (22-25°C).

One to three days after injection, voltage clamp measurements were performed using the custom acquisition program GePulse (available at http://users.ge.ibf.cnr.it/pusch/programs-mik.htm) and a Turbo-

Tec-05X amplifier (npi electronics, Tamm, Germany). The standard extracellular solution contained (in mM): 100 NaCl, 2 KCl, 1.8 $CaCl_2$, 1 $MgCl_2$ and 10 HEPES (pH 7.3, osmolarity: 215 mOsm). Hypotonic solution contained (in mM): 48 NaCl, 2 KCl, 1.8 $CaCl_2$, 1 $MgCl_2$ and 10 HEPES (pH 7.3, osmolarity: 120 mOsm). Oxidizing reagents were freshly added at the desired concentration of 0.1–2 mM (chloramine-T), 0.25–1 mM (*tert*-butyl hydroperoxide (TBHP)).

Holding potential was kept at −30 mV. The voltage and time dependence of currents were assayed with an IV protocol consisting of in the application of voltage steps ranging from −100 to 60 mV with 20 mV increments for 3000 ms. To determine the effects of oxidizing gents, a 200 ms pulse to 60 mV was applied every 5 s and currents were averaged over the pulse period and plotted as a function of time. In all figures, capacitive transients are blanked for clarity. For currents larger than 10 μA, series resistance was measured and compensated as follows. For the voltage clamp protocols, the effective command voltage, *V*eff, was adjusted offline according to the calculated series resistance error by *V*eff = *V*command – $I \times R$s, where *I* is the measured current. The current response at 60 mV was then corrected assuming a linear current–voltage relationship and the measured reversal potential. All chemicals were purchased from Sigma-Aldrich.

3.5 FRET measurements

Acceptor photobleaching and seFRET experiments were performed on a high-speed setup from Leica microsystems (Dmi6000B stage, 63x/1.4 oil objective, high-speed external Leica filter wheels with Leica FRET set filters (11522073), EL6000 light source, DFC360 FX camera, controlled by Las AF). All experiments were performed at room temperature.

seFRET

HELA cells were washed three times with isotonic solution before starting measurements. The sensitized emission of FRET constructs (seFRET) was determined by measuring in short succession the CFP channel (I^{DD}), the YFP channel (I^{AA}), and the FRET channel (I^{DA}). Acquisition parameters were maintained constant for all channels (100ms exposure, gain 1, illumination intensity 2) to correctly evaluate the correction factors. Spatial resolution was sacrificed for temporal resolution and sensitivity by 8x8 binning. Out of the three acquired channels, cFRET maps were calculated with the PixFRET plugin (Feige et al, 2005) according to the following equation (Jiang & Sorkin, 2002)

$$cFRET = (I^{DA}-I^{DD}*\beta-I^{AA}*\gamma)/I^{AA}$$

Where β is the correction factor for donor bleed through, and γ is the correction factor for acceptor cross excitation. Correction factors were determined with cells expressing either only donor (LRRC8A-CFP) or only acceptor (LRRC8A-VFP) constructs by the acquisition of I^{DD} and I^{DA} for donor only and I^{AA} and I^{DA} for acceptor only samples. Correction factors were obtained from the fraction of the intensity detected in I^{DA} to the absolute intensity detected in I^{DD} or I^{AA} ($\beta = I^{DA}/I^{DD}$ and $\gamma = I^{DA}/I^{AA}$). The final value of each correction

factor (β and γ) was finally determined by calculating the mean of the values measured on three different days of at least 10 samples per day and subsequently used to correct the cFRET of all performed experiments (β = 0.5645 and γ = 0.082).

For each field of view (FOV), cells showing membrane-localized signals in all three channels simultaneously were selected with hand-drawn ROIs. A background ROI was selected as well to subtract cFRET signals.

During the experiment, images and corresponding cFRET values were acquired every 10 seconds (1 cycle). The standard protocol was repeated for each measurement as follows: 15 cycles in isotonic bath, 15 cycles in hypotonic solution (or other stimuli according to the experiment), 15 cycles back to isotonic solution (to assess whether the FRET signal recovered back to the original value. Measured absolute cFRET values were normalized to the mean cFRET of the first timepoints while cells were kept in isotonic bath.

Images were processed in PixFRET using a Gaussian blur of 2 and threshold of 1. Since PixFRET does only process stacks of a single timepoint, a macro was programmed that ordered stacks according to the input demands of PixFRET and calculated automatically cFRET maps for all time points of an experiment (König, 2019; König et al, 2019).

3.6 YFP assay

The optical system used for fluorescence measurements is composed of a basic iMIC microscope with a QImaging Retiga EXI Blue camera and a dual-view port for the emission allowing the separation of the GFP and DsRed emissions (Till Photonics). For excitation we used Till Oligochrome, a wavelength-switching device containing a stable Xenon light-source.

The YFP(H148Q/I152L) quenching assay was performed 24-48 h after transfection. As a first step, the cell culture medium in each dish was exchanged with 200 µl of isotonic solution (in mM: 145 NaCl, 5 KCl, 1 $MgCl_2$, 2 $CaCl_2$, 10 glucose, 10 HEPES, pH 7.4, 320 mOsm) and fluorescence measurements were initiated.

YFP fluorescence was measured at 510 nm excitation wavelength and 540 nm emission wavelength (50 msec exposition).

After recording a baseline for ~ 60 s, the medium was exchanged by manual addition of iodide- containing isotonic solution (in mM: 150 NaI, 6 KCl; 1 $MgCl_2$, 1.8 $CaCl_2$, 10 glucose, 10 HEPES pH 7.4, 320 mOsm) and left for 2 minutes. Subsequently the iodide-containing isotonic was replaced by iodide-containing isotonic + 1 µM PMA till the end of the experiment (15 minutes overall).

All assay solutions were prepared freshly for each screening day and the osmolarity measured by a freezing point osmometer. The total duration of the measurements (500 s) was sufficient for YFP quenching to nearly reach steady state.

Fluorescence traces were then analysed by subtracting the signal from a background ROI of the same image and normalizing to the time point t=120 s (after the pipetting artifact).

Data analysis was performed with the custom analysis programs Anavision and Ana (freely available at http://users.ge.ibf.cnr.it/pusch/programs-mik.htm). A polygon was drawn on the border of the analysed cell and another on the background for background subtraction.

3.7 Construction of homology models

We used the "User template" mode of the Swiss Homology model server (https://swissmodel.expasy.org/interactive#structure) to create various homology models of heteromeric human LRRC8 channels of putative stoichiometry. All modelling was based on the pdb entry 6G9O (Deneka et al, 2018) of homomeric LRRC8A. In order to constrain the composition of a hexameric protein we artificially created a pdb file in which all 6 chains of the LRRC8A of the 6G9O entry were combined to a single chain, used as template. To create a model of a hexamer with 8A-8E-8A-8E-8A-8E composition we concatenated the sequences of 8A and 8E subunits accordingly in a single file using this as the target sequence for Swiss Model. The resulting homology model pdb file was then again split into different chains for the various subunits. In this way, we constructed model corresponding to the following subunits stoichiometry: A-E-A-E-A-E, E-A-E-A-E-A (note that these two are not equivalent due to the symmetry breaking at the level of the LRRC domains (Deneka et al, 2018)), A-C-A-C-A-C, C-A-C-A-C-A, A-D-A-D-A-D.

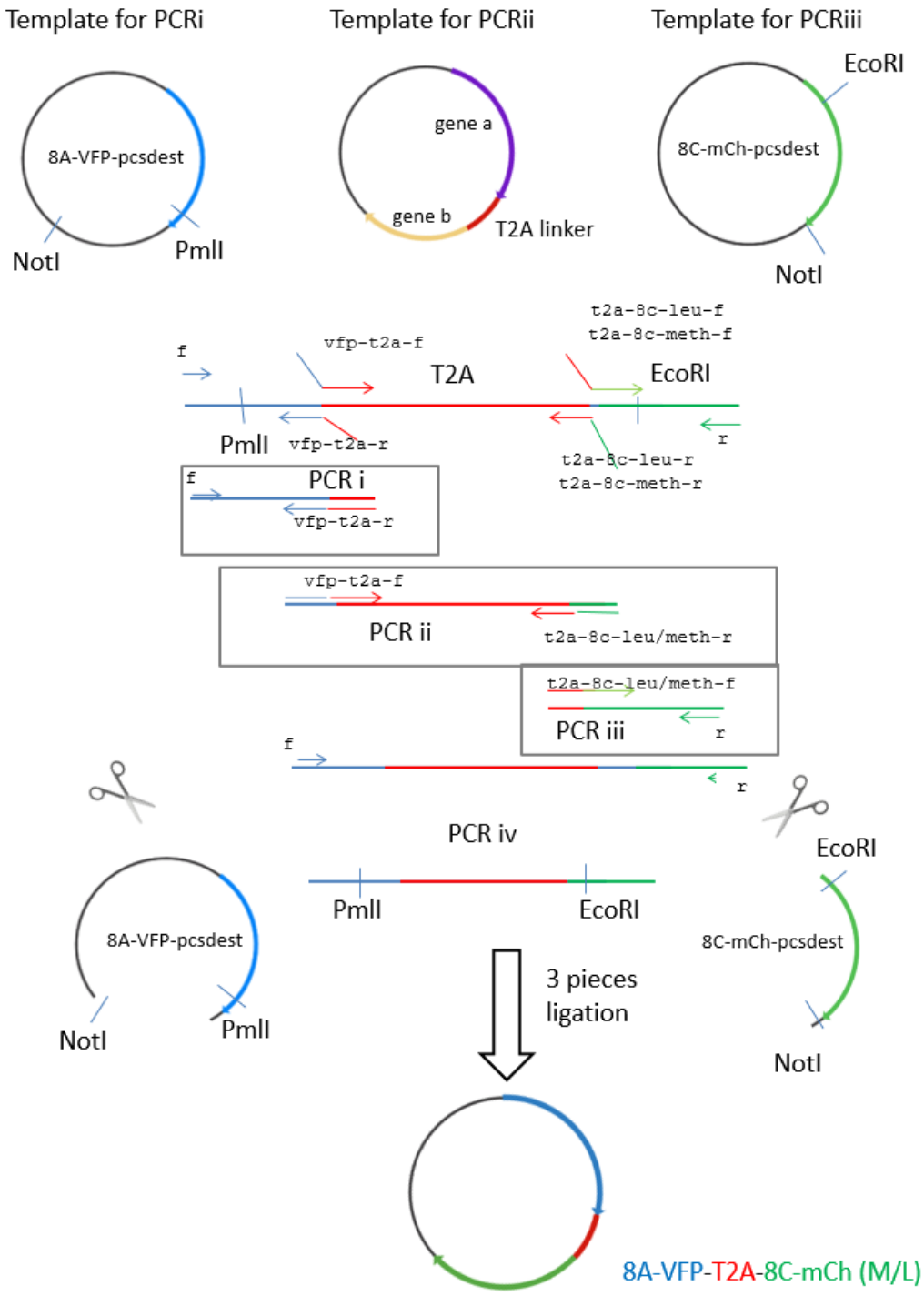

Figure 6. Generation of a bicistronic construct.
Scheme of the cloning strategy used to generate the bicistronic constructs 8A-VFP-T2A-8C-mCh and 8A-VFP-T2A-8C-mCh(M1L). To introduce a change at the first position of 8C (Met → Leu) different primers were designed. For details see the text.

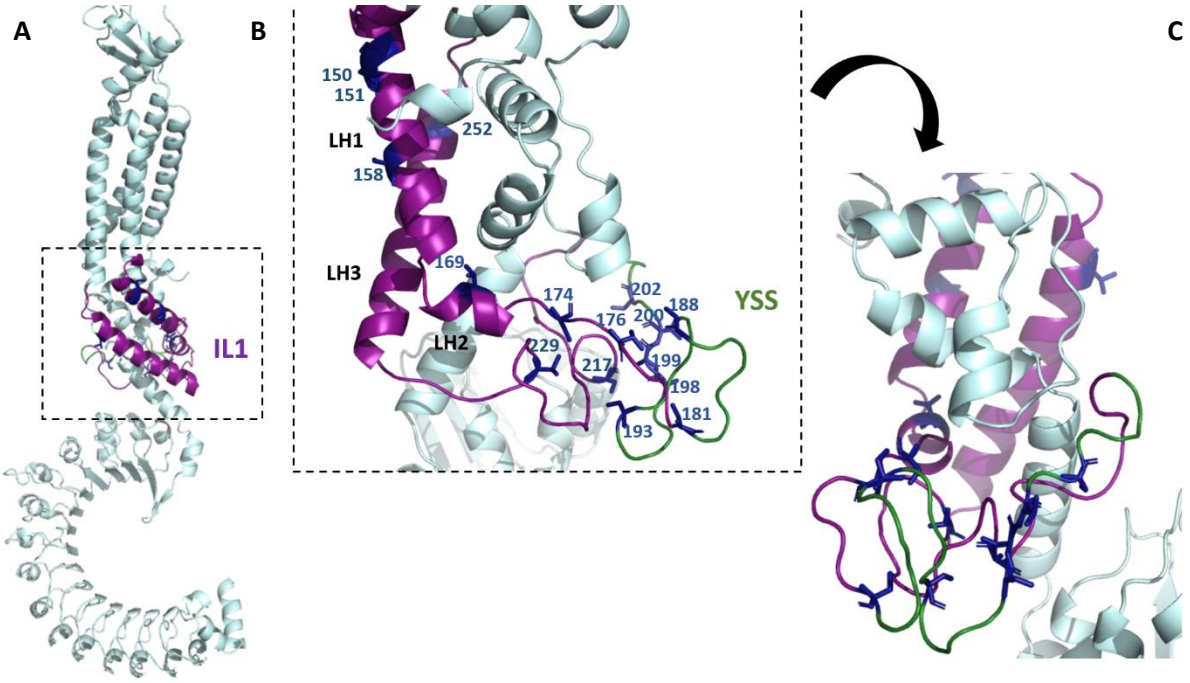

Figure 7. Overview of the intracellular loop IL1.
A) Full length structure of 8A subunit with the intracellular loop IL1 highlighted in purple. Residues 177-229 are actually not resolved in any of the cryoEM structures and were added artificially using Swiss Homology Modelling server. Their location is uncertain, and the region might actually be disordered (Strange et al, 2019). B) The insight evidences all motifs of IL1 that are relevant for the porpoise of the thesis. LH1, LH2, LH3, are respectively the first, second and third alpha helices of IL1. In blue, shown as sticks, are labelled all residues (Ser/Thr) mutated to Ala to generate the $IL1_{\Delta p}$ constructs. YSS, highlighted in green, is the stretch of 25 aminoacids identified in the work of (Yamada & Strange, 2018) that partially overlaps with some residues of $IL1_{\Delta p}$ (S188, S193, S198, S199, T200, S202). C) same as B, rotated as indicated.

RESULTS

Previous results obtained in oocytes suggested that the effects observed upon Chl-T application on 8A/8C and 8A/8E heteromers are mediated by the oxidation of intracellularly localized residues. We first intended to determine which domain might be the target of Chl-T among the various cytosolic regions of LRRC8 subunits. In addition to the LRRD, these include the N-terminus, the intracellular loop (IL1) between TM2-TM3, and the linker connecting the C-terminal end of TM4 with the first LRR.

To this end, we exploited Xenopus oocytes as heterologous expression system, employing LRRC8 subunits containing a fluorescent tag at the C-terminus. Expression of these constructs results in constitutively active channels, that are ideal to monitor activation or inactivation of current, without the need of pre-stimulation (Gaitán-Peñas et al, 2016; Gaitán-Peñas et al, 2018). Importantly, the (partially) constitutively active channels can be further activated by hypotonicity, demonstrating that the machinery of volume-sensitivity is fully active in the tagged constructs (Gaitán-Peñas et al, 2018).

We hypothesized that the LRRDs, might be the relevant target of Chl-T oxidation. To investigate this hypothesis, we swapped the LRRDs between 8C–mCh and 8E–mCh using a chimeric approach. Interestingly,

LRRD exchange resulted in a corresponding interchange of the respective oxidation sensitivity: 8A-VFP/8C(LRRD_8E)-mCh displayed a dramatic potentiation of the currents, while 8A-VFP/8E(LRRD_8C)-mCh currents were strongly inhibited (Fig. 8).

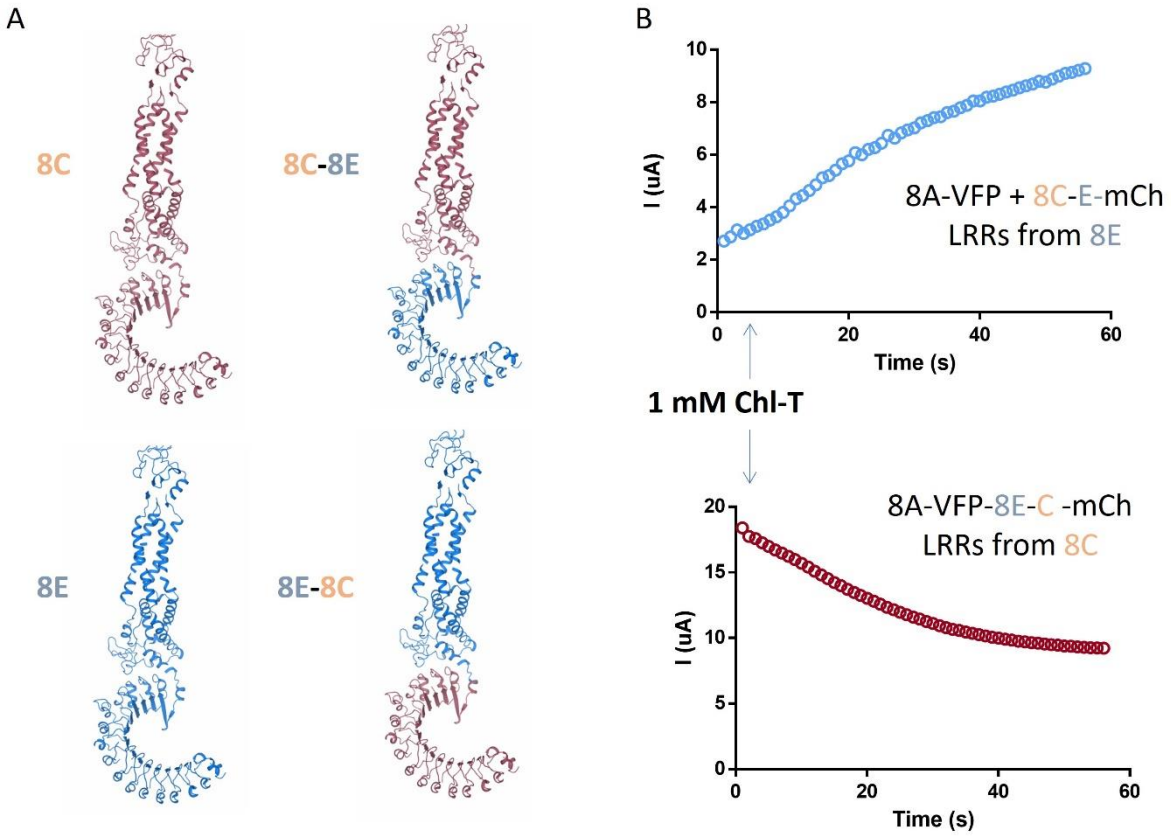

Figure 8. Effect of swapping of LRR domains between 8C and 8E subunits.
(A) Figures on the left were made with Pymol to highlight regions that were swapped between 8C and 8E subunits to give rise to $8C_{8E\text{-}LRRD}$, $8E_{8C\text{-}LRRD}$ chimeras (In red: sequences from 8C, in blue: sequences from 8A). In (B) are shown two representative traces showing that swaps of LRR domains corresponds to an interchange of the respective oxidation sensitivity between 8C and 8E: $8C_{8E\text{-}LRRD}$ and $8E_{8C\text{-}LRRD}$ are respectively activated and inhibited by the application of 1 mM Chl-T. Similar results were obtained in $8C_{8E\text{-}LRRD}$, n=6 and $8E_{8C\text{-}LRRD}$ n=7.

This finding confirmed the intracellular localization of the relevant residues underlying oxidation sensitivity and, more specifically, led us to conclude that these are localized in the LRRDs.

Next, we designed successive chimeras to further narrow down putative regions responsible for oxidant modulation. We first focused on residues responsible for current potentiation of 8A/8E heteromers upon Chl-T (Fig. 9D) or *tert*-Butyl hydroperoxide (TBHP) application. To this end, we screened all generated constructs by the application of Chl-T and TBHP), another organic oxidizing agent widely used in a variety of oxidation processes (Fig. 9D) and shown to potentiate 8A/8E complexes (Gradogna et al, 2017).

Successive chimeras dividing the LRRD in four pieces showed that activation of 8A/8E heteromers is most likely mediated by residues within leucine rich repeats 1 to 4 (LRRD1-4) (Fig. 9A-B). Indeed, only chimeras that contained this region form 8E behaved similarly to 8E upon Chl-T and TBHP oxidation (Fig. 9A-B).

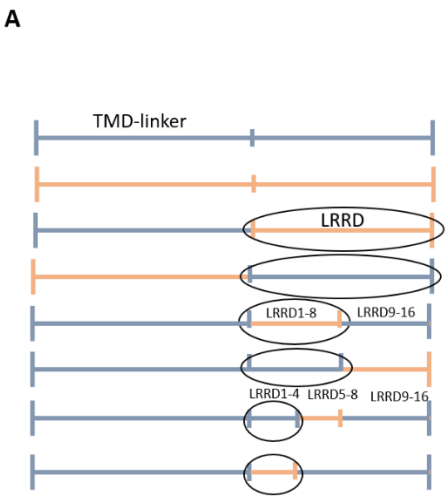

B

TMD-linker	LRR DOMAIN				OXIDANTS EFFECT		PHENOTYPE
	LRRD1-4	LRRD5-8	LRRD9-12	LRRD9-16	Chloramine-T	TBHP	
E					↑	↑	E
C					↓	—	C
E	C				↓	↓	C
C	E				↑	↑	E
E	E		C		↑	↑	E
E	C		E		mixed	—	mixed
E	E	C	E		↑	↑	E
E	C	E	E		mixed	—	mixed

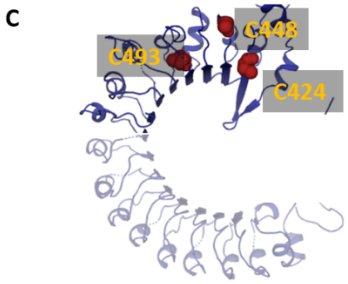

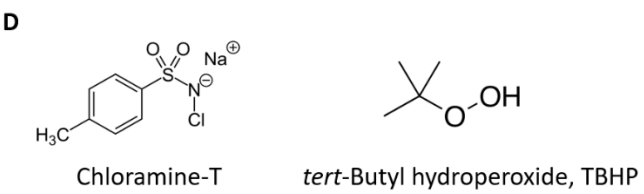

Chloramine-T *tert*-Butyl hydroperoxide, TBHP

Figure 9. Narrowing down the essential target of oxidation by generation of successive chimeras.
(A) Schematic view of all chimeras generated following the logic of bisection method. (B) In the table are highlighted in green the corresponding phenotypes observed upon application of Chl-T or TBHP. Overall, the results obtained with voltage clamp experiments suggested the region within LRRD1-4 as determinant for oxidation sensitivity of 8E.
Below are listed the corresponding positions of each LRR domain in the secondary structure: LRRC8C: LRRD 1-4 (426-518), LRRD 5-12 (519-615), LRRD 9-12(616-711), LRRD 13-16(612-803). LRRC8E: LRRD 1-4 (419-511), LRRD 5-12 (512-608), LRRD 9-12(609-704), LRRD 13-16(605-796). (C) Figure was made with Pymol to highlight cysteine residues within region LRRD1-4 of the 8E subunit (D) Chemical structures of Chl-T and TBHP.

It has to be kept in mind that Chl-T and TBHP exert different effects on 8A/8E vs. 8A/8C heteromers. Whereas both, Chl-T and TBHP, strongly activate 8A-VFP/8E-mCh heteromers, only Chl-T results in inhibition of, 8A-VFP/8C-mCh heteromers, while TBHP has no effect, indicating that the relative target is likely not modified by TBHP (Gradogna et al, 2017) (Fig. 9B).

The exclusion of residues external to LRRD1-4 domain as those responsible for 8A-VFP/8E-mCh potentiation left as cysteine candidates only three residues: C424, C448, and C493 (Fig. 9C).

We first generated a triple mutant in the background of 8E-mCh where cysteines 424, 448, and 493 were mutated to phenylalanine, serine and leucine, respectively (C424F-C448S-C493L). In full agreement with the chimeric approach, oocytes injected with 8A-VFP/8E$_{C424F-C448S-C493L}$-mCh mutant resulted in channels that were insensitive to both Chl-T and TBHP (Fig. 10 B, G). We next tested the single mutant 8A-VFP/8E$_{C493L}$mCh, which resulted sensitive to both oxidants as WT, excluding C493 as essential for mediating

oxidation effects (Fig. 10 C, G). The double mutant 8A-VFP/8E$_{C424F-C448S}$-mCh, was completely insensitive to Chl-T and TBHP, suggesting that one of the two residues might be the exact target (Fig. 10 D, G). Strikingly, both 8A-VFP/8E$_{C424F}$ as well as 8A-VFP/8E$_{C448S}$ single mutants, proved to be insensitive to oxidant application, i.e. no increase of the currents was observed upon oxidant application (Fig. 10 E,G). This result implied that both cysteines, C424 and C448 of 8E are targets of oxidation, and both are strictly required to elicit the potentiating effect observed upon Chl-T or TBHP application.

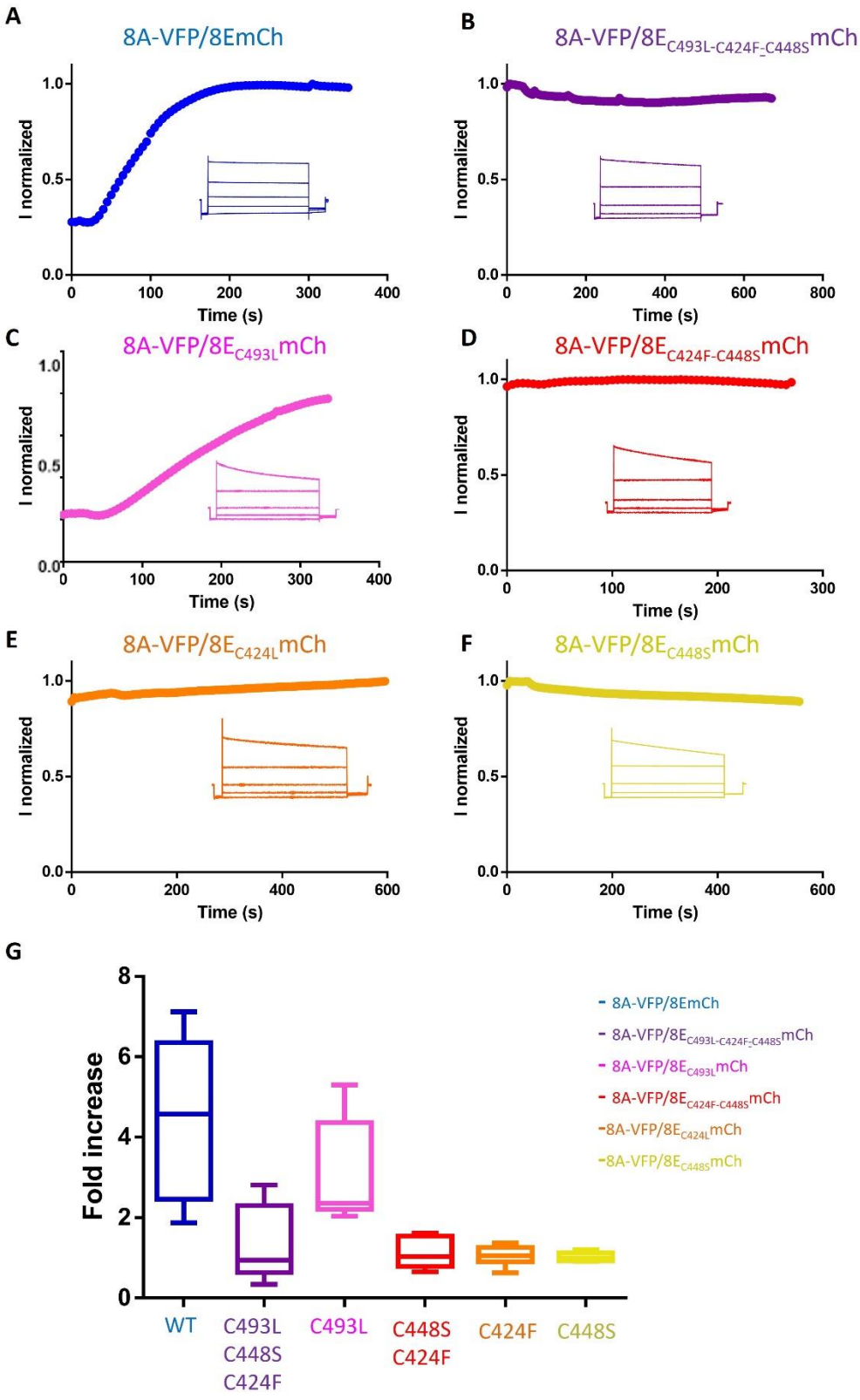

Figure 10. Effect of Chl-T in oocytes expressing 8A-VFP/8E-mCh channels harbouring different mutation within 8E-LRRD1-4.

Time course of currents recorded with a 200 ms test pulse to 60 mV applied every 5 secs from a holding potential of−30 mV after Chl-T application. Insets shows response to an *I–V* stimulation protocol from −80 to +80 mV every 40 mV before stimulus application. Oocytes were injected with 8A-VFP/8EmCh (A), 8A-VFP/8E$_{C493L-C424F-C448S}$mCh (B), 8A-VFP/8E$_{C493L}$mCh (C), 8A-VFP/8E$_{C424F-C448S}$mCh (D), 8A-VFP/8E$_{C424L}$mCh (E), 8A

VFP/8E$_{C448S}$mCh (F). (G) Average fold increase indicates the maximal activated current normalized to the initial current.

We made use of a homology model of 8A/8E heteromeric channels (described in the section ..Material and Methods) to obtain further insight into the structure-function relationship of the two cysteines. C424 is localized at the C-terminus of the beta strand of LRR1 while C448 lies in the linker connecting the LRR2 beta strand and the LRR2 alpha helix, thus resulting in a 3D conformation where C424 and C448 are close, almost facing each other (Fig. 11 A-B). According to the homology model, C424 and C448S are at a distance of ~ 7.1 Å. A similar structural proximity of residues, even though relying on an approximate model, suggested that Chl-T might possibly mediate a reaction between the cysteines, or conversely interfere with a pre-existing disulphide bond, thus disrupting it. The distance in the model is probably too high to be compatible with the formation of a disulphide bond. However, there is evidence that Chl-T and oxidants in general can mediate the formation of a disulphide bond when they encounter cysteines in close proximity with highly reactive participating thiols (*i.e.* low p*Ka*) (Cremers & Jakob, 2013, Rehder, 2010, #4007). In the proposed mechanism, cysteines are thereby drawn closer often leading to conformational rearrangement. Based on this possibility, we speculate that Chl-T may induce the formation of a disulphide bond between C424 and C448. The resulting bridge can act like a mechanic pin forcing the LRRDS toward an open conformation (Figure 11 B).

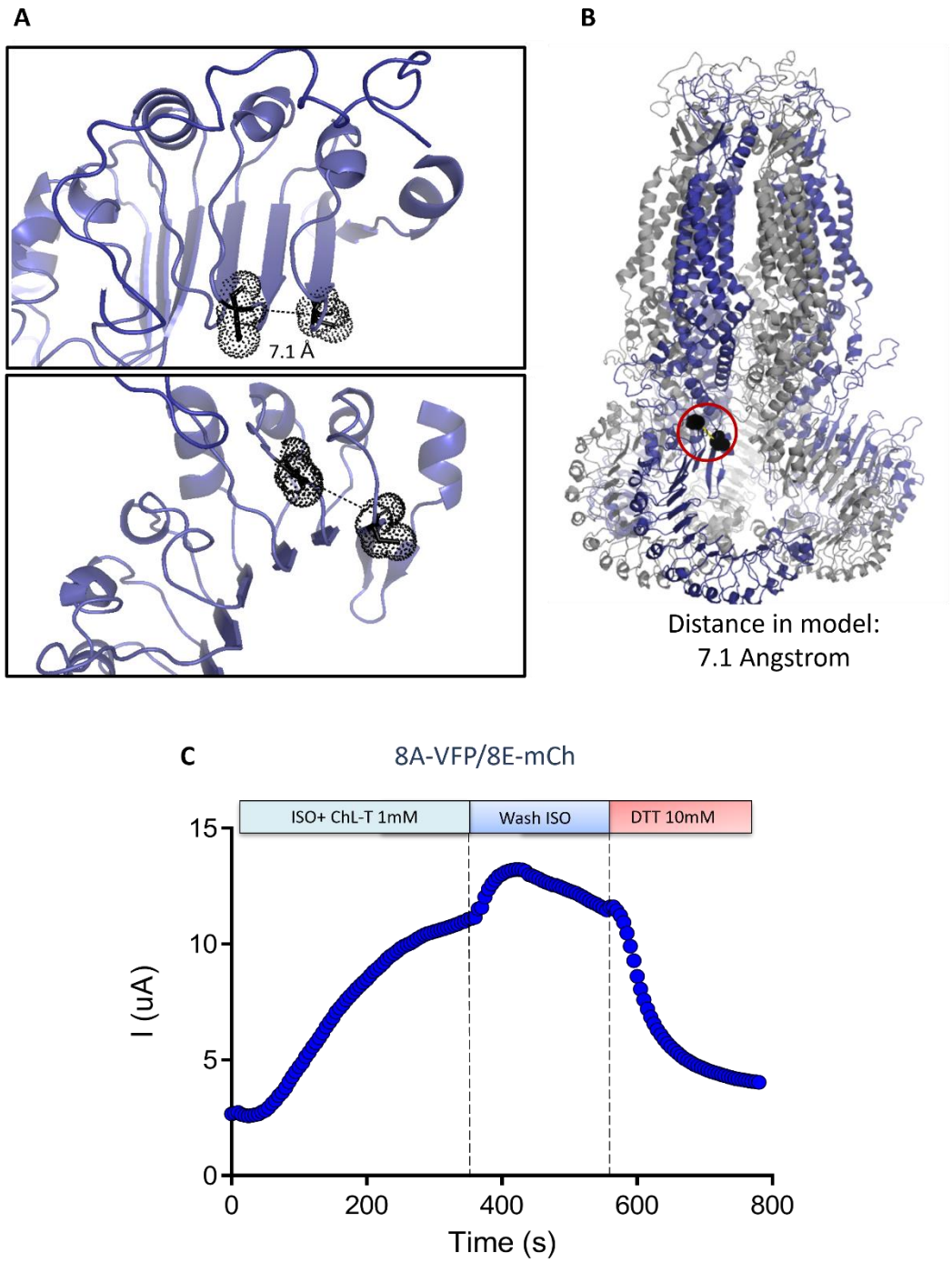

Figure 11. Homology model of 8A/8E heteromers and reversibility of Chl-T oxidation. (A) Figures were made with Pymol using the homology model of 8A/8E (8A-subunit: grey cartoon, 8E-subunit: blue cartoon) to provide a close-up view (top and side) of C424 and C448 mutual position in the backbone of the leucine-rich repeat domain. Cysteines 424 and 448 are evidenced with dots and 'sticks'. The distance within residues is 7.1 Angstrom according to the model. (B) Full structural view of the hexamer with C424 and C448 represented in one subunit as black spheres. (C) Representative time course of current change upon different stimulation of 8A-VFP/8E-mCh injected oocytes. The extent of current inhibition upon application of 10mM DTT is compatible with the disruption of a Chl-T induced disulphide bond.

To further explore this hypothesis and to evaluate whether Chl-T mediated oxidation could be reverted we applied the reducing agent DTT (dithiothreitol), commonly used to disrupt disulphide bonds. 8A-VFP/8E-

mCh heteromers were first activated with 1mM Chl-T till steady state was reached, and then perfuse with 10 mM DTT. As shown in Fig. 11 C, application of DTT led to a steep decrease of the current till complete inactivation.

Interestingly, C424 and C448 are not conserved among the LRRC8 isoforms, being unique to the 8E subunit. At this stage we tried to transplant the activation mechanism into 8C by inserting the two cysteines at the corresponding positions in LRR1 of 8C, i.e. I431 and K455, obtaining the $8C_{I431C\text{-}K455C}$-mCh construct.

As mentioned above, and illustrated in Fig. 12 A, currents mediated by 8A-VFP/8C-mCh heteromers are normally not modified by TBHB. Thus, to allow an easier identification of any effect introduced by the inserted cysteines we first employed TBHP. Application of TBHP in oocytes expressing 8A-VFP/$8C_{431C\text{-}455C}$-mCh resulted in a current increase that was very similar to that seen in oocytes expressing 8A-VFP/8E-mCh (Fig. 12 B). The overall fold change of the current was comparable (Fig. 12 E).

We next tested also Chl-T. A priori, it is not clear which of the two contrasting expected effects would prevail: activation induced by oxidation of the two introduced cysteines or inhibition mediated by the 8C background. Application of Chl-T to oocytes expressing 8A-VFP/$8C_{I431C\text{-}K455C}$-mCh led to an initial slight increase of the current, that was thereafter followed by a gradual decrease leading finally to inactivation, however only after a prolonged time (Fig. 12 C-D), and clearly different from the response of WT 8A-VFP/8C-mCh. This suggests that the I431C and K455C mutations introduce a new reaction site for Chl-T in the background of 8C, while in parallel Chl-T still reacts with another, so far unknown motif(s) present in 8C that leads to an inhibition of activity. Apparently, this leads to a temporary initial approximate balance of the two effects, such that neither activation nor inactivation prevail (Fig.12 C-D).

Only after several minutes, the inhibitory effect turns out to be predominant, leading to a slow irreversible inactivation of the current. Fig. 12 C shows two representative traces revealing that 3 min after Chl-T perfusion, 8A-VFP/8C-mCh mediated currents are reduced to about 50% of the initial value, while 8A-VFP/$8C_{K431C/I455C}$ mediated current are still close to 100%.

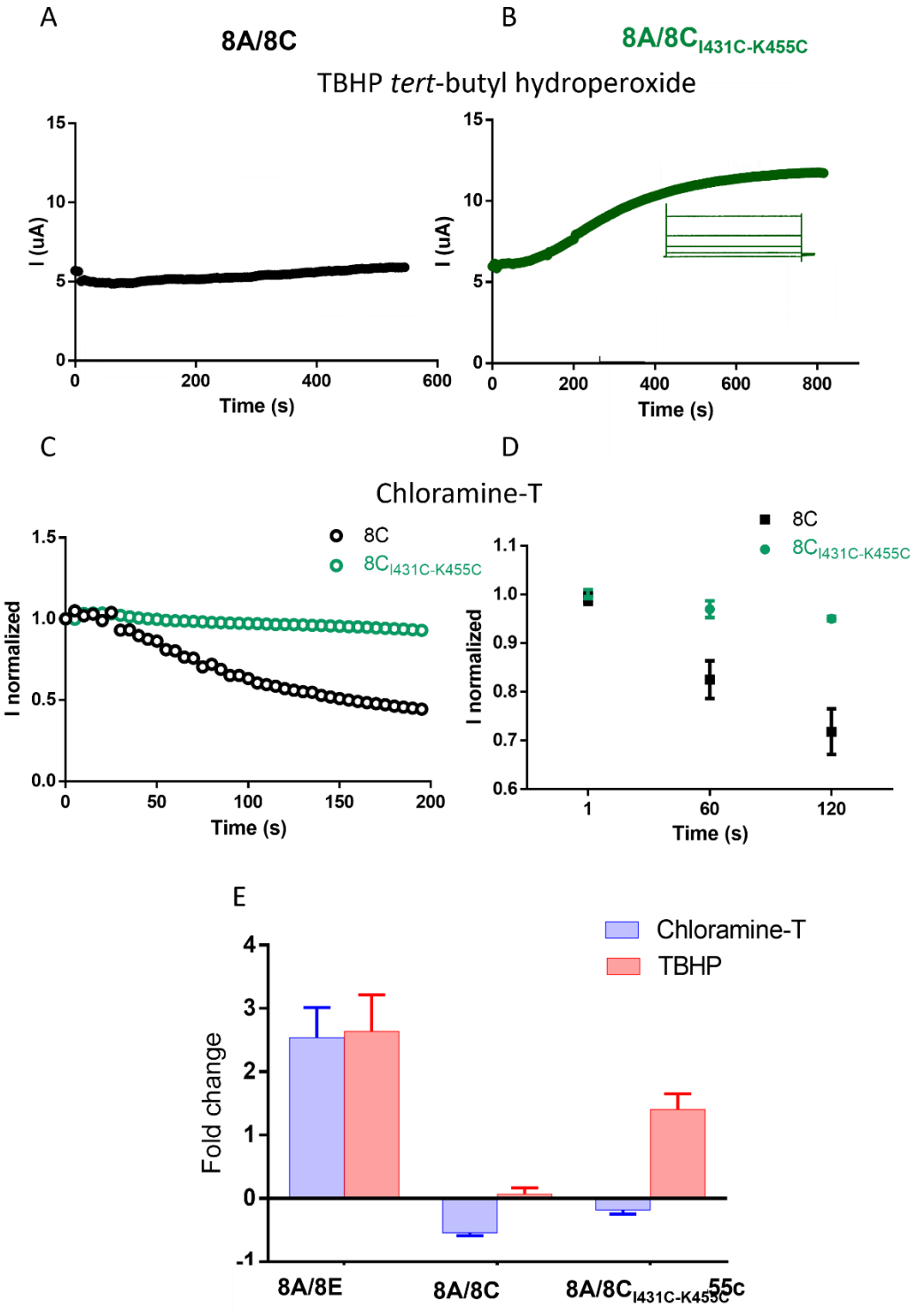

Figure 12. Characterization of 8A-VFP/8C$_{I431C-K455C}$mCh mutant.
Representative traces of 8A-VFP/8C$_{I431C-K455C}$mCh (A) and 8A-VFP/8CmCh (B) current upon application of *tert*-butyl hydroperoxide (TBHP) or chloramine T (Chl-T). Timecourse of current was recorded with a test 200 ms pulse to +60 mV from a holding potential of−30 mV applied every 5 secs. C) Normalized current traces of 8A-VFP/8C$_{I431C-K455C}$mCh and 8A-VFP/8CmCh highlight differences in the time course of inactivation after Chl-T application. D) Plot of average ± SEM amplitudes at 1, 60 and 120s after Chl-T application. (E) Bar charts showing average fold changecurrent upon application of chloramine-T and TBHP to oocytes expressing 8A-VFP/8EmCh , 8A-VFP/8CmCh and 8A/8C$_{431C-K455C}$mCh.

Having unambiguously identified the residues underlying potentiation of 8E harbouring heteromers we sought to similarly identify residues responsible of Chl-T mediated 8A-VFP/8C-mCh inhibition. Initially we adopted the chimera based screening strategy similar to what done for the 8E subunit. Results with the first chimera exchanging the LRRD between 8E and 8C suggested that also for 8C residues within the LRRD underlie oxidation sensitivity. However, results obtained with the subsequent sub-chimeras were of difficult interpretation (Fig. 9 B) because of mixed effects of Chl-T. Thus, we initially considered the first half of the LRRD and mutated all cysteine and methionine residues within this region (LRRD 1-8). However, none of the mutants abolished Chl-T inhibitory effect (Table 5). We thus extended mutagenesis to all cysteine and methionine residues within the entire LRRD domain, but again this approach failed to find a good candidate (Table 5). We therefore concluded that for the specific case of 8C subunit, the chimeric strategy was misleading (discussed in depth in 'conclusion' section).

We proceeded screening all methionine and most cysteines (excluding those involved in cysteine bridges in the extracellular domains) of the full length 8C subunit. Since there is evidence that hypochlorite, can also oxidize histidine residues, even though at a lower rate compared to cysteines and methionine (Hawkins et al, 2003), we included this amino acid in the list of residues to be mutated, selecting several histidines in the LRRD. Surprisingly, none of the candidates turned out to abolish or attenuate Chl-T mediated inhibition (Table 5).

Table 5. List of single-point mutations introduced in the background of 8C-mCh.

8C-Met residues mutated	Domain	Effect	8C-Cys residues mutated	Domain	Effect
M48L	ECL1	wt	C477S	LRRD	wt
M96L	ECL1	wt	C493F	LRRD	wt
M114L	ECL1	wt	C571S	LRRD	wt
M139L	TM2	wt	C599S	LRRD	wt
M193L	TM2-TM3 linker	wt	C682S	LRRD	wt
M300L	ECL2	wt	C715S	LRRD	wt
M312L	ECL2	wt	C728S	LRRD	wt
M376L	TM4-LRR linker	wt	C774S	LRRD	wt
M432L	LRRD	wt	**8C-His residues mutated**	**Domain**	**Effect**
M458T	LRRD	wt	H423N	LRRD	wt
M503L	LRRD	wt	H475N	LRRD	wt
M510L	LRRD	wt	H482N	LRRD	wt
M570L	LRRD	wt	H527N	LRRD	wt
M581L	LRRD	wt	H598N	LRRD	wt
M588L	LRRD	wt	H669N	LRRD	wt
M800L	LRRD	wt	H678N	LRRD	wt
M458T-M503L-M510V-M570L-M588L-M800L	LRRD	wt	H763N	LRRD	wt

The only residue we had excluded (or did not consider) in the screening was the start methionine (M1). The N-terminus of LRRC8 proteins has been shown to be essential for channel functioning with several mutants within the first 15 amino acids resulting in a loss of function of VRAC channels (Zhou et al, 2018). Moreover, since the first methionine is mandatory for initiation of protein synthesis, it is intrinsically difficult to modify and we needed to find a strategy to bypass this constraint. A simple approach might be to use a

concatamer of 8A and 8C subunits in which the 8C start methionine could be mutated at will. However, it has been shown that the N-terminus of LRRC8 subunits has to be “free” in order to form functional channels (T.J. Jentsch, personal communication). To circumvent this problem, we employed a self-cleaving peptide sequence (T2A) separating 8A and 8C subunits in the concatamer (Tang et al, 2009). (see Materials and Methods). While being encoded in only one mRNA, the cleavage at the translational level produces two separate peptides. We generated two variants: a control concatamer 8A-VFP$_{T2A}$8C-mCh supposed to mimic WT 8A-VFP/8C-mCh heteromeric channels, and a concatamer in which M1 of 8C was substituted with a leucine residue (L1) 8A-VFP$_{T2A}$8C$_{M1L}$-mCh.

Concatamers expressed in Xenopus oocytes yielded currents significantly above background but much lower than those obtained by co-expressing the single subunits. Nevertheless, as expected, the control concatamer 8A-VFP$_{T2A}$8C-mCh was consistently inhibited by Chl-T (Fig.13 A). Most importantly, currents measured in oocytes injected with 8A-VFP$_{T2A}$8C$_{M1L}$-mCh, in which the start methionine of 8C is mutated to leucine, completely abolished the inhibitory effect of Chl-T (Fig. 13 A).

These results strongly suggest that oxidation of the start methionine of 8C subunits underlies inhibition of 8A/8C heteromers. To further cement this conclusion, we inserted into the 8A-VFP$_{T2A}$8C$_{L1}$-mCh concatamer the two cysteine residues at positions 431 and 455 that conferred activation by TBHP and partial decrease of Chl-T mediated inactivation to 8C subunits (construct 8A-VFP$_{T2A}$8C$_{M1L\text{-}I431C\text{-}K455C}$-mCh).

First, applying TBHP to the 8A-VFP$_{T2A}$8C$_{M1L\text{-}I431C\text{-}K455C}$-mCh concatamer resulted in a significant increase of currents (data not shown), confirming that the concatamer is able to reproduce the results obtained by co-injection of the single subunits. More importantly, also the application of Chl-T led to a strong activation of currents (Fig.13 A-B), demonstrating the absence of the inhibitory effect of Chl-T seen in WT 8A/8C heteromers. Furthermore, DTT application rapidly reverted the Chl-T induced activation (Fig.13 C), in a manner compatible with disulphide disruption, again reproducing the 8E phenotype.

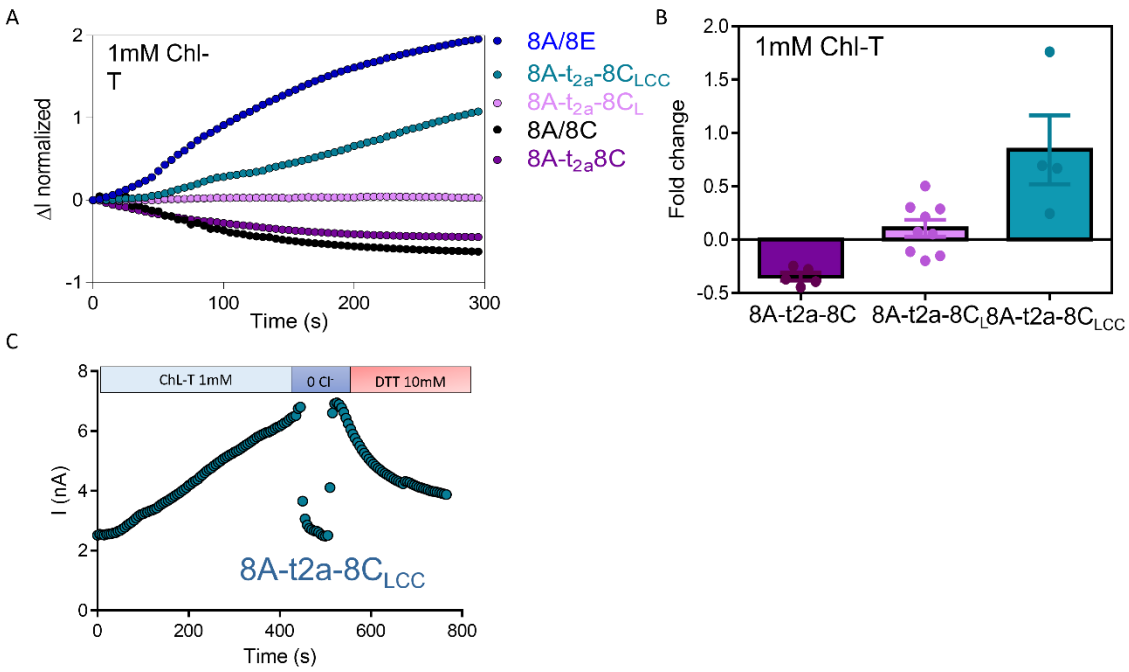

Figure 13. The first Methionine of 8C subunit is the target of chloramine-T.
(A) Representative traces of 8A/8E, 8A-t2a-8C$_{LCC}$,8A-t2a-8C$_{L}$,8A/8C, 8A-t2a-8C reveals that the first methionine (M1) of 8C subunit is the target of chloramine-T.
The control concatamer 8A-t2a-8C behaves like 8A/8C, inhibiting upon chl-T application. Conversly, the elimination of the first methionine in 8A-t2a-8C$_{L}$completely abolished the inhibitory effect of chloramine-T. The insertion of the two corresponding cysteines of 8E in 8A-t2a-8C$_{LCC}$ nicely reproduced phenotype of 8E. In (B) is shown the fold change (ΔI/I initial) of the respective concatemers that highliths the reverted phenotype of 8A-t2a-8C$_{LCC}$.(C) Similarly to 8E the application of DTT after Chl-t leads to a rapid decrease of the current again in line with the disruption of a disulphide bond.

Interestingly, 8A-VFP$_{T2A}$8C$_{I431C-K455C}$-mCh mediated channels (i.e. channels with intact 8C start methionine and introduced activating cysteines from 8E) displayed a slight current activation upon Chl-T perfusion (data not shown). This might seem at odds with the overall inhibitory effect of Chl-T on currents induced by the "equivalent" co-injection of 8A-VFP with 8C$_{I431C-K455C}$-mCh (Fig. 12 C-D). This apparent discrepancy might be related to the fact that concatemers generated with the T2A linker introduce small changes both at the 3' end of the first ORF and at 5' end of the second ORF. In particular a proline residue is added in front of the second ORF. In this scenario M1 of 8C in the construct 8A-VFP$_{T2A}$8C$_{I431C-K455C}$-mCh is preceded by a proline residue and this might explain the reduced inhibitory effect of Chl-T.
Moreover, the addition of a proline residue might explain the overall smaller expression levels elicited by expression of concatemers This is also coherent with previous findings concerning the relevance of the N-terminus for VRAC functioning (Zhou et al, 2018). In the conclusion section this aspect is discussed in depth and major speculation are derived.

Role of phosphorylation in swelling induced VRAC activation.

In a set of parallel experiments, I intended to explore the physiological mechanism underlying VRAC activation upon swelling, with the major goal to elucidate the long-standing dilemma of the role of phosphorylation. Moreover, latest findings about the relevance of the first intracellular loop (IL1) in VRAC functioning (Strange et al, 2019; Yamada & Strange, 2018), and clues suggesting this portion of the channel as a putative target of post-translational modification (Abascal & Zardoya, 2012; Strange et al, 2019) led us to investigate whether there might be a correlation between VRAC activity and the requirement of specific modification (e.g., phosphorylation) in residues localized inside the IL1 .

On this purpose we made use of prediction servers to screen for sites with a high prediction score to undergo phosphorylation. Exploiting the NetPhos 3.1 server, 16 residues in the stretch of the intracellular loop (IL1) of LRR8A covering a region of ~120aa (144-265) turned out to be putative targets of phosphorylation, most of which were serine and threonine residues (see table 2). The same analysis was performed for LRRC8E and led to identify 9 residues in 8E(IL1) with a score >0.5 for phosphorylation. Interestingly, part of the 16 residues of 8A(IL1) overlapped with the stretch of 25 amino acids (YSS) identified in the work of Yamada & Strange (Yamada & Strange, 2018) to be essential for channel functioning (see Figures 6 and 14).

In order to test for a possible importance of phosphorylation in VRAC activation, we designed a construct in which the residues with high score to undergo phosphorylation were mutated to alanine and subcloned in the background of LRRC8A and LRRC8E, respectively, giving rise to what we called 8A-IL (Δp), 8E-IL (Δp) (see Materials and Methods and Figure 14).

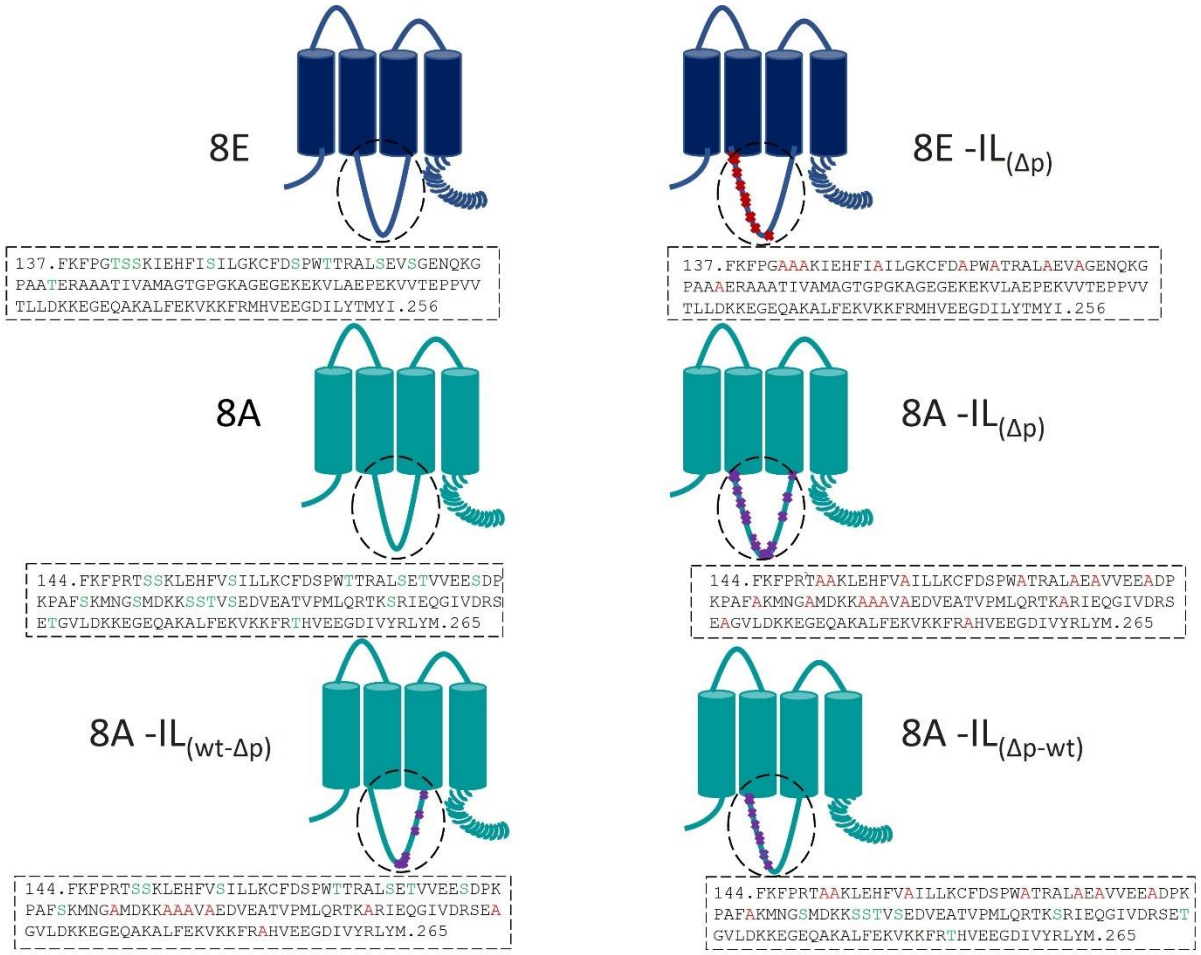

Figure 14. Schematic representation of 8A and 8E constructs harbouring mutations inside IL1.
Different constructs were designed to generate channels harbouring different mutations within the first intracellular loop (IL1) to investigate relevance of underlined residues for VRAC activation.

These constructs were first tested in HEK-5X-KO, a cell line in which all LRRC8 genes have been deleted, providing a background free of LRRC8 genes, kindly provided by Thomas Jentsch. Patch clamp experiments in the whole cell configuration showed that cells co-transfected with 8A-IL$_{(\Delta p)}$/8E completely lost any response to the application of a hypotonic extracellular solution. On the contrary, cells co-transfected with 8A/8E-IL$_{(\Delta p)}$ showed a response to a hypotonic challenge comparable to cells transfect with 8A/8E (Figure 15A). Surprisingly, 8A-IL$_{(\Delta p)}$/8E heteromers turned out to be responsive to a stimulation with a pipette solution with a low ionic strength. Even though low-ionic strength activated currents of 8A-IL$_{(\Delta p)}$/8E heteromers were significantly smaller compared to 8A/8E mediated currents, this result asserts that 8A-IL$_{(\Delta p)}$/8E channels are, in principle, still functional. Similar experiments were performed by transfecting HEK-5X-KO with 8A-IL$_{(\Delta p)}$ CFP/8E-VFP or 8A-CFP/8E-VFP (Figure 15 B-D). Both channels showed a clear and comparable basal current while kept in isotonic bath, but notably only 8A/8E channel were capable to undergo further activation upon hypotonic stimulation.

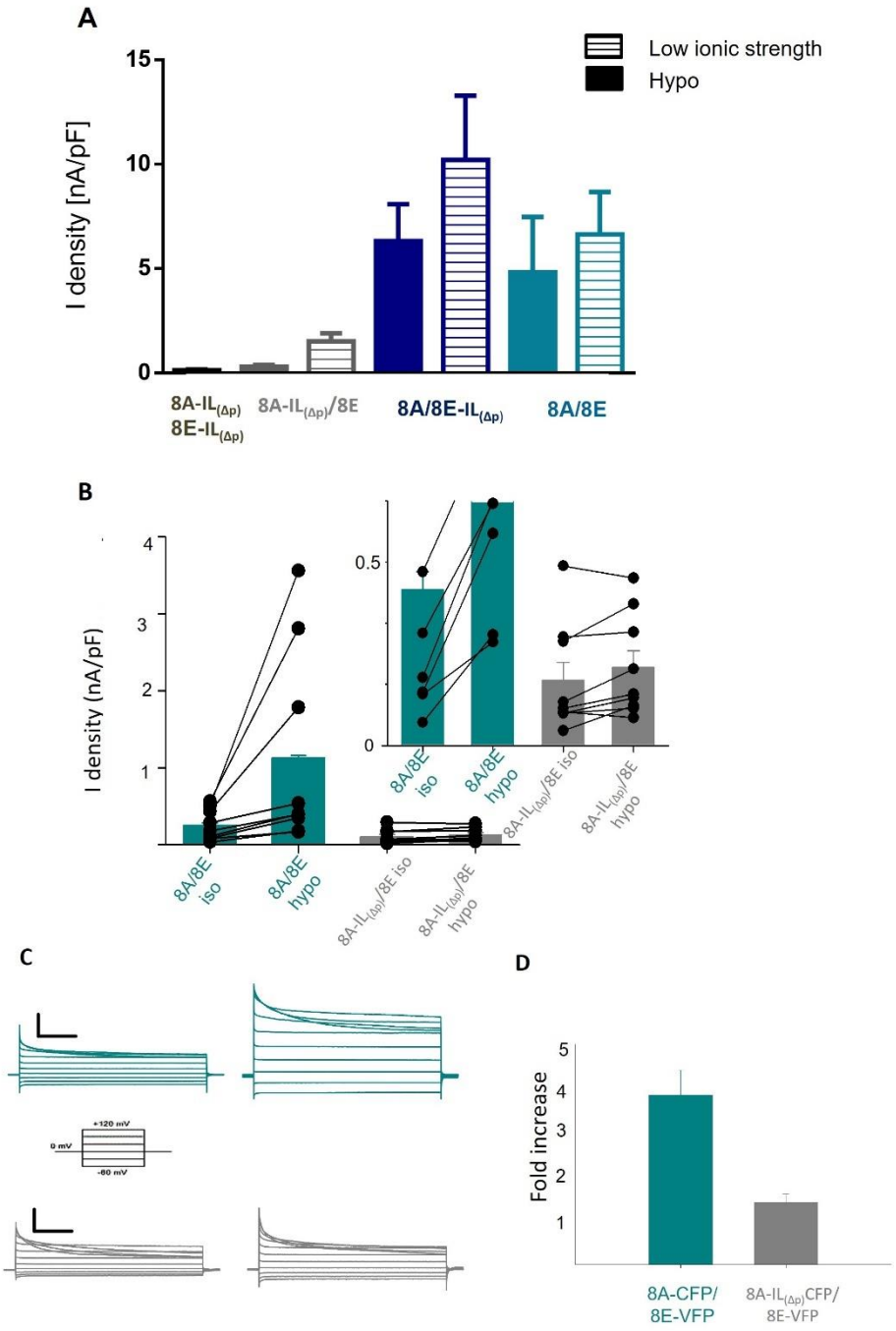

Figure 15. Depletion of serine/threonine residues within 8A-IL1 impairs VRAC activation upon hypotonic stimulation.

Whole cell recordings of HEK-5X-KO transfected with different heteromers. (A) Average current density of different mutant upon hypotonic stimulation or application of low ionic strength pipette solution. Current response to various stimuli was monitored using the time course protocol, consisting of successive steps of 50 ms pulses to −75, −25, 0, 25 and 75 mV every 5 s. Maximal current at 75 mV was normalized to membrane capacity. Mean currents ± SEM is indicated. (B-C-D) Addition of a fluorescent tag to C-terminus leads to constitutive currents. Average current density (B) and representative IV traces (C) before and after hypotonic stimulation. (D) Fold increase indicating maximal activated current normalized to basal current. Note that 8A-IL$_{(\Delta p)}$CFP/8E-VFP channels display a constitutive current comparable to 8A-CFP/8E-VFP, but do not increase further in hypotonic condition.

The latter finding provided a first evidence that the mutation of 16 putative phosphorylation sites within IL1 loop (i.e. $IL_{(\Delta p)}$) in 8A did not impair channel targeting to the plasma membrane, in that mutated channels were still functional upon the application of the low-ionic strength stimulus. Indeed, intracellular low ionic strength is thought to elicit a strong, but likely non-physiological activation of VRAC channels, putatively by electrostatic interactions between LRR domains. Moreover, the fact that similarly mutating 16 putative phosphorylation sites in the background of 8E did not impair the responsiveness of 8A/8E-$IL_{(\Delta p)}$ to swelling, confirmed that these residues in the IL1 loop are fundamental only within the LRRC8A subunit.

Successive chimeras were built to identify the portion of the IL1 underlying the reduced ability of the channel to undergo activation upon swelling. The details concerning each construct are summarized in table 1.

To this end, we designed 8A-$IL_{(\Delta p\text{-}WT)}$ and 8A-$IL_{(WT\text{-}\Delta p)}$ sub-chimeras, in which the mutated residues were maintained only in the first or second half of $IL_{(\Delta p)}$, respectively (Figure 14). We also designed and tested a triple and quadrupole mutant: $8A_{S217E\text{-}S229E\text{-}S252E}$ (8A-IL(3E)) and $8A_{S198A\text{-}S199A\text{-}T200A\text{-}S202A}$ (8A-IL(4A)). For details see the section Material and Methods. Our interest in 8A-IL(4A) derived from the fact that the stretch within aa 198-202 contains 4 Ser/Thr residues in sequence (with only a Valine interrupting the continuity) highly suspected to be a target of PKC (Abascal & Zardoya, 2012). Moreover the underlined residues overlap with the YSS stretch (Strange et al, 2019).

Patch clamp experiments revealed that 8A-$IL_{(\Delta p\text{-}WT)}$/8E heteromers failed to activate under hypotonic conditions (Figure 16). On the contrary, 8A-$IL_{(WT\text{-}\Delta p)}$/8E channels fully activated in response to a hypotonic challenge, with a current density similar to WT 8A/8E channels (Figure 16).

Both 8A-IL(3E)/8E and 8A-IL(4A)/8E resulted in a robust current activation upon hypotonic perfusion.

These results clearly indicated that the second half of IL1 is not essential for mediating volume-sensitivity, while one or more of the 8 residues mutated in the first half of IL1 are essential for channel functioning.

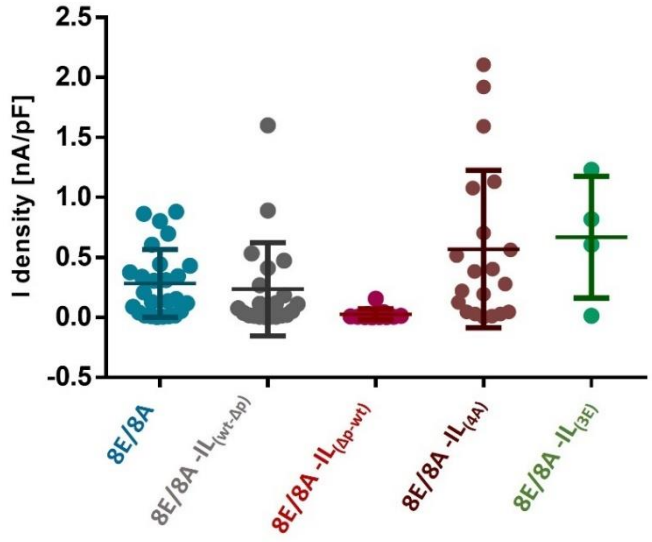

Figure 16. Narrowing down 8A-IL1 relevant regions by creating successive sub-chimeras. Average current density indicating maximal activated current normalized to membrane capacity. To monitor current activation it was used the same time course protocol shown in 15 (A) and (B).

To further corroborate our findings and to obtain a deeper insight into the significance of our results I complemented some experiments using a particular FRET assay. Namely, as pipette dialysis is one of the limitations of the whole cell patch clamp technique, I intended to obtain similar evidence by exploiting a system that creates less disturbances in the intracellular milieu. On this purpose we collaborated with the group of Prof. Tobias Stauber that recently established a FRET sensor assay capable to monitor VRAC activity in a spatio-temporal manner. The sensor consists of CFP and YFP fluorescent proteins fused at the C-terminus of LRRC8A and LRRC8E, respectively. Sensitized-emission FRET changes can detect movement of the intracellular C-terminal domains upon switch from isotonic (340 mOsm) to hypotonic (250 mOsm) solution, by leading to a robust decrease in cFRET by 5–10% within 90 s in both HeLa and HEK293 cells (König et al, 2019). An advantage of this technique is that the intracellular milieu is not disturbed by pipette dialysis occurs during patch-clamp experiments, avoiding artifacts due to the impairment of the physiological cytosolic environment. I exploited the FRET sensor assay to test some of the chimeras of 8A in Hela cells. The results well overlapped with those obtained by patch clamp measurements (Figure 17), i.e. 8A-IL $_{(wt-\Delta p)}$ /8E responded with a decrease of FRET upon hypotonic stimulation similar to 8A-CFP/8E-YFP, while 8A-IL $_{(\Delta p-wt)}$ /8E was almost completely unresponsive.

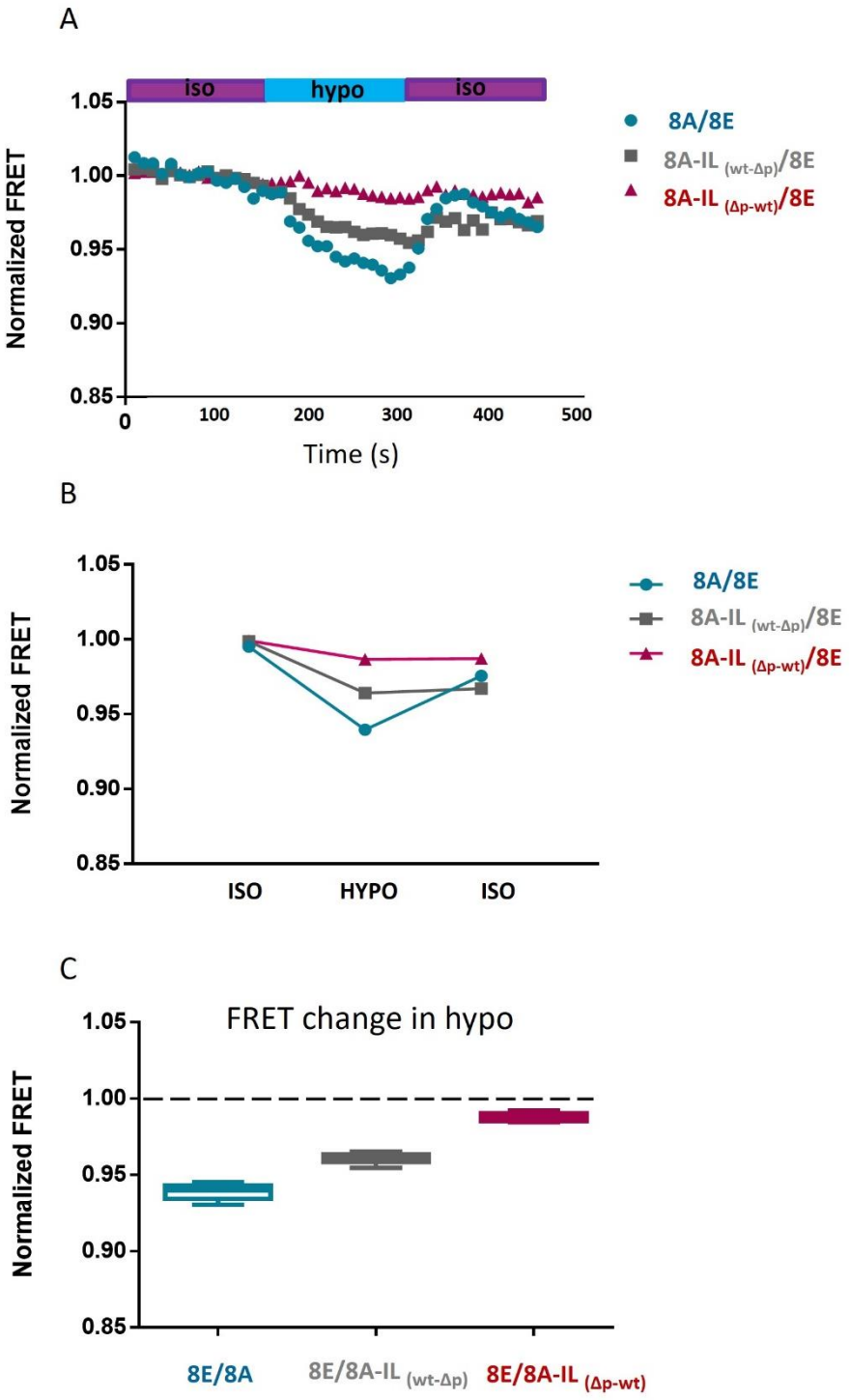

Figure 17. FRET experiments in HELA cells confirmed 8A-IL $_{(\Delta p\text{-}wt)}$ /8E channels insensitivity to swelling.
(A) normalized cFRET values during buffer exchange experiments with 8A-CFP/8E-YFP, 8A-IL $_{(wt\text{-}\Delta p)}$ /8E and 8A-IL $_{(\Delta p\text{-}wt)}$ /8E. (B) Average cFRET change in iso-hypo-iso buffer switch .(C) Average normalized cFRET in hypotonic buffer taken from (B). Data represent mean of last five time points in hypotonic buffer ofindividual cells, and mean of all cells ±s.e.m. Baseline cFRET in isotonic buffer indicated by dashed line.

Next, we decided to mutate these 8 residues one by one using PCR mutagenesis. Among these, T169 is the first residue after the highly conserved helix-loop-helix turn involving proline P167. In fact, the stretch (D/E)SPWT$_{169}$T(R/K)ALS, is conserved in all LRRC8 isoforms in mouse and humans. We first tested the construct 8A$_{T169A}$-VFP/8E-mCh in Xenopus oocytes. The mutation T169A led to a complete abolishment of the normally present constitutive currents, as well as a response to hypotonic stimulation, in agreement with a critical function of T169. Surprisingly, a similar effect was observed with the conservative mutation T169S (data not shown). To confirm the latter result, we performed experiments in HEK-5X-KO cells transfected with untagged 8A$_{T169S}$/8E. In agreement with the oocyte data, the T169S mutation resulted in a phenotype unresponsive to hypotonicity (Figure 18). Importantly, the patch clamp experiments revealed that the T169S mutation maintained responsiveness to low intracellular ionic strength (Figure 18A). In order to test if the variants of T169 affected protein stability and/or membrane targeting, we inserted the T169S mutation in the fluorescently tagged 8A-Cerulean construct (normally used in the FRET experiments), allowing to quantify membrane localization via the fluorescence of the tag.

Importantly, both 8A-Cerulean and 8A$_{T169S}$-Cerulean showed a clear expression in the cell membrane together with 8E-Venus (Figure 18B).

Since the targeting of 8E subunits at the plasma membrane is strictly dependent on its association with the 8A subunit (Voss et al, 2014), this also excluded the possibility that the mutation could somehow interfere with the ability of the two subunits to heteromerize.

To investigate if a negative charge could mimic the effect of a phosphorylated threonine group, we mutated T169 to glutamate (E). Notably patch clamp measurement revealed that this mutation maintains channel functionality: indeed, both 8A$_{T169E}$/8E and 8A/8E displayed similar current activation upon hypotonic perfusion, with an even more pronounced increase by direct application of a low ionic strength solution in the pipette. Moreover, cells transfected with 8A$_{T169E}$/8E showed a constitutive current even in the absence of a fluorescent tag at the C-terminus (Figure 18A). This result suggested that the insertion of a negative charge at position 169 might mimic the effect of phosphorylation or might introduce some rearrangement of the 3D conformation favouring channel opening.

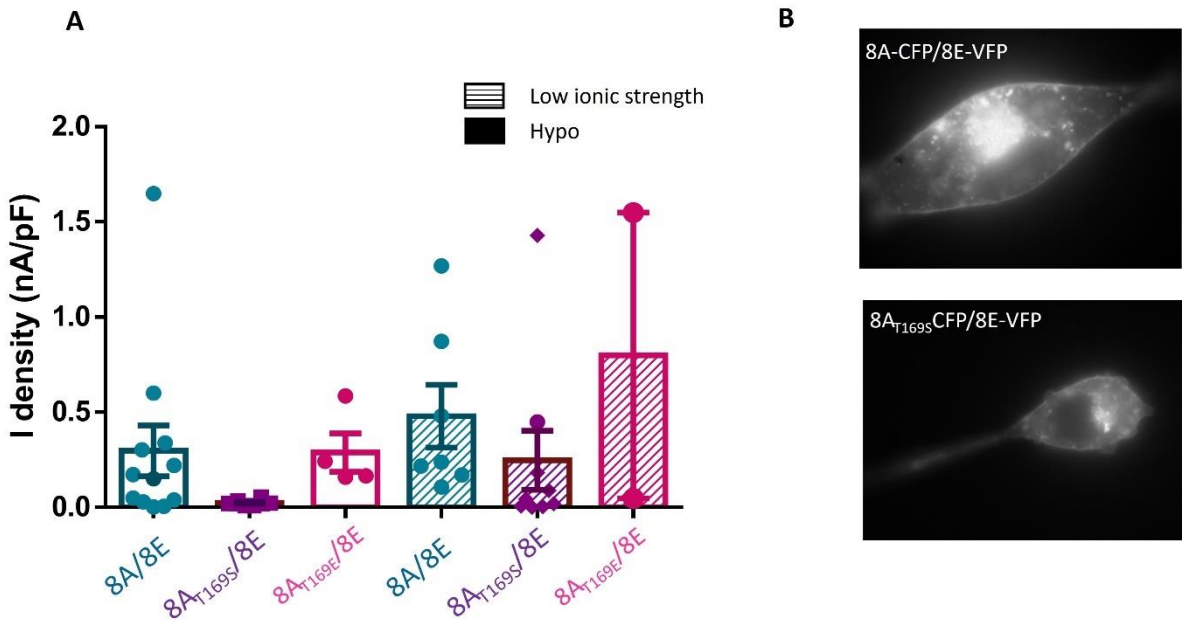

Figure 18. Residue T169 is critical for channel functioning and responsiveness to hypotonic stimulation. Average current density of 8A/8E, $8A_{T169S}$/8E and $8A_{T169E}$/8E upon hypotonic stimulation or application of low ionic strength pipette solution. Note that even $8A_{T169S}$/8E channels that are unresponsive to hypotonic stimulation can be activated by a low intracellular ionic strength solution and (B) are nicely expressed on plasma membrane, ruling out the hypothesis of an impaired targeting of the channel to cell membrane.

As a next step, we asked whether activation of specific kinase signalling pathways could interfere with VRAC activation upon swelling. As already discussed in detail in the introduction, protein kinase C (PKC) has been proposed as a key player in the modulation of the channel with publications proposing either stimulating or inhibitory effect. The protein kinase C family comprises several paralogs which phosphorylate their substrates on serine or threonine residues. PKCs are activated and recruited to the plasma membrane by diacylglycerol (DAG), which is the product of phospholipase C catalyzing the cleavage of phosphatidylinositol-4,5-bisphosphate (PIP2) to DAG and inositol-1,4,5-triphosphate (IP3). Activation of PKCs is experimentally accomplished by the addition of phorbol esters, which serve as DAG analogues, for example phorbol-12-myristate-13-acetate (PMA).

We thus used PMA to directly test its effect on VRAC modulation. As a first attempt we performed patch clamp experiment to monitor VRAC current after application of PMA at several time points (data not shown). However, we soon realised that patch clamp is not an ideal technique for this kind of experiments for two main reason. First it is possible to measure only one cell per time and given the short window of PMA activity the risk is to lose information. Secondarily, the whole-cell configuration might impair cell signalling by diluting cellular components including signalling molecules, thus masking possible effects of PMA.

We thus proceeded to monitor VRAC activity using an iodide influx assay based on YFP quenching (Galietta et al, 2001), being less invasive and allowing parallel screening of a higher number of cells within the same field of view.

Details of the experiments are summarized in Material and Methods (section).

Results are shown in Figure 19. PMA application exerted a small effect, in a way that was comparable between 8A/8E, $8A_{T169E}$/8E, and $8A_{T169S/}$8E, all co-transfected with an iodide sensitive variant of YFP (Galietta et al, 2001). On the contrary, when the same cells were subjected to a hypotonic solution containing iodide (in place of Cl^-) we could observe a large drop of fluorescence of 8A/8E transfected cells, smaller but comparable to that of $8A_{T169E}$/8E, while for $8A_{T169s}$/8E neither PMA nor hypotonicity could elicit a significant change of fluorescence (Figure 19 A-B).

To further test if PMA can activate VRAC, we performed voltage clamp measurement applying the compound to oocytes injected with 8A-VFP/8E-mCh. Oocytes were perfused with 1 µM PMA or 0.1% DMSO as a vehicle control. These experiments revealed a small but significant activation of 8A-VFP/8E-mCh channels (Figure 19C). However, successive application of a hypotonic solution led to a much larger increase in the current compared to PMA (data not shown).

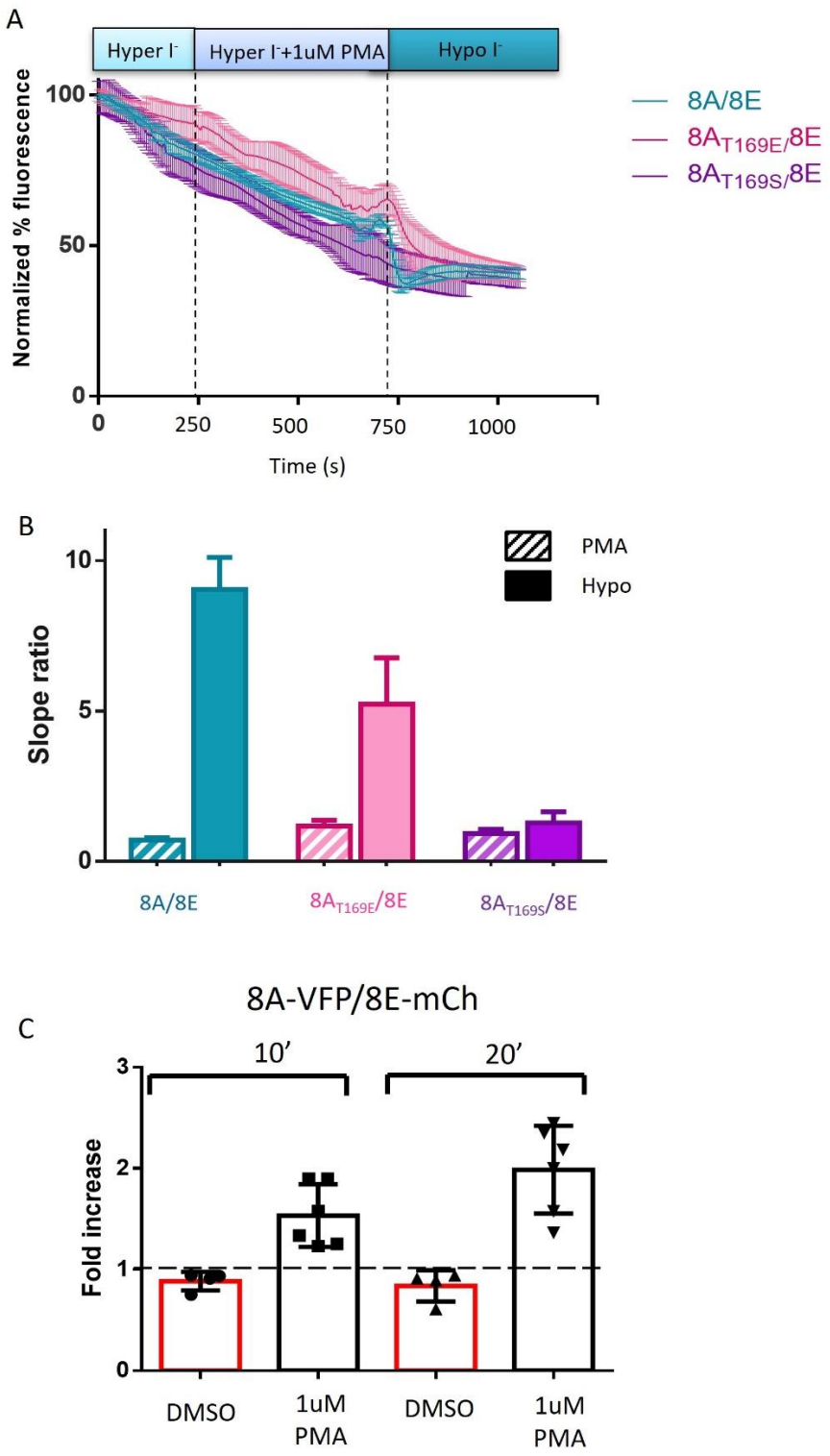

Figure 19. Effect of PMA by means of iodide sensitive YFP quenching assay and voltage clamp experiments. (A) Example traces, normalized to initial fluorescence showing the time course of YFP quenching upon different conditions. (B) Bar charts indicate the slope of fluorescence drop observed upon perfusion of hyper I^-+1uM PMA solution normalized to the slope fluorescence drop while cells were kept in hyper I^- solution (dashed pattern). Similarly, solid filled chart indicates slope of fluorescence drop upon hypo I^- solution normalized to the slope of fluorescence drop while cells were kept in hyper I^- solution. (C) Voltage clamp experiments in oocytes expressing 8A-VFP/8E-mCh. Average fold increase indicates the current at 10' or 20' after 1uM PMA or 0.1% DMSO application normalized to the basal current. Time course of current was measured using same protocol shown in Figure 11A.

In conclusion, experiments performed so far did not provide evidence of a strong effect of PMA on VRAC activation, even though results do not allow to clearly exclude this possibility. Several possible explanations, including the variability of the time required for the availability of PKC in the plasma membrane, can explain a failure of similar experiments.

5. DISCUSSION

Thirty years after its discovery, the puzzle to link VRAC physiology with the molecular events underlying its activation are yet to be solved. Yet, the molecular identification of LRRC8 proteins as those underlying VRAC channels was a milestone that paved the way to a deep characterization of the biophysical properties of the channel with regard to distinct subsets of subunit combinations (Qiu et al, 2014; Voss et al, 2014). Noteworthy, it laid the groundwork to obtaining cryo-EM structures of homomeric LRRC8A and homomeric LRRC8D complexes (Deneka et al, 2018; Kasuya et al, 2018; Kefauver et al, 2018; Kern et al, 2019; Nakamura et al, 2020).

Despite these important achievements, several critical aspects regarding VRAC channels remain enigmatic. Among these are: What is the fundamental trigger mechanism underlying VRAC activation? What is the physiologically relevant stoichiometry and subunit composition of heteromers? Which are the domains involved in the gating of the channel?

Considerable progress has been obtained in recent years, employing site directed mutagenesis and chimeric approaches, that elucidated the relevance of specific regions of LRRC8 subunits. For example, the first 15 residues at the N-terminus of LRRC8 subunits, that are not resolved in the structures described so far, are functionally important and might line the cytoplasmic side of the VRAC pore folding back into the ion permeation pathway (Zhou et al, 2018). Also, a stretch of 25 residues in the loop of the 8A subunit (YSS) was shown to be essential for channel functioning, since when introduced in place of corresponding residues of 8C, 8D, or 8E could give rise to homomeric-chimeras of the respective subunits which could undergo activation without need of co-expression with 8A. So far, no current was observed in any LRRC8 homomeric channel, with the only exception of 8A homomers that were shown to elicit a tiny current (Yamada et al, 2020; Yamada & Strange, 2018; Zhou et al, 2018).

In this thesis I focus on the mechanism of VRAC activation, putting particular emphasis in the investigation of two molecular events that has been implicated with VRAC gating: oxidation and phosphorylation.

The coupling between VRAC activity and reactive oxygen species (ROS) is not yet fully understood. Given the broad physiological and pathophysiological relevance of the ROS sensitivity of VRAC it is important to decipher the molecular mechanisms underlying this regulation.

On the one hand ROS have been shown to directly modulate VRAC activity in several cellular systems, but in parallel extracellular hypotonic conditions has been reported to influence ROS level, leading to an increase (Browe & Baumgarten, 2004; Crutzen et al, 2012; Shimizu et al, 2004; Varela et al, 2004). In addition, it has been recently proposed that VRAC activation impacts on the oxidation status, also by the release of reduced glutathione (Friard et al, 2019).

An important matter of debate is whether ROS may directly act on VRAC channels or indirectly through the modulation of upstream regulator. A previous report provided evidence that Chl-T and TBHP have

divergent effect when applied on oocytes injected with 8A/8E compared to those injected with 8A/8C or 8A/8D subunits, and suggested a direct oxidation of intracellular cysteines of 8E and of methionines of 8C (Gradogna et al, 2017). However, which residues were affected by oxidation remained unclear.

In the present work we succeeded to identify the targets of oxidation in 8E as well as in 8C subunits. Based on successive chimeras of 8E and 8C subunits, we finally disclosed C424 and C448 of LRRC8E as the targets of Chl-T and TBHP oxidation. Surprisingly, the results showed that both cysteines are essential to elicit the strong potentiation of VRAC activity upon Chl-T application: both single mutations, C424F and C448S, abolished responsiveness to Chl-T.

Interestingly, the two cysteines are likely close to each other in the 3D structure, with C424 localized at the beginning of LRR1 and C448 at the beginning of LRR2. We speculate that Chl-T/TBHP might induce a disulphide bond formation between the two cysteines.

In the homology model of 8A/8E heteromers the distance between the two cysteines is around 7.1 Å. Such a distance is not compatible with a direct formation of a disulphide bond, that usually occurs when two cysteines are spatially closer (within 3 Å). However, it needs to be taken into account that the 8A/8E "structure" is a homology-model based on the homomeric and un-physiological LRRC8A structure. Being a model, it is difficult to predict the real spatial distance occurring in the natural conformation. However, there is considerable evidence regarding the potential role of oxidants in mediating disulfide bond formation. When reactive cysteine thiols meet reactive oxygen, sulfenic acid (RSOH) formation occurs. Sulfenic acids are highly unstable oxidation intermediates that rapidly interact with nearby cysteines to form inter- or intramolecular disulphide bonds (RSSR), making this a primary route for oxidant-mediated disulphide bond formation (Cremers & Jakob, 2013). The formation of an intramolecular disulphide bond can bring closer two cysteines that are distant in the reduced form (even by 17 Å) leading to conformational changes that might affect the function of proteins. We speculated that this could be the case of C424 and C448 (Fig. 12).

Interestingly, the insertion of two cysteines in the corresponding position in 8C subunits, which normally are not functionally modified by TBHP, resulted in TBHP sensitive channels, similar to 8E containing heteromers. This finding further corroborated our hypothesis.

Notably, the biphasic effect observed upon application of Chl-T on 8A/8C$_{I431C/K455C}$, that namely led to a slight activation followed by a very slow inactivation of the current, indicates that C431 and C455 introduce into 8C a reaction site for Chl-T, that is distinct from that present in WT 8C subunit.

The generation of concatemers exploiting the T2A cleavable-linker technology allowed the mutation of the start Methionine (M1) and made it possible to disclose M1 as the target of 8C oxidation leading to inhibition of 8A/8C heteromers. The N-terminus was previously reported to be critical for channel gating (Zhou et al, 2018) and to play a role in pore constriction in native channels composed of 8A/8C heteromers. Moreover, whole-cell currents mediated by 8A-T5C/8C are strongly suppressed upon the addition of MTSES

(Kefauver et al, 2018). All these findings suggested that the N-terminus might line the cytoplasmic side of the VRAC pore folding back into the ion permeation pathway. We speculate that M1 is part of a constriction narrow enough to block the pore upon covalent modification by Chl-T. However, a critical open question is why the oxidation of the first methionine has an inhibitory effect only in 8C. Indeed, the chimera "E-C", which contains only the LRRD of 8C is inhibited by Chl-T (Fig. 8A). This puzzling finding let us initially to believe that the target of oxidation in 8C has to be localized in the LRRD. However singly mutating all Met and Cys residues in the LRRD of 8C did not eliminate the inhibition. Thus, the results with the chimera "E-C" indicate that also the start methionine of 8E is oxidized by Chl-T, but an inhibitory effect is only seen if the LRRD is from the 8C subunit. Since oxidized methionines have one or two oxygen atoms added to the sulphur atom, the oxidized Meth side chain is bulkier. Thus it is tempting to speculate that an N-terminus with oxidized M1 is able to occlude the pore if the LRRD is from 8C but not if it is from 8E. This speculation points again to a highly critical role of the conformation of the LRRD domains for channel activation.
Ironically, this is the same conclusion we obtained regarding the disulphide bond formation in 8E subunits: bringing closer to each other C424 and C448 in LRR1 by a few Angstroms leads to strong channel activation. Thus, our results provided important insights into the mechanism of channel activation and the involvement of specific molecular parts of the LRRDs and the N-terminus.
The oxidation of Met1 is unlikely of physiological relevance in that for example TBHP was not sufficient to induce Met1 oxidation in 8C. In contrast, the necessary ROS concentration needed for disulphide bond formation in 8E subunits might be achieved locally in specific conditions of oxidative stress, and we cannot exclude that this is of physiological relevance. This question requires further investigation.
Finally, the molecular targets underlying oxidation induced inhibition of 8A/8D subunits (Gradogna et al, 2017) need to be identified.
The second major aim of my thesis project had the main goal of elucidating the relevance of post-translational modification in VRAC function. In particular, a large body of literature hinted at a determinant role of phosphorylation in the signalling cascade leading to VRAC activation. However, even though several works suggested that the inhibition of kinase activity could hinder VRAC activation upon hypotonic stimulation, it has never been clarified whether this might rely on a direct effect on VRAC subunits or on an upstream regulator. Also, most of the works on the topic were performed before the molecular identification of LRRC8 genes.
I thereby used the NetPhos phosphorylation prediction server to identify regions of each LRRC8 subunit that are likely target of phosphorylation. The IL1 of LRRC8A, and in particular 16 Ser/Thr residues within a stretch of ~120 aa of IL1, that partially overlapped with YSS (Yamada & Strange, 2018), turned out to have a high score for being targets of phosphorylation.
Here again I adopted the strategy of building successive chimeras, to furtherly narrow down the regions of the IL1 that, when mutagenized, rendered the channel unresponsive to hypotonic stimulation.

This approach led me to identify threonine 169 of LRRC8A as a highly critical residue for VRAC functioning. Indeed, replacement of T169 by alanine (A) eliminated the activation by hypotonicity. On the contrary, mutant T169E retained activation by hypotonicity and even induced a certain degree of constitutive activity. This result is in agreement with the interpretation that the insertion of a negative charged residue at position 169 mimics the presence of a phosphate group, and thus that, in vivo, phosphorylation of T169 promotes channel activation.

However surprisingly, when T169 was replaced by a serine, similarly to what happened for T169A, the channel turned to be insensitive to hypotonic stimulation. Overall, while the effect observed with $8A_{T169E}$/8E support the hypothesis of a role of phosphorylation in the gating of the channel, the loss of activity of $8A_{T169S}$/8E apparently argues against it. Serine and threonine possess a similar sidechain that is a possible target of serine/threonine kinases which react with their OH group transferring a phosphate to the oxygen atom. Nevertheless, serine is smaller in size and possesses only a OH group, unlike threonine, which has an additional methyl group. In is insightful to highlight the position of threonine 169 in the IL1. T169 lies in a stretch of residues at the beginning of IL1 that show a very high level of conservation in all LRRC8 subunits, conferring to the structure a peculiar conformation (Figure 13). The first alpha helix of the IL1 (called LH1) points into the cytoplasmic side, and is interrupted by proline 167. P167 causes a kink in the helix, generating a motif known as helix-turn-helix. The kink creates an angle followed by another short helix in which T169 is localized at the second position.

Kern et al. captured two predominant conformations of LRRC8A homomers, a ‘constricted ‘ and a ‘relaxed’ form, which were interpreted as representing a closed versus an active state of the channel (Kern et al, 2019). A morph between the two structures shows the motion of the linker region upon channel gating (https://static-movie-usa.glencoesoftware.com/mp4/10.7554/452/4d81c05158bf7c77fd0823af84a1db9045171161/elife-42636-video2.mp4). Here it is possible to see that the helix-turn-helix motif maintains its rigidity and keeps the same lean while sliding-up to achieve the presumably active conformation. This causes a sequential rearrangement of the remaining part of the linker that might finally contribute to an upward push of the TM3 (Kern et al, 2019).

It is difficult to distinguish whether the importance of threonine 169 reflects its property to undergo phosphorylation/dephosphorylation that is abolished by substitution with other residues (including serine), or whether T169 might be critical for structural integrity, such that alterations caused by replacement by other aminoacids with different size or chemical properties, results in impossibility of volume induced channels opening. In any case, we can rather confidently speculate that a change at position 169 might introduce flexibility in a highly conserved rigid region thus affecting the following (allosteric) conformational rearrangements required to gate the channel.

Remarkably, $8A_{T169S}$/8E channels are still capable to undergo activation by application of a low intracellular ionic strength solution through the patch pipette. On the one hand, this finding highlights the physiological relevance of T169 in the background of 8A for what concerns the mechanism underlying VRAC activation upon cell swelling and, more in general, hints at the importance of the stretch of highly conserved aminoacids in close proximity, whose precise 3D conformation might be determinant to guarantee channel activity under physiological condition, characterizing an important constraint for VRAC gating.

Furthermore, our results clearly demonstrate that the ability of VRAC channels to sense low ionic strength is not physiologically relevant and do not support the mechanism by which cells respond to the hypotonic challenge, how was previously hypothesized (Nilius et al, 1998; Syeda et al, 2016; Voets et al, 1999) . On the contrary, corroborates the hypothesis of an artifact effect that most likely rely on electrostatic interaction within the LRR domain of neighbouring subunits (Strange et al, 2019).

Unfortunately, experiments performed with phorbol 12-myristate 13-acetate (PMA), that mimic DAG signalling leading to PKC activation, did not provide evidence of a strong effect on VRAC activation, so far.

Further investigations are required to elucidate a possible involvement of phosphorylation in the hypotonic challenge for VRAC activity.

6. BIBLIOGRAPHY

Abascal F, Zardoya R (2012) LRRC8 proteins share a common ancestor with pannexins, and may form hexameric channels involved in cell-cell communication. *Bioessays* **34:** 551-560

Ackerman MJ, Wickman KD, Clapham DE (1994) Hypotonicity activates a native chloride current in Xenopus oocytes. *J Gen Physiol* **103:** 153-179

Akita T, Fedorovich SV, Okada Y (2011) Ca^{2+} nanodomain-mediated component of swelling-induced volume-sensitive outwardly rectifying anion current triggered by autocrine action of ATP in mouse astrocytes. *Cell Physiol Biochem* **28:** 1181-1190

Akita T, Okada Y (2014) Characteristics and roles of the volume-sensitive outwardly rectifying (Vsor) anion channel in the central nervous system. *Neuroscience* **275:** 211-231

Anderson JW, Jirsch JD, Fedida D (1995) Cation regulation of anion current activated by cell swelling in two types of human epithelial cancer cells. *J Physiol* **483 (Pt 3):** 549-557

Bao J, Perez CJ, Kim J, Zhang H, Murphy CJ, Hamidi T, Jaubert J, Platt CD, Chou J, Deng M, Zhou MH, Huang Y, Gaitan-Penas H, Guenet JL, Lin K, Lu Y, Chen T, Bedford MT, Dent SY, Richburg JH, Estevez R, Pan HL, Geha RS, Shi Q, Benavides F (2018) Deficient LRRC8A-dependent volume-regulated anion channel activity is associated with male infertility in mice. *JCI insight* **3**

Bertelli S, Remigante A, Zuccolini P, Barbieri R, Ferrera L, Picco C, Gavazzo P, Pusch M (2021) Mechanisms of Activation of LRRC8 Volume Regulated Anion Channels. *Cell Physiol Biochem* **55:** 41-56

Botchkin LM, Matthews G (1993) Chloride current activated by swelling in retinal pigment epithelium cells. *Am J Physiol* **265:** C1037-C1045

Bowens NH, Dohare P, Kuo YH, Mongin AA (2013) DCPIB, the proposed selective blocker of volume-regulated anion channels, inhibits several glutamate transport pathways in glial cells. *Mol Pharmacol* **83:** 22-32

Braun AP, Schulman H (1996) Distinct voltage-dependent gating behaviours of a swelling-activated chloride current in human epithelial cells. *J Physiol* **495 (Pt 3):** 743-753

Browe DM, Baumgarten CM (2004) Angiotensin II (AT1) receptors and NADPH oxidase regulate Cl- current elicited by beta1 integrin stretch in rabbit ventricular myocytes. *J Gen Physiol* **124:** 273-287

Bryan-Sisneros A, Sabanov V, Thoroed SM, Doroshenko P (2000) Dual role of ATP in supporting volume-regulated chloride channels in mouse fibroblasts. *Biochim Biophys Acta* **1468:** 63-72

Burg MB (2002) Response of renal inner medullary epithelial cells to osmotic stress. *Comp Biochem Physiol A Mol Integr Physiol* **133:** 661-666

Cahalan MD, Lewis RS (1988) Role of potassium and chloride channels in volume regulation by T lymphocytes. *Soc Gen Physiol Ser* **43:** 281-301

Carton I, Trouet D, Hermans D, Barth H, Aktories K, Droogmans G, Jorgensen NK, Hoffmann EK, Nilius B, Eggermont J (2002) RhoA exerts a permissive effect on volume-regulated anion channels in vascular endothelial cells. *Am J Physiol Cell Physiol* **283:** C115-C125

Chen L, Becker TM, Koch U, Stauber T (2019) The LRRC8/VRAC anion channel facilitates myogenic differentiation of murine myoblasts by promoting membrane hyperpolarization. *J Biol Chem* **294:** 14279-14288

Chen L, Konig B, Stauber T (2020) LRRC8 channel activation and reduction in cytosolic chloride concentration during early differentiation of C2C12 myoblasts. *Biochem Biophys Res Commun* **532:** 482-488

Chen LX, Zhu LY, Jacob TJ, Wang LW (2007) Roles of volume-activated Cl- currents and regulatory volume decrease in the cell cycle and proliferation in nasopharyngeal carcinoma cells. *Cell proliferation* **40:** 253-267

Chou CY, Shen MR, Hsu KS, Huang HY, Lin HC (1998) Involvement of PKC-alpha in regulatory volume decrease responses and activation of volume-sensitive chloride channels in human cervical cancer HT-3 cells. *J Physiol* **512 (Pt 2):** 435-448

Coca-Prados M, Anguita J, Chalfant ML, Civan MM (1995) PKC-sensitive Cl^- channels associated with ciliary epithelial homologue of pICln. *Am J Physiol* **268:** C572-579

Cremers CM, Jakob U (2013) Oxidant sensing by reversible disulfide bond formation. *J Biol Chem* **288:** 26489-26496

Crepel V, Panenka W, Kelly ME, MacVicar BA (1998) Mitogen-activated protein and tyrosine kinases in the activation of astrocyte volume-activated chloride current. *J Neurosci* **18:** 1196-1206

Crutzen R, Shlyonsky V, Louchami K, Virreira M, Hupkens E, Boom A, Sener A, Malaisse WJ, Beauwens R (2012) Does NAD(P)H oxidase-derived H_2O_2 participate in hypotonicity-induced insulin release by activating VRAC in beta-cells? *Pflugers Arch* **463:** 377-390

Darby M, Kuzmiski JB, Panenka W, Feighan D, MacVicar BA (2003) ATP released from astrocytes during swelling activates chloride channels. *J Neurophysiol* **89:** 1870-1877

de Tassigny AD, Souktani R, Henry P, Ghaleh B, Berdeaux A (2004) Volume-sensitive chloride channels (I-Cl,(vol)) mediate doxorubicin-induced apoptosis through apoptotic volume decrease in cardiomyocytes. *Fund Clin Pharmacol* **18:** 531-538

Decher N, Lang HJ, Nilius B, Bruggemann A, Busch AE, Steinmeyer K (2001) DCPIB is a novel selective blocker of I(Cl,swell) and prevents swelling-induced shortening of guinea-pig atrial action potential duration. *Br J Pharmacol* **134:** 1467-1479

DeCoursey TE (2003) Voltage-gated proton channels and other proton transfer pathways. *Physiol Rev* **83:** 475-579

Deneka D, Sawicka M, Lam AKM, Paulino C, Dutzler R (2018) Structure of a volume-regulated anion channel of the LRRC8 family. *Nature* **558:** 254-259

Dolan J, Walshe K, Alsbury S, Hokamp K, O'Keeffe S, Okafuji T, Miller SF, Tear G, Mitchell KJ (2007) The extracellular leucine-rich repeat superfamily; a comparative survey and analysis of evolutionary relationships and expression patterns. *BMC genomics* **8:** 320

Doroshenko P (1991) Second messengers mediating activation of chloride current by intracellular GTP gamma S in bovine chromaffin cells. *J Physiol* **436:** 725-738

Doroshenko P (1998) Pervanadate inhibits volume-sensitive chloride current in bovine chromaffin cells. *Pflugers Arch* **435:** 303-309

Doroshenko P, Neher E (1992) Volume-sensitive chloride conductance in bovine chromaffin cell membrane. *J Physiol* **449:** 197-218

Du XL, Gao Z, Lau CP, Chiu SW, Tse HF, Baumgarten CM, Li GR (2004) Differential effects of tyrosine kinase inhibitors on volume-sensitive chloride current in human atrial myocytes: evidence for dual regulation by Src and EGFR kinases. *J Gen Physiol* **123:** 427-439

Dubois JM, Rouzaire-Dubois B (2004) The influence of cell volume changes on tumour cell proliferation. *Eur Biophys J* **33:** 227-232

Dusterwald KM, Currin CB, Burman RJ, Akerman CJ, Kay AR, Raimondo JV (2018) Biophysical models reveal the relative importance of transporter proteins and impermeant anions in chloride homeostasis. *Elife* **7**

Enkhbayar P, Kamiya M, Osaki M, Matsumoto T, Matsushima N (2004) Structural principles of leucine-rich repeat (LRR) proteins. *Proteins* **54:** 394-403

Estevez AY, Bond T, Strange K (2001) Regulation of I(Cl,swell) in neuroblastoma cells by G protein signaling pathways. *Am J Physiol Cell Physiol* **281:** C89-98

Feige JN, Sage D, Wahli W, Desvergne B, Gelman L (2005) PixFRET, an ImageJ plug-in for FRET calculation that can accommodate variations in spectral bleed-throughs. *Microsc Res Tech* **68:** 51-58

Fisher SK, Cheema TA, Foster DJ, Heacock AM (2008) Volume-dependent osmolyte efflux from neural tissues: regulation by G-protein-coupled receptors. *J Neurochem* **106:** 1998-2014

Fisher SK, Heacock AM, Keep RF, Foster DJ (2010) Receptor regulation of osmolyte homeostasis in neural cells. *J Physiol* **588:** 3355-3364

Franco R, Panayiotidis MI, de la Paz LD (2008) Autocrine signaling involved in cell volume regulation: the role of released transmitters and plasma membrane receptors. *J Cell Physiol* **216:** 14-28

Friard J, Corinus A, Cougnon M, Tauc M, Pisani DF, Duranton C, Rubera I (2019) LRRC8/VRAC channels exhibit a noncanonical permeability to glutathione, which modulates epithelial-to-mesenchymal transition (EMT). *Cell Death Dis* **10:** 925

Fujii T, Takahashi Y, Takeshima H, Saitoh C, Shimizu T, Takeguchi N, Sakai H (2015) Inhibition of gastric H+,K+-ATPase by 4-(2-butyl-6,7-dichloro-2-cyclopentylindan-1-on-5-yl)oxybutyric acid (DCPIB), an inhibitor of volume-regulated anion channel. *European journal of pharmacology* **765:** 34-41

Gaitán-Peñas H, Gradogna A, Laparra-Cuervo L, Solsona C, Fernández-Dueñas V, Barrallo-Gimeno A, Ciruela F, Lakadamyali M, Pusch M, Estévez R (2016) Investigation of LRRC8-mediated volume-regulated anion currents in *Xenopus o*ocytes. *Biophysical journal* **111:** 1429-1443

Gaitán-Peñas H, Pusch M, Estevez R (2018) Expression of LRRC8/VRAC currents in Xenopus oocytes: Advantages and caveats. *Int J Mol Sci* **19**

Galietta LJ, Haggie PM, Verkman AS (2001) Green fluorescent protein-based halide indicators with improved chloride and iodide affinities. *FEBS Lett* **499:** 220-224

Gay NJ, Symmons MF, Gangloff M, Bryant CE (2014) Assembly and localization of Toll-like receptor signalling complexes. *Nature reviews Immunology* **14:** 546-558

Gong W, Xu H, Shimizu T, Morishima S, Tanabe S, Tachibe T, Uchida S, Sasaki S, Okada Y (2004) ClC-3-independent, PKC-dependent activity of volume-sensitive Cl channel in mouse ventricular cardiomyocytes. *Cell Physiol Biochem* **14:** 213-224

Gradogna A, Gavazzo P, Boccaccio A, Pusch M (2017) Subunit-dependent oxidative stress sensitivity of LRRC8 volume-regulated anion channels. *J Physiol* **595:** 6719-6733

Groulx N, Boudreault F, Orlov SN, Grygorczyk R (2006) Membrane reserves and hypotonic cell swelling. *J Membr Biol* **214:** 43-56

Grubb S, Poulsen KA, Juul CA, Kyed T, Klausen TK, Larsen EH, Hoffmann EK (2013) TMEM16F (Anoctamin 6), an anion channel of delayed Ca(2+) activation. *The Journal of general physiology* **141:** 585-600

Gründer S, Thiemann A, Pusch M, Jentsch TJ (1992) Regions involved in the opening of CIC-2 chloride channel by voltage and cell volume. *Nature* **360:** 759-762

Habela CW, Sontheimer H (2007) Cytoplasmic volume condensation is an integral part of mitosis. *Cell Cycle* **6:** 1613-1620

Hartzell HC, Yu K, Xiao Q, Chien L-T, Qu Z (2009) Anoctamin/TMEM16 family members are Ca2+-activated Cl− channels. *The Journal of Physiology* **587:** 2127-2139

Hawkins CL, Pattison DI, Davies MJ (2003) Hypochlorite-induced oxidation of amino acids, peptides and proteins. *Amino acids* **25:** 259-274

Hazama A, Okada Y (1988) Ca^{2+} sensitivity of volume-regulatory K^+ and Cl^- channels in cultured human epithelial cells. *J Physiol* **402:** 687-702

Hermoso M, Olivero P, Torres R, Riveros A, Quest AF, Stutzin A (2004) Cell volume regulation in response to hypotonicity is impaired in HeLa cells expressing a protein kinase Calpha mutant lacking kinase activity. *J Biol Chem* **279:** 17681-17689

Hernandez-Carballo CY, De Santiago-Castillo JA, Rosales-Saavedra T, Perez-Cornejo P, Arreola J (2010) Control of volume-sensitive chloride channel inactivation by the coupled action of intracellular chloride and extracellular protons. *Pflugers Arch* **460:** 633-644

Hoffmann EK, Lambert IH, Pedersen SF (2009) Physiology of cell volume regulation in vertebrates. *Physiol Rev* **89:** 193-277

Hoffmann EK, Sorensen BH, Sauter DP, Lambert IH (2015) Role of volume-regulated and calcium-activated anion channels in cell volume homeostasis, cancer and drug resistance. *Channels (Austin)* **9:** 380-396

Jackson PS, Morrison R, Strange K (1994) The volume-sensitive organic osmolyte-anion channel VSOAC is regulated by nonhydrolytic ATP binding. *Am J Physiol* **267:** C1203-C1209

Jackson PS, Strange K (1995) Characterization of the voltage-dependent properties of a volume-sensitive anion conductance. *J Gen Physiol* **105:** 661-676

Jentsch TJ (2016) VRACs and other ion channels and transporters in the regulation of cell volume and beyond. *Nat Rev Mol Cell Biol* **17:** 293-307

Jiang X, Sorkin A (2002) Coordinated traffic of Grb2 and Ras during epidermal growth factor receptor endocytosis visualized in living cells. *Mol Biol Cell* **13:** 1522-1535

Jiao JD, Xu CQ, Yue P, Dong DL, Li Z, Du ZM, Yang BF (2006) Volume-sensitive outwardly rectifying chloride channels are involved in oxidative stress-induced apoptosis of mesangial cells. *Biochem Biophys Res Commun* **340:** 277-285

Jurman ME, Boland LM, Liu Y, Yellen G (1994) Visual identification of individual transfected cells for electrophysiology using antibody-coated beads. *Biotechniques* **17:** 876-881

Juul CA, Grubb S, Poulsen KA, Kyed T, Hashem N, Lambert IH, Larsen EH, Hoffmann EK (2014) Anoctamin 6 differs from VRAC and VSOAC but is involved in apoptosis and supports volume regulation in the presence of Ca2+. *Pflugers Arch* **466:** 1899-1910

Kang C, Xie L, Gunasekar SK, Mishra A, Zhang Y, Pai S, Gao Y, Kumar A, Norris AW, Stephens SB, Sah R (2018) SWELL1 is a glucose sensor regulating beta-cell excitability and systemic glycaemia. *Nat Commun* **9:** 367

Kasuya G, Nakane T, Yokoyama T, Jia Y, Inoue M, Watanabe K, Nakamura R, Nishizawa T, Kusakizako T, Tsutsumi A, Yanagisawa H, Dohmae N, Hattori M, Ichijo H, Yan Z, Kikkawa M, Shirouzu M, Ishitani R, Nureki O (2018) Cryo-EM structures of the human volume-regulated anion channel LRRC8. *Nature structural & molecular biology* **25:** 797-804

Kefauver JM, Saotome K, Dubin AE, Pallesen J, Cottrell CA, Cahalan SM, Qiu Z, Hong G, Crowley CS, Whitwam T, Lee WH, Ward AB, Patapoutian A (2018) Structure of the human volume regulated anion channel. *eLife* **7**

Kern DM, Oh S, Hite RK, Brohawn SG (2019) Cryo-EM structures of the DCPIB-inhibited volume-regulated anion channel LRRC8A in lipid nanodiscs. *eLife* **8**

Klausen TK, Bergdahl A, Hougaard C, Christophersen P, Pedersen SF, Hoffmann EK (2007) Cell cycle-dependent activity of the volume- and Ca2+-activated anion currents in Ehrlich lettre ascites cells. *J Cell Physiol* **210:** 831-842

Kobe B, Kajava AV (2001) The leucine-rich repeat as a protein recognition motif. *Curr Opin Struct Biol* **11:** 725-732

König B (2019) Establishment and application of a FRET sensor for VRAC activity reveals a key role for diacylglycerol signaling in channel regulation. Ph.D. Thesis, Department of Biology, Chemistry and Pharmacy, Freie Universit□at Berlin, Berlin

König B, Hao Y, Schwartz S, Plested AJ, Stauber T (2019) A FRET sensor of C-terminal movement reveals VRAC activation by plasma membrane DAG signaling rather than ionic strength. *eLife* **8**

Kubo M, Okada Y (1992) Volume-regulatory Cl^- channel currents in cultured human epithelial cells. *J Physiol* **456:** 351-371

Kubota K, Kim JY, Sawada A, Tokimasa S, Fujisaki H, Matsuda-Hashii Y, Ozono K, Hara J (2004) LRRC8 involved in B cell development belongs to a novel family of leucine-rich repeat proteins. *FEBS Lett* **564:** 147-152

Kumar A, Xie L, Ta CM, Hinton AO, Gunasekar SK, Minerath RA, Shen K, Maurer JM, Grueter CE, Abel ED, Meyer G, Sah R (2020) SWELL1 regulates skeletal muscle cell size, intracellular signaling, adiposity and glucose metabolism. *eLife* **9**

Lahey LJ, Mardjuki RE, Wen X, Hess GT, Ritchie C, Carozza JA, Bohnert V, Maduke M, Bassik MC, Li L (2020) LRRC8A:C/E heteromeric channels are ubiquitous transporters of cGAMP. *Mol Cell*

Lang F, Ritter M, Gamper N, Huber S, Fillon S, Tanneur V, Lepple-Wienhues A, Szabo I, Gulbins E (2000) Cell volume in the regulation of cell proliferation and apoptotic cell death. *Cell Physiol Biochem* **10:** 417-428

Lewis RS, Ross PE, Cahalan MD (1993) Chloride channels activated by osmotic stress in T lymphocytes. *J Gen Physiol* **101:** 801-826

Liu HT, Akita T, Shimizu T, Sabirov RZ, Okada Y (2009) Bradykinin-induced astrocyte-neuron signalling: glutamate release is mediated by ROS-activated volume-sensitive outwardly rectifying anion channels. *J Physiol* **587:** 2197-2209

Lück JC, Puchkov D, Ullrich F, Jentsch TJ (2018) LRRC8/VRAC anion channels are required for late stages of spermatid development in mice. *J Biol Chem* **293:** 11796-11808

Lutter D, Ullrich F, Lueck JC, Kempa S, Jentsch TJ (2017) Selective transport of neurotransmitters and modulators by distinct volume-regulated LRRC8 anion channels. *J Cell Sci* **130:** 1122-1133

Manolopoulos VG, Droogmans G, Nilius B (1997) Hypotonicity and thrombin activate taurine efflux in BC3H1 and C2C12 myoblasts that is down regulated during differentiation. *Biochem Biophys Res Commun* **232:** 74-79

Manolopoulos VG, Liekens S, Koolwijk P, Voets T, Peters E, Droogmans G, Lelkes PI, De Clercq E, Nilius B (2000) Inhibition of angiogenesis by blockers of volume-regulated anion channels. *Gen Pharmacol* **34:** 107-116

Matsushima N, Takatsuka S, Miyashita H, Kretsinger RH (2019) Leucine Rich Repeat Proteins: Sequences, Mutations, Structures and Diseases. *Protein Pept Lett* **26:** 108-131

Meyer K, Korbmacher C (1996) Cell swelling activates ATP-dependent voltage-gated chloride channels in M-1 mouse cortical collecting duct cells. *J Gen Physiol* **108:** 177-193

Michalski K, Syrjanen JL, Henze E, Kumpf J, Furukawa H, Kawate T (2020) The Cryo-EM structure of pannexin 1 reveals unique motifs for ion selection and inhibition. *eLife* **9**

Michea L, Ferguson DR, Peters EM, Andrews PM, Kirby MR, Burg MB (2000) Cell cycle delay and apoptosis are induced by high salt and urea in renal medullary cells. *Am J Physiol Renal Physiol* **278:** F209-218

Minieri L, Pivonkova H, Caprini M, Harantova L, Anderova M, Ferroni S (2013) The inhibitor of volume-regulated anion channels DCPIB activates TREK potassium channels in cultured astrocytes. *Br J Pharmacol* **168:** 1240-1254

Mongin AA (2016) Volume-regulated anion channel--a frenemy within the brain. *Pflugers Arch* **468:** 421-441

Mongin AA, Kimelberg HK (2005) ATP regulates anion channel-mediated organic osmolyte release from cultured rat astrocytes via multiple Ca2+-sensitive mechanisms. *Am J Physiol Cell Physiol* **288:** C204-213

Muralidharan S, Mandrekar P (2013) Cellular stress response and innate immune signaling: integrating pathways in host defense and inflammation. *J Leukoc Biol* **94:** 1167-1184

Nakamura R, Numata T, Kasuya G, Yokoyama T, Nishizawa T, Kusakizako T, Kato T, Hagino T, Dohmae N, Inoue M, Watanabe K, Ichijo H, Kikkawa M, Shirouzu M, Jentsch TJ, Ishitani R, Okada Y, Nureki O (2020) Cryo-EM structure of the volume-regulated anion channel LRRC8D isoform identifies features important for substrate permeation. *Commun Biol* **3:** 240

Nietsch HH, Roe MW, Fiekers JF, Moore AL, Lidofsky SD (2000) Activation of potassium and chloride channels by tumor necrosis factor alpha. Role in liver cell death. *J Biol Chem* **275:** 20556-20561

Nilius B, Droogmans G (2001) Ion channels and their functional role in vascular endothelium. *Physiol Rev* **81:** 1415-1459

Nilius B, Droogmans G (2003) Amazing chloride channels: an overview. *Acta physiologica Scandinavica* **177:** 119-147

Nilius B, Eggermont J, Voets T, Buyse G, Manolopoulos V, Droogmans G (1997) Properties of volume-regulated anion channels in mammalian cells. *Prog Biophys Mol Biol* **68:** 69-119

Nilius B, Oike M, Zahradnik I, Droogmans G (1994) Activation of a Cl^- current by hypotonic volume increase in human endothelial cells. *J Gen Physiol* **103:** 787-805

Nilius B, Prenen J, Voets T, Eggermont J, Droogmans G (1998) Activation of volume-regulated chloride currents by reduction of intracellular ionic strength in bovine endothelial cells. *J Physiol* **506:** 353-361

Nilius B, Voets T, Eggermont J, Droogmans G (1999) VRAC: A multifunctional volume-regulated anion channel in vascular endothelium. In *Chloride Channels*, pp 47–64. Oxford: Isis Medical Media Ltd

Okada Y (1997) Volume expansion-sensing outward-rectifier Cl^- channel: fresh start to the molecular identity and volume sensor. *The American journal of physiology* **273:** C755-789

Okada Y, Okada T, Sato-Numata K, Islam MR, Ando-Akatsuka Y, Numata T, Kubo M, Shimizu T, Kurbannazarova RS, Marunaka Y, Sabirov RZ (2019) Cell volume-activated and volume-correlated anion channels in mammalian cells: their biophysical, molecular, and pharmacological properties. *Pharmacol Rev* **71:** 49-88

Okada Y, Shimizu T, Maeno E, Tanabe S, Wang X, Takahashi N (2006) Volume-sensitive chloride channels involved in apoptotic volume decrease and cell death. *The Journal of membrane biology* **209:** 21-29

Pappas CA, Ritchie JM (1998) Effect of specific ion channel blockers on cultured Schwann cell proliferation. *Glia* **22:** 113-120

Pedersen SF, Klausen TK, Nilius B (2015) The identification of a volume-regulated anion channel: an amazing Odyssey. *Acta Physiol (Oxf)***:** 1-14

Pedersen SF, Okada Y, Nilius B (2016) Biophysics and physiology of the volume-regulated anion channel (VRAC)/volume-sensitive outwardly rectifying anion channel (VSOR). *Pflugers Arch* **468:** 371-383

Pedersen SF, Prenen J, Droogmans G, Hoffmann EK, Nilius B (1998) Separate swelling- and Ca2+-activated anion currents in Ehrlich ascites tumor cells. *The Journal of membrane biology* **163:** 97-110

Pendergrass WR, Angello JC, Kirschner MD, Norwood TH (1991) The relationship between the rate of entry into S phase, concentration of DNA polymerase alpha, and cell volume in human diploid fibroblast-like monokaryon cells. *Experimental cell research* **192:** 418-425

Pifferi S, Dibattista M, Menini A (2009) TMEM16B induces chloride currents activated by calcium in mammalian cells. *Pflügers Archiv: European journal of physiology* **458:** 1023-1038

Planells-Cases R, Lutter D, Guyader C, Gerhards NM, Ullrich F, Elger DA, Kucukosmanoglu A, Xu G, Voss FK, Reincke SM, Stauber T, Blomen VA, Vis DJ, Wessels LF, Brummelkamp TR, Borst P, Rottenberg S, Jentsch TJ (2015) Subunit composition of VRAC channels determines substrate specificity and cellular resistance to Pt-based anti-cancer drugs. *Embo J* **34:** 2993-3008

Qiu Z, Dubin AE, Mathur J, Tu B, Reddy K, Miraglia LJ, Reinhardt J, Orth AP, Patapoutian A (2014) SWELL1, a plasma membrane protein, is an essential component of volume-regulated anion channel. *Cell* **157:** 447-458

Ren Z, Baumgarten CM (2005) Antagonistic regulation of swelling-activated Cl- current in rabbit ventricle by Src and EGFR protein tyrosine kinases. *Am J Physiol Heart Circ Physiol* **288:** H2628-2636

Rouzaire-Dubois B, Milandri JB, Bostel S, Dubois JM (2000) Control of cell proliferation by cell volume alterations in rat C6 glioma cells. *Pflugers Arch* **440:** 881-888

Rouzaire-Dubois B, O'Regan S, Dubois JM (2005) Cell size-dependent and independent proliferation of rodent neuroblastoma x glioma cells. *J Cell Physiol* **203:** 243-250

Ruan Z, Orozco IJ, Du J, Lu W (2020) Structures of human pannexin 1 reveal ion pathways and mechanism of gating. *Nature* **584:** 646-651

Schroeder BC, Cheng T, Jan YN, Jan LY (2008) Expression cloning of TMEM16A as a calcium-activated chloride channel subunit. *Cell* **134:** 1019-1029

Schumann MA, Gardner P, Raffin TA (1993) Recombinant human tumor necrosis factor alpha induces calcium oscillation and calcium-activated chloride current in human neutrophils. The role of calcium/calmodulin-dependent protein kinase. *J Biol Chem* **268:** 2134-2140

Schwab A, Fabian A, Hanley PJ, Stock C (2012) Role of ion channels and transporters in cell migration. *Physiol Rev* **92:** 1865-1913

Shen MR, Droogmans G, Eggermont J, Voets T, Ellory JC, Nilius B (2000) Differential expression of volume-regulated anion channels during cell cycle progression of human cervical cancer cells. *J Physiol* **529 Pt 2:** 385-394

Shimizu T, Numata T, Okada Y (2004) A role of reactive oxygen species in apoptotic activation of volume-sensitive Cl(-) channel. *Proc Natl Acad Sci U S A* **101:** 6770-6773

Smits G, Kajava AV (2004) LRRC8 extracellular domain is composed of 17 leucine-rich repeats. *Mol Immunol* **41:** 561-562

Sorota S (1995) Tyrosine protein kinase inhibitors prevent activation of cardiac swelling-induced chloride current. *Pflugers Arch* **431:** 178-185

Strange K, Emma F, Jackson PS (1996) Cellular and molecular physiology of volume-sensitive anion channels. *Am J Physiol* **270:** C711-730

Strange K, Yamada T, Denton JS (2019) A 30-year journey from volume-regulated anion currents to molecular structure of the LRRC8 channel. *J Gen Physiol* **151:** 100-117

Stuhlmann T, Planells-Cases R, Jentsch TJ (2018) LRRC8/VRAC anion channels enhance beta-cell glucose sensing and insulin secretion. *Nat Commun* **9:** 1974

Stühmer W (1998) Electrophysiologic recordings from Xenopus oocytes. *Methods Enzymol* **293:** 280-300

Syeda R, Qiu Z, Dubin AE, Murthy SE, Florendo MN, Mason DE, Mathur J, Cahalan SM, Peters EC, Montal M, Patapoutian A (2016) LRRC8 Proteins form volume-regulated anion channels that sense ionic strength. *Cell* **164:** 499-511

Szücs G, Heinke S, De Greef C, Raeymaekers L, Eggermont J, Droogmans G, Nilius B (1996) The volume-activated chloride current in endothelial cells from bovine pulmonary artery is not modulated by phosphorylation. *Pflugers Arch* **431:** 540-548

Takano T, Kang J, Jaiswal JK, Simon SM, Lin JH, Yu Y, Li Y, Yang J, Dienel G, Zielke HR, Nedergaard M (2005) Receptor-mediated glutamate release from volume sensitive channels in astrocytes. *Proc Natl Acad Sci U S A* **102:** 16466-16471

Tang W, Ehrlich I, Wolff SB, Michalski AM, Wolfl S, Hasan MT, Luthi A, Sprengel R (2009) Faithful expression of multiple proteins via 2A-peptide self-processing: a versatile and reliable method for manipulating brain circuits. *J Neurosci* **29:** 8621-8629

Thiemann A, Gründer S, Pusch M, Jentsch TJ (1992) A chloride channel widely expressed in epithelial and non-epithelial cells. *Nature* **356:** 57-60

Thoroed SM, Bryan-Sisneros A, Doroshenko P (1999) Protein phosphotyrosine phosphatase inhibitors suppress regulatory volume decrease and the volume-sensitive Cl- conductance in mouse fibroblasts. *Pflugers Arch* **438:** 133-140

Tilly BC, Edixhoven MJ, Tertoolen LG, Morii N, Saitoh Y, Narumiya S, de Jonge HR (1996) Activation of the osmo-sensitive chloride conductance involves P21rho and is accompanied by a transient reorganization of the F-actin cytoskeleton. *Mol Biol Cell* **7:** 1419-1427

Tilly BC, van den Berghe N, Tertoolen LG, Edixhoven MJ, de Jonge HR (1993) Protein tyrosine phosphorylation is involved in osmoregulation of ionic conductances. *J Biol Chem* **268:** 19919-19922

Tominaga K, Kondo C, Kagata T, Hishida T, Nishizuka M, Imagawa M (2004) The novel gene fad158, having a transmembrane domain and leucine-rich repeat, stimulates adipocyte differentiation. *J Biol Chem* **279:** 34840-34848

Ullrich F (2016) Molecular identification and electrophysiological characterization of the volume-regulated anion channel VRAC. Ph.D. Thesis, Department of Biology, Chemistry and Pharmacy Freie Universität Berlin, Berlin

Ullrich F, Reincke SM, Voss FK, Stauber T, Jentsch TJ (2016) Inactivation and anion selectivity of volume-regulated anion channels (VRACs) depend on C-terminal residues of the first extracellular loop. *J Biol Chem* **291:** 17040-17048

Varela D, Simon F, Olivero P, Armisen R, Leiva-Salcedo E, Jorgensen F, Sala F, Stutzin A (2007) Activation of H_2O_2-induced VSOR Cl^- currents in HTC cells require phospholipase Cgamma1 phosphorylation and Ca^{2+} mobilisation. *Cell Physiol Biochem* **20:** 773-780

Varela D, Simon F, Riveros A, Jorgensen F, Stutzin A (2004) NAD(P)H oxidase-derived H(2)O(2) signals chloride channel activation in cell volume regulation and cell proliferation. *J Biol Chem* **279:** 13301-13304

Voets T, Droogmans G, Nilius B (1997a) Modulation of voltage-dependent properties of a swelling-activated Cl- current. *J Gen Physiol* **110:** 313-325

Voets T, Droogmans G, Raskin G, Eggermont J, Nilius B (1999) Reduced intracellular ionic strength as the initial trigger for activation of endothelial volume-regulated anion channels. *Proc Natl Acad Sci U S A* **96:** 5298-5303

Voets T, Manolopoulos V, Eggermont J, Ellory C, Droogmans G, Nilius B (1998) Regulation of a swelling-activated chloride current in bovine endothelium by protein tyrosine phosphorylation and G proteins. *J Physiol* **506 (Pt 2):** 341-352

Voets T, Szucs G, Droogmans G, Nilius B (1995) Blockers of volume-activated Cl- currents inhibit endothelial cell proliferation. *Pflugers Arch* **431:** 132-134

Voets T, Wei L, De Smet P, Van Driessche W, Eggermont J, Droogmans G, Nilius B (1997b) Downregulation of volume-activated Cl- currents during muscle differentiation. *Am J Physiol* **272:** C667-674

Voss FK, Ullrich F, Munch J, Lazarow K, Lutter D, Mah N, Andrade-Navarro MA, von Kries JP, Stauber T, Jentsch TJ (2014) Identification of LRRC8 heteromers as an essential component of the volume-regulated anion channel VRAC. *Science* **344:** 634-638

Wehner F (2006) Cell volume-regulated cation channels. *Contributions to nephrology* **152:** 25-53

Wondergem R, Gong W, Monen SH, Dooley SN, Gonce JL, Conner TD, Houser M, Ecay TW, Ferslew KE (2001) Blocking swelling-activated chloride current inhibits mouse liver cell proliferation. *J Physiol* **532:** 661-672

Yamada T, Figueroa EE, Denton JS, Strange K (2020) LRRC8A homohexameric channels poorly recapitulate VRAC regulation and pharmacology. *Am J Physiol Cell Physiol*

Yamada T, Strange K (2018) Intracellular and extracellular loops of LRRC8 are essential for volume-regulated anion channel function. *J Gen Physiol* **150:** 1003-1015

Zhou C, Chen X, Planells-Cases R, Chu J, Wang L, Cao L, Li Z, Lopez-Cayuqueo KI, Xie Y, Ye S, Wang X, Ullrich F, Ma S, Fang Y, Zhang X, Qian Z, Liang X, Cai SQ, Jiang Z, Zhou D, Leng Q, Xiao TS, Lan K, Yang J, Li H, Peng C, Qiu Z, Jentsch TJ, Xiao H (2020) Transfer of cGAMP into bystander cells via LRRC8 volume-regulated anion channels augments STING-mediated interferon responses and anti-viral immunity. *Immunity* **52:** 767-781 e766

Zhou P, Polovitskaya MM, Jentsch TJ (2018) LRRC8 N termini influence pore properties and gating of volume-regulated anion channels (VRACs). *J Biol Chem* **293:** 13440-13451

Ziegelhoeffer T, Scholz D, Friedrich C, Helisch A, Wagner S, Fernandez B, Schaper W (2003) Inhibition of collateral artery growth by mibefradil: possible role of volume-regulated chloride channels. *Endothelium : journal of endothelial cell research* **10:** 237-246

ACKNOWLEDGEMENTS

I would like to thank Anna Menini for her essential contribution and great support and for making it possible to pursue my PhD project in an open collaboration between SISSA and IBF.

I would like to express my gratitude to Michael Pusch for granting me the privilege of working in his laboratory. His unconditional support and constant interest in my work have been of great help. Thank you for the time and effort you invested in this project and for contributing to the development of my personal academic skills, which is of immense value to me.

Special thanks go to all the members of the 'IBF team' in Genova: Paola Gavazzo, Raffaella Barbieri, Loretta Ferrera, Paolo Zuccolini, Alessia Remigante, Cristiana Picco, Gianni Zifarelli. I would also like to thank Anna Boccaccio for her important help and scientific support especially in the final rush before my PhD defence.

I also thank all my 'close' and 'distant' colleagues at IBF and SISSA for all the special and funny moments we shared, stimulating discussions, technical help, and the great working environment.

Finally, I would like to thank my family who supported me constantly over the years.